SOLAR CYCLE EFFECTS ON GNSS-DERIVED IONOSPHERIC TOTAL ELECTRON CONTENT OBSERVED OVER SOUTHERN AFRICA

A thesis submitted in fulfillment of the
requirements for the degree of

DOCTOR OF PHILOSOPHY

of

RHODES UNIVERSITY

by

DANIEL MOJALEFA MOEKETSI

December 2007

Abstract

The South African Global Navigation Satellite System (GNSS) network of dual frequency receivers provide an opportunity to investigate solar cycle effects on ionospheric Total Electron Content (TEC) over the South Africa region by taking advantage of the dispersive nature of the ionospheric medium. For this task, the global University of New Brunswick Ionospheric Modelling Technique (UNB-IMT) was adopted, modified and applied to compute TEC using data from the southern African GNSS Network. TEC values were compared with CODE International GNSS services TEC predictions and Ionosonde-derived TEC (ITEC) measurements to test and validate the UNB-IMT results over South Africa. It was found that the variation trends of GTEC and ITEC over all stations are in good agreement and show pronounced seasonal variations with high TEC values around equinoxes for a year near solar maximum and less pronounced around solar minimum. Signature TEC depletions and enhanced spikes were prevalently evident around equinoxes, particularly for a year near solar maximum. These observations were investigated and further discussed with an analysis of the midday Disturbance Storm Time (DST) index of geomagnetic activity. The residual GTEC – ITEC corresponding to plasmaspheric electron content and equivalent ionospheric foF2 and total slab thickness parameters were computed and comprehensively discussed. The results verified the use of UNB-IMT as one of the tools for ionospheric research over South Africa. The UNB-IMT algorithm was applied to investigate TEC variability during different epochs of solar cycle 23. The results were investigated and further discussed by analyzing the GOES 8 and 10 satellites X-ray flux (0.1 – 0.8 nm) and SOHO Solar Extreme Ultraviolet Monitor higher resolution data. Comparison of UNB-IMT TEC derived from collocated HRAO and HARB GNSS receivers was undertaken for the solar X17 and X9 flare events, which occurred on day 301, 2003 and day 339, 2006. It was found that there exist considerable TEC differences between the two collocated receivers with some evidence of solar cycle dependence. Furthermore, the daytime UNB TEC compared with the International Reference Ionosphere 2001 predicted TEC found both models to show a good agreement. The UNB-IMT TEC was further applied to investigate the capabilities of geodetic Very Long Baseline Interferometry (VLBI) derived TEC using the Vienna TEC Model for space weather monitoring over HartRAO during the CONT02 and CONT05 campaigns conducted during the years 2002 (near solar maximum) and 2005 (near solar minimum). The results verified the use of geodetic VLBI as one of the possible instruments for monitoring space weather impacts on the ionosphere over South Africa.

ACKNOWLEDGEMENTS

I would like to acknowledge the contribution of the following people and express my gratitude to them, in no particular order:

- *Dr. L. A. McKinnell, my supervisor, for her support, motivation, advice and useful discussions throughout this study. Furthermore, the support from the staff of Department of Physics and Electronics.*
- *Dr. W. L. Combrinck, my co-supervisor, for his support and encouragement throughout this study.*
- *Dr. M. Fedrizzi of the University of Colorado, NOAA/SEC CIRES, USA, for her insight, advices, and helpful discussions about the UNB-IMT algorithm.*
- *Prof. R. Langley of the University of New Brunswick, Canada, for providing the UNB-IMT Unix version code, for research purposes.*
- *Mr. S. Ngcobo and Dr. A. Combrink for their assistance in porting the UNB-IMT Unix version to a Linux compatible version.*
- *Dr. N. Jakowski for his useful suggestions and discussions about this work.*
- *Dr. Hobiger for providing me with the VLBIonos TEC data and the interest he has shown in this work.*
- *Mr. J. Botai, Mr. S Madiseng and Mr. M. V. Molusi for friendship, and useful discussions.*
- *Mrs. Marisa Nichola for editing of this thesis.*
- *National Research Foundation/HartRAO for financial support, and Center for High Performance Computing of CSIR Meraka Institute for offering me a research position.*

A special thank to the following:

- *All mighty GOD, for enabling me to study a small portion of his magnificent creation.*
- *My parents (Mr. E. T. Moeketsi and Mrs. A. L. Moeketsi) for the support, love, encouragement, prayers which made me to arrive at this point in my academic career.*
- *My sisters; Maria, Veronica, and Roseline Moeketsi and brothers; Benjamin and David Moeketsi for the support and encouragements throughout this study.*
- *My wife Cleopatra, who sacrificed a comfortable life with her parents for the challenging one, of " student's wife". I would like to thank her for love, motivation and support she gave me throughout this study.*

This thesis is dedicated to her and my sons Katleho and Lefa.

E-mail: dmoeketsi@csir.co.za

List of Acronyms and Abbreviations

ATS	Application Technology Satellites
CELIAS	Charge Element and Isotope Analysis System
COSPAR	Committee on Space Research
EUV	Extreme Ultraviolet
DST	Disturbance Storm Time Index
GNSS	Global Navigation Satellite System
GLONASS	Global Orbiting Navigation Satellite System
GOES	Global Earth Observation Satellite
GPS	Global Position System
GTEC	GNSS Total Electron Content
HRAO/HartRAO	Hartebeesthoek Radio Astronomy Observatory
HF	High Frequency
IGS	International GNSS Service
ITEC	Ionosonde Total Electron Content
IRI	International Reference Ionosphere
NOAA	National Oceanic and Atmospheric Administration
PRN	Pseudorandom Number
RINEX	Receiver Exchange Format
SADC	Southern African Development Community
SEC	Space Enviroment Center
SEM	Solar Enviroment Monitor
SEPs	Solar Energetic Particles
SKA	Square Kilometer Array

SOHO	Solar and Heliospheric Observatory
SXI	Solar X-ray Imager
TEC	Total Electron Content
VLBI	Very Long Baseline Interferrometry
VTEC	VLBI Total Electron Content
VTM	Vienna Total Electron Content Model
UNB-IMT	University of New Brunswick Ionospheric Modelling Technique
ULMCAR	University of Massachusetts Lowel Center for Atmospheric Research
URSI	International Union of Radio Science
US	United States
UT	Universal Time

TABLE OF CONTENTS

LIST OF FIGURES

LIST OF TABLES

Chapter 1

INTRODUCTION

1.1 Background

The early studies of ionospheric Total Electron Content (TEC) were carried out using measurements from geostationary radio beacon satellites using the Faraday rotation technique (e.g. Garriott and Little, 1960; Garriott et al., 1965; Titheridge, 1973; Davies, 1980). Those studies were based mainly on measurements obtained either from single frequency or a ground network of instruments. Due to the declining number of special experiments on board Faraday satellites and the advent of Global Navigation Satellite Systems (GNSS) such as the Russian Global Navigation Satellite System (GLONASS) and the United States (US) Global Positioning System (GPS) in the last two decades, it became possible to use the GPS technique for a comprehensive monitoring of the ionosphere.

In particular, the current trend in ionospheric physics research has proven that the dual frequency (L1 = 1575.42 MHz and L2 = 1227.60 MHz) signals transmitted by GNSS and received by the network of Global Positioning System (GPS) receivers distributed worldwide, provide a unique opportunity to determine the higher resolution spatial and temporal ionospheric TEC at a regional and global level (e.g. Klobuchar, 1991; Komjathy and Langley, 1996; Jakowski, 1996; Komjathy, 1997; Mannucci et al. 1998). This is possible due to the dispersive nature of the ionospheric medium (Ratclife, 1959). Electromagnetic waves, such as GPS signals, experience time delays and phase advances when traversing the ionosphere due to the interaction with free electron gas. The net effect of the delay is directly proportional to the integrated free-electron density (TEC) along the signal path from the broadcasting position (~22 200 km) in space to the receiver on Earth (Lanyi and Roth,

1988; Klobuchar, 1991; Coco, 1991; Langley, 1996). The magnitude of TEC is highly variable and depends on several factors such as local time, geographical location, season and solar activity cycle (e.g. Jakowski, 1996; Jakowski et al., 1999; Jakowski, et al., 2002; Immel et al., 2003; Tsurutani, et al., 2004; Skoug et al., 2004; Jee, et al., 2005; Mannucci et al., 2005; Fedrizzi, et al., 2001). Recent studies (Jakowski et al., 2001; 2002) illustrate that TEC monitoring using the GNSS network can contribute to space weather monitoring. These studies were mainly conducted using GPS data densely distributed in the Northern Hemisphere, and are very rare over southern Africa.

On the other hand, ionospheric research over South Africa has been carried out for more than a decade using data from three Ionosondes located at Madimbo (28.28° S, 30.38° E), Grahamastown (33.32° S, 26.50° E) and Louisvale (28.51° S, 21.24° E). The area of interest has been modelling bottomside ionospheric parameters using neural networks (Willicroft and Poole, 1996; McKinnell and Poole, 2000; Poole and McKinnell, 2000; McKinnell, 2002; Oyeyemi and Poole, 2004; McKinnell and Poole, 2004; Oyeyemi, 2005; Oyeyemi et al., 2007). Recently, efforts have been undertaken to use GNSS as a new technique to monitor the dynamics and variations of the ionosphere over South Africa (Cilliers et al., 2004; Ngcobo et al., 2005; Moeketsi et al., 2007a,b; Opperman et al., 2007; Mckinnell et al., 2007). The advantage of using the GPS technique for regional modelling is that it provides high resolution temporal and spatial data coverage, and can provide detailed information on the dynamics and variations of the plasmasphere-ionospheric total electron content (Reinisch and Huang, 2001; McKinnell, 2007). This technique therefore should complement the Ionosondes over South Africa but not replace them. It is crucial to note that since the early experiments by Breit and Tuve (1926), vertical high frequency (HF) radio sounding techniques, such as Ionosondes, have provided the global ionospheric communities with a wealth of information about the physics of the upper atmospheric layers.

In this thesis, the University of New Brunswick Ionospheric Modelling Technique (UNB-IMT) (Komjathy, 1997), which applies a spatial linear approximation of the vertical TEC above each

station using stochastic parameters in Kalman filter estimation is adopted and applied to study the solar cycle effects on GNSS derived TEC over southern Africa. The UNB-IMT Unix compatible version was developed in 1997, by the Department of Geodesy and Geomatics Engineering at the University of New Bruwnswick (UNB) Canada, to compute global and regional TEC from GNSS data mainly distributed in the Northern Hemisphere in order to provide ionospheric corrections to communications, surveillance and navigation systems operating at a single frequency (Komjathy and Langley, 1996; Komjathy, 1997; Komjathy et al., 1998). Recently, Fedrizzi et al. (2005) also used the same model to study TEC variability associated with geomagnetic storm activity over locations in the South American sector.

However, efforts were undertaken by the Space Geodesy Group of the Hartebeesthoek Radio Astronomy Observatory (HartRAO) to modify the Unix version of the UNB model to compile on a Linux platform for the purpose of this work, to be used for the application in ionospheric research and future high frequency radio communication over southern Africa. Extracts of this work have been published in Ngcobo et al. (2005) and Moeketsi et al. (2007a,b). The current data available from HartRAO, the International GNSS Service (IGS) and the Chief Directorate Surveys and Mapping (CDSM) Trignet network of dual frequency GPS receivers distributed over southern Africa make this study possible (Combrinck et al., 2003; Cilliers et al., 2003; Combrink, 2006).

1.2 Aim and Structure of Thesis

The main aim of the thesis is:

- To investigate effects of solar activity such as solar flares, and geomagnetic storm activity on GNSS-derived ionospheric TEC over southern Africa during different periods of solar cycle 23.

- To validate UNB-IMT with ionosonde TEC measurements over South Africa during different periods of solar cycle 23 using more regional GPS data sets, so that it can be verified and adopted as one of the tools for ionospheric research in this region.
- To investigate the capabilities of the TEC derived from the geodetic Very Long Baseline Interferometer (VLBI) technique using the Vienna TEC Model (Hobiger et al., 2006; Hobiger, 2007; *private communication*) over HartRAO for space weather monitoring over South Africa using the UNB-IMT TEC results.

The structure of the thesis follows:

An introduction to the Sun and its activity cycle, Earth's ionosphere and its structure, ionospheric perturbations, solar terrestrial indices, and basic theory of ionospheric effects on propagation of electromagnetic waves is presented in **Chapter 2**, along with all related major concepts and definitions used in this study. The South African Ionosondes, and satellite missions such as GNSS, Global Earth Observation Satellite (GOES) and Solar Heliospheric Observatory (SOHO) instruments and sensors are also briefly described which provide data used for processing, analysis, validations and investigations in this study.

Chapter 3 gives a detailed description of the Ionospheric TEC Model used in this study (Komjathy, 1997). It starts with a concise history of ionospheric TEC modelling techniques with the main emphasis on regional models using the GNSS technique and describes the UNB-IMT model and its modification for application over South Africa region. A brief description of the International Reference Ionosphere (IRI) 2001 model (Bilitza, 2001), also used in this work is presented. Extracts from this chapter have been published in Ngcobo et al. (2005) and Moeketsi et al. (2007a,b).

Validation of UNB-IMT with Ionosonde TEC measurements over South Africa during different periods of the solar cycle is described in **Chapter 4**. In particular, a comparison of GNSS TEC

(GTEC) computed using UNB-IMT with Ionosonde TEC (ITEC) derived from ionogram measurements using techniques described in Reinisch and Huang (2001). The corresponding vertical equivalent slap-thickness parameter is computed. This is important for characterizing the width of the electron density profile and contributes to the study of the dynamic forces that can change the profile shape, especially under perturbed conditions. Consequently, the residual GTEC – VTEC is computed, which correspond to plasmaspheric electron content and is further discussed to understand its contribution to the TEC over South Africa.

After verifying UNB-IMT as a tool for ionospheric studies over South Africa in the preceding Chapter, it is then applied in **Chapter 5** for mapping TEC during different epochs of solar cycle 23. The results are discussed and further investigated by analyzing the GOES X-ray flux (0.1 – 0.8 nm) and SOHO Charge, Element and Isotope Analysis/Solar Extreme Ultraviolet Monitor (CELIAS/SEM) 26.0 – 24.0 nm higher resolution data (e.g. Judge et al., 1998). GTEC is compared comprehensively with IRI 2001 model predictions (Bilitza, 2001). The effects of particular solar X-ray flares over HartRAO on collocated GNSS receivers are also illustrated. Extracts from this work have been published in Moeketsi et al. (2007a,b).

In **Chapter 6**, TEC derived from the geodetic VLBI technique using the Vienna TEC Model (Hobiger et al., 2006; Hobiger, 2007; *private communication*) is investigated for space weather monitoring using UNB-IMT TEC results for a year 2002 near solar maximum for different months of the season and a year 2005 near solar minimum during CONT02 and CONT05, respectively. The current shortcomings of geodetic VLBI in providing near real-time ionospheric parameters are discussed and recommendations are made related to VLBI2010.

Chapter 7 presents a summary, conclusions and recommendations for future work based on the outcome of this work. This chapter highlights the contribution of the thesis to ionospheric research;

in particular in providing capabilities for future near real-time space weather monitoring over South Africa using space geodetic techniques.

Chapter 2

THE SUN, EARTH`S IONOSPHERE AND SATELLITE MISSIONS

2.1 Introduction

This chapter presents theoretical background on the Sun and its activity cycle, the Earth's ionosphere and its structure and effects on the propagation of electromagnetic waves such as GNSS signals, which are important for this work. A brief description of the operation of ground based Ionosondes as a tool for ionospheric research is also presented. Furthermore, important satellite missions such as the GNSS constellations, SOHO Charge, Element and Isotope Analysis System/Solar Extreme Ultraviolet Monitor (CELIAS/SEM) sensor and GOES Solar Environment Monitor (SEM) are briefly described as related to this work.

2.2 The Sun, solar cycle and Earth`s magnetic field

Our nearest star, the Sun located at an average distance of 1 AU (1AU = $1,49\times10^{8}$ km) from the planet Earth, is a middle aged, main sequence star. Its surface is not solid but a spherical plasmatic gas with radius of about 0.005 AU and has a differential rotation period which increases in latitude from an average value of ~ 25 days at the equator to ~ 32 days near the polar region. The Sun is mainly composed of Hydrogen (~90%) and Helium (~10%) with signatures of other heavy elements. The light of the Sun comes from the photosphere, which has a temperature of about 5800 K (Kelvin). Around this lies a region of hot gas, the chromosphere, visible during solar eclipses, and it extends $\sim10^{3}$ km from the photosphere. Above that there is a tenuous and even hotter layer, the corona that extends 10^{6} km out into space from the chromosphere.

The visible dark areas of irregular shape on the photosphere that are cooler than the entire solar surface are called sunspots. Detailed records of the sunspot number, which is a direct indication of the level of solar activity have been kept since 1749 and are shown in Figure 2.1 up to September 2007. From these monthly averaged values, it is evident that the Sun has a quasi-periodic ~11 year solar cycle. Approximately every 11 years the Sun moves through a period of fewer and smaller sunspots termed solar minimum, followed by a period of larger and more sunspots termed solar maximum (e.g. Smith and Marsden, 2003; Moeketsi, 2004). Solar activity such as solar flares and Coronal Mass Ejections (CMEs) occur more frequently around solar maximum.

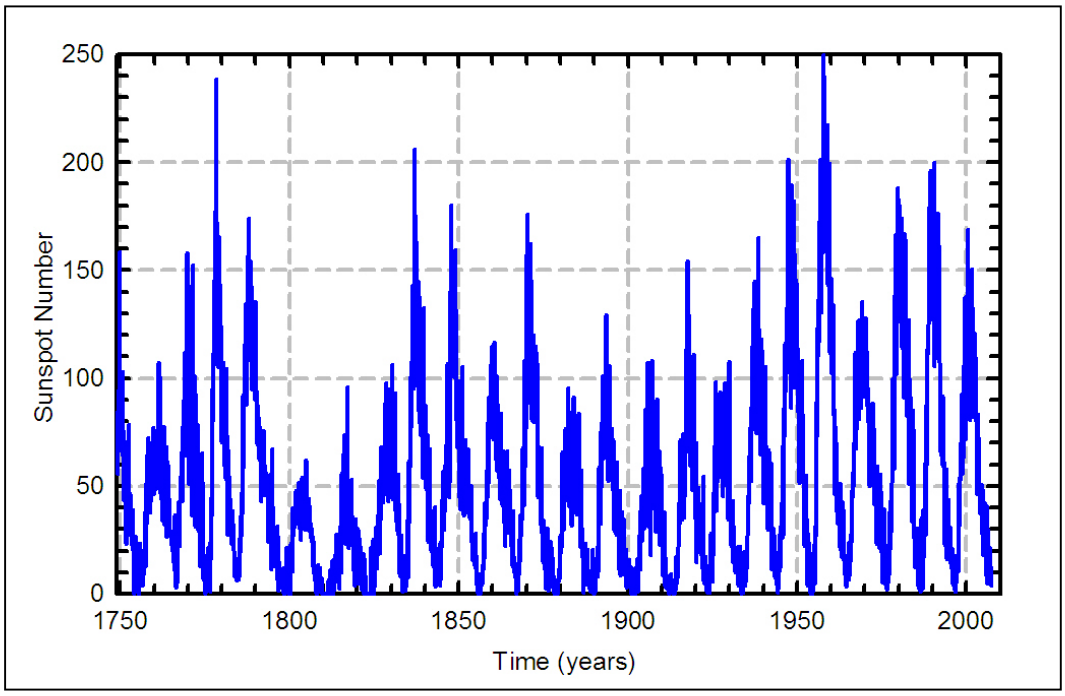

Figure 2.1: Monthly averaged sunspot number from the year 1749 up to the end of August 2007 (data from http://www.spaceweather.com).

The plasmatic atmosphere of the Sun constantly blows away from its surface to maintain equilibrium (Parker, 1958; 1963). This occurs because the temperatures in the corona are so high

that the solar material is not gravitationally bound to the Sun. The escaping hot coronal plasma from the Sun is termed the solar wind (Biermann, 1961). The solar wind will carry the solar magnetic field into interplanetary space, forming the Heliospheric Magnetic Field (HMF), which is mostly responsible for heliospheric modulation of cosmic radiation and can cause terrestrial geomagnetic disturbances.

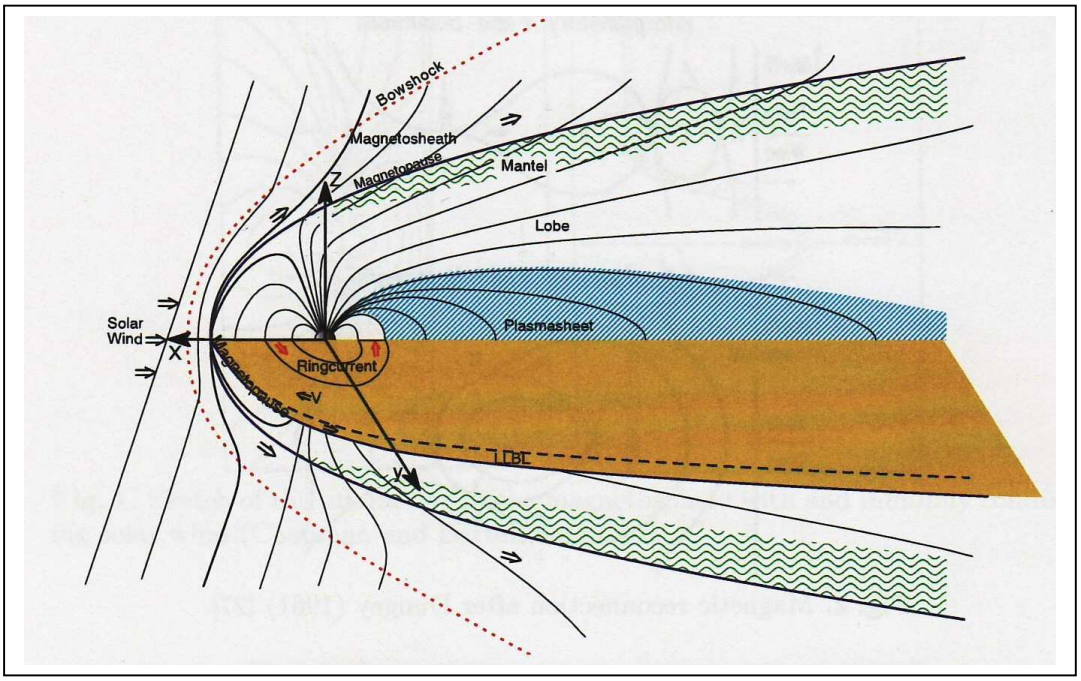

Figure 2.2: The solar wind interaction with the Earth's magnetosphere (Otto, 2005).

The radial blowing solar wind interacts with the Earth's geomagnetic field known as the magnetosphere, compresses the dayside portion and generates a tail as depicted in Figure 2.2. The magnetosphere is a large plasma cavity dominated by the Earth's magnetic field and solar wind plasma (Otto, 2005). On the other hand, the Sun also emits background electromagnetic radiation in the Extreme Ultraviolet and X-ray spectrum, which does not interact directly with the Earth's magnetic field, and therefore penetrates the magnetosphere, getting absorbed into the lower part of the atmosphere. Nevertheless, the Earth's magnetic field plays an important role in the formation of

the ionised region of the upper atmosphere, which will be discussed in the next section. This emphasises the importance of using geomagnetic coordinates to describe and model the ionised upper atmospheric region (Komjathy, 1997).

The first approximation to the Earth's magnetic field is that of a sphere, uniformly magnetised in the direction of the centered dipole axis. This axis cuts the surface of the Earth at a point known as austral (south) and boreal (north) dipoles. The intersection between the plane through the Earth's center perpendicular to the dipole axis and the Earth`s surface is called the geomagnetic equator. However, the dip latitude is often used to describe the Earth's magnetic field. In such scenarios, the poles are referred to as dip poles, i.e. locations where the geomagnetic field is vertical to the Earth surface, and the dip equator is where the geomagnetic field is horizontal. Detailed descriptions of the Earth's magnetic field, and relationships between geographic, geomagnetic, and dip latitudes have been given by Tascione (1988), McNamara (1994), and Davies (1990).

2.3 The Earth's Ionosphere

The partially-ionised region of the Earth's upper atmosphere, which extends from ~50 km above the surface of the Earth to ~1000 km, is called the ionosphere. Sir Robert Watson-Watt first coined the term ionosphere in 1926, in a letter to the secretary of the British Radio Research Board. The expression came into wide use during the period 1932-1934 by Watson-Watt, Appleton, Ratcliffe and others. Before the term ionosphere gained worldwide acceptance, it was called the Kennedy-Heaviside layer, or the upper conducting layer (Hunsucker, 1991).

The ionosphere is mainly formed by the interaction of solar X-ray and EUV ionizing radiation with neutral atmospheric constituents. Cosmic radiation also contributes to the formation of the ionosphere, but to a lesser extent. However, the incident solar radiation's energetic photons interact with neutral atoms and molecules in the upper atmosphere, giving the outer electron of such neutral species enough energy to escape the attraction of the positively charged nucleus. Thus a positively

charged ion is created, and the negatively charged electron becomes free. This process is called photoionisation. The reverse process occurs when the ions and electrons combine to form neutral atoms. This phenomenon is known as recombination. The detailed explanations of these processes can be found in McNamara (1991) and Davies (1990).

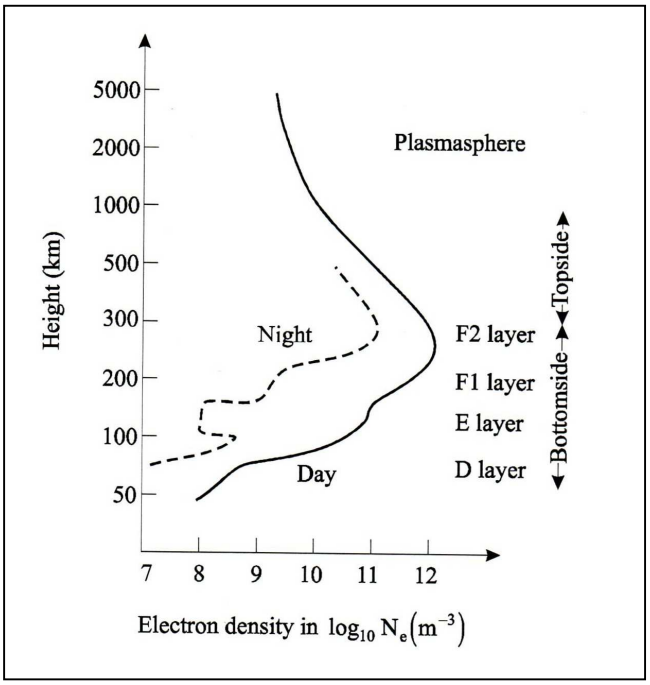

Figure 2.3: Typical vertical profile of the ionosphere adopted from Davies (1990) and Komjathy (1997).

Above the upper boundary of the ionosphere there is a region termed the plasmasphere, in which the density of neutral atoms are small and where the positive ions are predominantly protons, hence sometimes this region is termed the protonsphere. At an altitude of ~ 40 000 km the plasmasphere decays out to the plasmapause and the electron densities of the plasmasphere drops significantly to an order of ~2 magnitudes (Davies, 1990). The shape and density of the plasmasphere is constantly changing primarily due to changes in the underlying ionosphere and geomagnetic disturbances (Webb and Essex, 2002). During quiet times, the density of plasmaspheric constituents drops rapidly to geocentric distances (Carpenter, 1970; Huang et al., 2003). However, during periods of high solar

activity, plasmaspheric tails are formed that extend away down to the ionosphere, affecting Earth communication (Forster and Jakowski, 2000).

Due to the different molecules and atoms in the atmosphere and their differing rates of absorption, a series of distinct regions or layers of electrons exist. These are denoted by letters D, E, F1, F2 and are usually referred to as the bottom side ionosphere as shown in Figure 2.3. The portion of the upper atmosphere between the F2 layer and the upper boundary is termed the topside ionosphere. It is in the F2 layer where the maximum electron density usually occurs as a result of the combined effect of solar EUV radiation and the increase of neutral atmospheric density as the altitude decreases.

The maximum frequency at which a radio wave would be reflected from an ionospheric layer is called the critical plasma frequency of the particular layer and is denoted by foD, foE, foF1, and foF2 according to the designation of the ionospheric layer. The square of a critical frequency is linearly proportional to the maximum electron density of the individual layer, denoted by NmD, NmE, NmF1 and NmF2 respectively. The changes in foD, foE and foF1 are in phase with solar variation and foF2 is in anti-phase (Komjathy, 1997). The existence of the D, E, and F1 layers seems to be primarily controlled by the solar zenith angle showing a strong diurnal, seasonal and latitudinal variation. The diurnal variation of the D, E, and F1 layers also implies that they tend to vanish or greatly reduce in size at night. The F1 layer disappears in winter when the solar zenith angle is higher than in summer, at which the F1 layer is consistently present. The critical frequency of the layers follows the 11-year solar cycle variation caused by the change in the intensity of solar radiation. A brief description of individual ionospheric layers is given below. For further information the reader is referred to Davies (1990), McNamara (1990) and Stubbe (1996).

2.3.1 The D layer

The D layer is the lowest portion of the ionosphere, extending in height from ~50 to ~90 km above the Earth's surface. The primary source of ionization in this layer is cosmic rays (Davies, 1990; Stubbe, 1996), which manifest in a solar cycle variation in the D layer's electron density. During nighttime, the electrons may become attached to atoms and molecules, forming negative ions that cause the D layer to disappear. During daytime, as a result of background solar radiation, photoionization occurs causing the recovery of the D layer electron densities. In principle, the electron density in the D region increases monotonically with altitude, and a typical daytime electron number density at 90 km is ~ 10^{10} m^{-3}. The uppermost D layer region – above 80 km is mainly dominated by NO^+ and O_2^+ ions, whereas in the lower region complex positively charged water cluster ions, and also negative ions, play a significant role. The latter is often referred to as the C layer (Davies, 1990).

2.3.2 The E layer

The ionosphere in the altitude range from about 90 km to about 140 km is termed the E region, which has a typical peak electron density of ~ 10^{11} m^{-3} occurring at an altitude of approximately 105 km. The E region is characterized by molecular ions and chemical processes and the reaction between charged particles are not important. The primary source of ionization is solar X-ray emission, resulting in electron densities showing distinct solar cycle, seasonal and diurnal variation. In particular, the molecular N_2^+ and O_2^+ ions are the primary ionization products of photoionisation of N_2 and O_2. Most of the N_2^+ ions are lost in rapid secondary reactions with atomic and molecular oxygen. As a result, O_2^+ and NO^+ are the main molecular ions. Furthermore, most of O_2^+ ions react with N_2 to form NO and NO^+, rather than dissociatively recombining with electrons. As a consequence, the NO^+ leads to neutralization (Stubbe, 1996; Shetti, 2006).

2.4.3 The F layer

The ionosphere above the E region, beginning at ~140 km, is termed the F region. The main source of ionization in this region is the solar EUV radiation. At altitudes below ~180 km, the dominant ions are NO^+ and O_2^+. The behaviour is described by photochemical equilibrium, as in the E region. Above ~180 km, O^+ becomes the dominant ion. A typical altitude range for the F region peak electron density is from about 300 km to about 400 km, depending on the level of solar activity, and a representative daytime maximum electron density value is ~ 10^{12} m^{-3}. The F region ends by definition were O_2^+ ceases to be and H^+ ions begin to be the dominant ion species. The upper boundary of the F region thereby becomes the lower boundary of the plasmasphere.

However, the F region can split into two layers, namely F1 and F2 respectively, depending on the local time and geographical location. In particular, the F1 is mainly observed during the day since the electron densities are controlled by the zenith angle of the sun. When this layer is present, it can change rapidly within minutes. It is more pronounced during the summer than the winter season for low solar activity and for periods of ionospheric perturbations. On the other hand, the F2 layer is the most important for the propagation of HF radio waves. The F2 layer does not follow the zenith angle dependence. The winter anomaly occurs during the daytime only which is thought to be due to the large summer electron loss caused by the increased molecular to atomic composition of the neutral atmosphere. In summer, foF2 shows a less pronounced diurnal variation. The global spatial distribution of foF2 reveals a strong geomagnetic and solar cycle dependence.

2.3.4 Major geographic regions of the ionosphere

In principle, there are three major geographical regions of the ionosphere: the high latitude, mid-latitude, and equatorial regions. In this section, the main characteristics of each region illustrated in Figure 2.4 are briefly described (Komjathy, 1997).

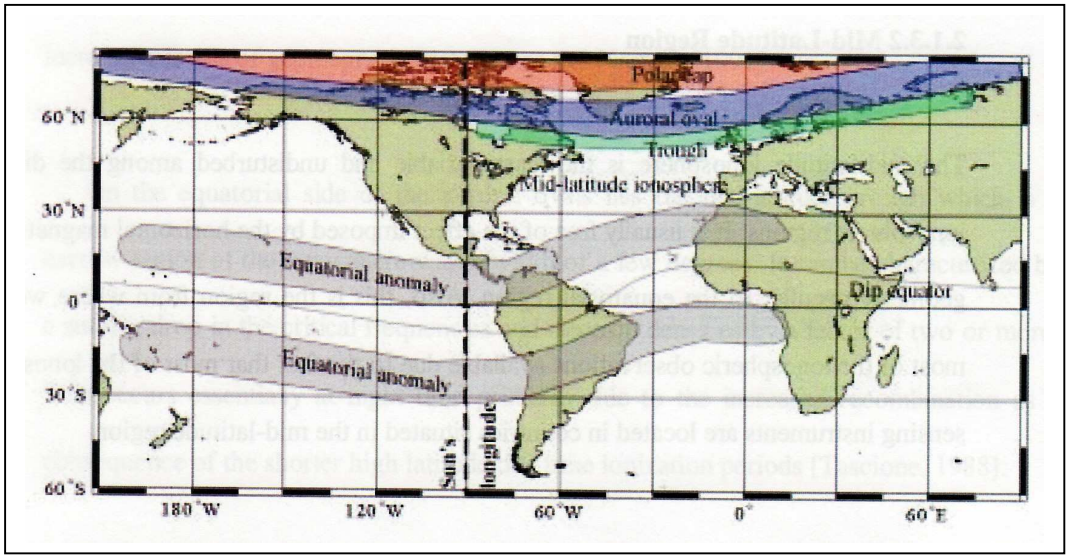

Figure 2.4: Major geographic regions of the ionosphere (e.g. Komjathy, 1997)

2.3.4.1 The equatorial region

The equatorial region is sometimes referred to as the low-latitude zone, spans ~20° to ~30° either side of the magnetic equator, and is strongly influenced by electromagnetic forces that arise due to the geomagnetic field which runs horizontally over the magnetic equator. This region can be characterized as having the highest values of peak electron density with the most pronounced amplitude and phase scintillation effects. In particular, the combined effect of the high intensity of radiation from the Sun, the electric and magnetic fields of the Earth results in the electrons rising and moving along the horizontal magnetic field lines. This phenomenon is known as the fountain effect. The electrons move as far as geomagnetic latitude of about 10° to 20° causing a high concentration of electrons, which are often termed ionospheric equatorial anomalies (IEA).

2.3.4.2 The mid-latitude region

The mid-latitude region is the least variable and undisturbed among ionospheric regions. However, it is mainly influenced by energetic solar EUV and X-ray radiation, which results in ionization of the daytime ionosphere. During the nighttime ionization is overwhelmed by chemical recombination processes, which may involve the neutral atmosphere as well as ionized species. However, their

movement of ions, and the balance between the production and loss, are affected by thermospheric winds. Most ionospheric observations are done over this region because most of the ionospheric sensing instruments are located in countries situated in the mid-latitude (Komjathy, 1997)

2.3.4.3 The high latitude region

At high latitudes, the geomagnetic field lines run nearly vertical, leading to the existence of an ionosphere that is considerably more complex than that in either the middle or the low-latitude regions. Besides photoionisation, collisional ionisation is another source of ionisation in the high latitude region. This is due to the fact that the magnetic field lines connect the high latitudes to the outer part of the magnetosphere, which essentially leads to the charged particles descending to E layer altitudes. These particles can collide with neutral atmospheric gases, causing local enhancements of electron densities, a phenomenon associated with auroral activity. Auroral activity can be regarded as the interaction between the magnetosphere, ionosphere and atmosphere. Typically auroral zones are relatively narrow rings situated in high southern and northern geomagnetic latitudes. In general, the intensity of the position of the auroral oval has a linkage with the magnetosphere and is related to geomagnetic perturbations (McNamara, 1991). The auroral regions are particularly complex for radio propagation.

On the equatorial side of the auroral oval lies the mid-latitude trough of lesser ionization. It is a narrow region of the ionosphere with a width of a few degrees. It can be characterised by a sudden drop in the critical frequencies and electron densities by a factor of two or one. However, this occurs at nighttime primarily due to increased recombination as a consequence of the shorter high latitude daytime ionisation periods (Tascione, 1988).

The direct interaction between the interplanetary magnetic field and the Earth's magnetosphere results in the dayside cusp or cleft. It is typically 2° to 4° wide and located at the geomagnetic

latitude of 78° to 80° near local noon. The phenomenon is characterized by an enhancement in electron densities at all altitudes.

The geographical regions enclosed by auroral rings are called the polar caps. The polar caps are severely affected by solar flares and coronal mass ejections causing D region electron enhancements.

2.4 Ionospheric perturbations

Ionospheric perturbations are mainly triggered by solar activity such as solar flares and coronal mass ejections, which have impinged on the terrestrial magnetosphere-ionosphere system. These events affect the outermost geomagnetic field lines and compress the geomagnetic field causing geomagnetic disturbances (e.g. Otto, 2005).

2.4.1 Ionospheric storms

Ionospheric storms can be caused by clouds of ionised gas ejected from the Sun during solar flares. However, electromagnetic radiation such as X-rays produced during the flare, can penetrate as far as the D-region causing a phenomenon known as short-wave fadeout. The energetic particles also produced during the flares can hit the Earth's magnetosphere, causing ionospheric storms. This can manifest itself as sudden, unpredictable changes in ionospheric parameters, such as foF2, and electron concentrations. Whether these parameters are increased or decreased will depend on the time of the day, the season, and geographical location when the plasma cloud hit the Earth, as well as the magnitude of the storm.

Ionospheric storms can also be caused by a high speed solar wind stream (HSSWS), which emanates from coronal holes. The Sun's magnetic field lines stretch into the interplanetary medium forming what is known as a heliospheric magnetic field (HMF) (Parker, 1963). The HMF makes it possible for ionized material such as solar wind particles to travel along the field lines by a diffusion process

and eventually reach the Earth. The effect of HSSWS on the ionosphere is usually not as devastating as those of a large solar flare. This happens because the HSSWS does not overtake the Earth as fast as the ionized cloud from solar flares (e.g. Komjathy, 1997; Shetti, 2006).

Sudden disappearing filaments on the solar surface could also cause ionospheric storms. They are a large, relatively cool structure on the solar surface potentially blowing out magnetised plasma into interplanetary space, affecting the Earth's geomagnetic field (Tascione, 1988; McNamara, 1991; Komjathy, 1997).

2.4.2 Geomagnetic storms

Geomagnetic storms result from a major disturbance of the magnetosphere that occurs when the HMF turns southward and remains southward for a prolonged period of time. Geomagnetic storms occur in conjunction with ionospheric storms and can be caused by solar flares, HSSWS and sudden disappearing filaments. A geomagnetic storm usually starts with an increase in the intensity of the Earth's geomagnetic field (the initial phase), followed by a large decrease termed the main phase, and finally the recovery phase with possible sub-storms. These result in a significant variation in electron density in the ionosphere, and a simultaneous increase in absorption of radio waves. However, a solar flare initiated geomagnetic storm usually starts with the sudden commencement as an initial phase. On the other hand, a high speed solar wind induced geomagnetic storm is expected to start with a gradual commencement with storms tending to reoccur every 27 days as a result of solar rotation (McNamara, 1991; Tascione, 1988).

2.4.3 Ionospheric scintillations

The small-scale structures in the electron content of the ionosphere can range from a few meters to a few kilometers, which can cause both refraction and diffraction of electromagnetic waves propagating through the ionosphere. In particular, diffraction is associated with the bending of electromagnetic waves, which takes place when the wave front moves obliquely across to media

with different propagation velocities. However, bending can also take place when electromagnetic waves pass by an obstacle such as a localised ionospheric perturbation. As a consequence of refraction, the wave front becomes crinkled, giving rise to amplitude and phase fluctuations of the signal. These fluctuations caused by small scales plasma density irregularities, are termed ionospheric scintillation (Wanninger, 1993). The phase scintillations are rapid changes in signal phase that can be attributed to rapid but very small changes in the ionospheric electron content. A change of 1 radian in phase is required at 1.5 GHz to cause problems for the GNSS receivers' tracking loop (Langley, 1996; Komjathy, 1997).

2.5 Solar Terrestrial Indices

Most of the solar-terrestrial empirical and physics-based models require geomagnetic indices to specify the solar and geomagnetic level. These indices are usually parameters that can be monitored continuously with ground-based equipment or that can be derived from continuously monitored parameters. The DST, Kp and Ap indices are the most commonly used indices and are briefly described as follows:

2.5.1 The DST index

The DST is a geomagnetic index (Sugiura, 1964), which indicates the severity of a geomagnetic storm and the development of the ring current. It is constructed by averaging the horizontal component of the geomagnetic field from mid-latitude and equatorial magneto-grams from the worldwide network of magnetometers. However, the negative DST values indicate a magnetic storm in progress, even more negative DST values indicate a more intense magnetic storm. The negative reflections in the DST are caused by the storm time ring current, which flows around the Earth from east to west in the equatorial plane. The ring current results from differential gradient and curvature drift of electrons and protons in the near Earth region, and its strength is coupled to the solar wind conditions. This happens when there is an electric field, due to magnetospheric convections resulting from the interconnection between the southward interplanetary magnetic field and the geomagnetic

fields. Through understanding the solar wind conditions and the form of coupling functions between the solar wind and ring current, an estimate of the DST index can be made. The DST index is used during investigations in Chapter 4, 5 and 6.

2.5.2 The Kp, and Ap indices

The Kp (planetarische Kennziffer) index (Bartels et al., 1939), for each 3 hour period of every Universal Time (UT) day, is a measure of variations in the Cartesian components of the Earth's magnetic field (x, y, z). These irregular variations are associated with geomagnetic field disturbances measured in gammas (nano Tesla). The range R between the largest and the smallest of the three geomagnetic field components, measured in gammas is used to define a particular K. About thirteen observatories which lie between 46° and 63° north and south geomagnetic latitude determine their own integer K, ranging from 0 to 9 for each 3 hour period of the day based on the measured ranges in the geomagnetic field components. A particular K scale is adopted for each observatory but the scale differs from one observatory to another. The highest values for R is about 500 gammas at a typical midlatitude station and about 2000 gammas for a station at the auroral zone. The planetary 3 hour index Kp is designed to give a global measure of geomagnetic activity and is computed as an arithmetic mean of the K values calculated at the thirteen observatories. The Kp index has 28 steps from zero (quiet) to 9 (highly disturbed) with fractional parts expressed in a third of a unit (see also Komjathy, 1997).

Equivalent planetary amplitude index "ap" of geomagnetic field variation is derived from Kp values. The Ap index is defined as the earliest occurring maximum 24 hour value obtained by computing an 8-point running average of successive 3 hour ap indices during a geomagnetic storm event without regard to the starting and ending times of the day. These indices are not used in this study, but are of importance to the space physics community. More information about these indices can be found at http://www.ngdc.noaa.gov.

2.6 Ionospheric effects on propagation of electromagnetic waves

The theory of propagation of electromagnetic waves through a partially-ionised medium such as the ionosphere is well described in the literature (e.g. Ratcliffe, 1959; Davies, 1966; 1990). In most literature, the derivation of the complex index of the ionosphere as a magneto-ionic medium is mainly associated with Sir Edward Appleton who first pointed out that plane polarized waves will split into two opposite rotating circularly polarized waves when entering a magnetized plasma (Hunsucker, 1991). In 1931, Hartree suggested inclusion of the Lorenz polarization term, after which the complex index was often referred to as the Appleton-Hartree formula (Komjathy, 1997). The detailed derivation of the formula can be found in Davies (1966; 1990). The first approach in deriving the latter is to invoke Maxwell's wave equation and to apply the properties of the medium (see review by Combrink et al., 2004).

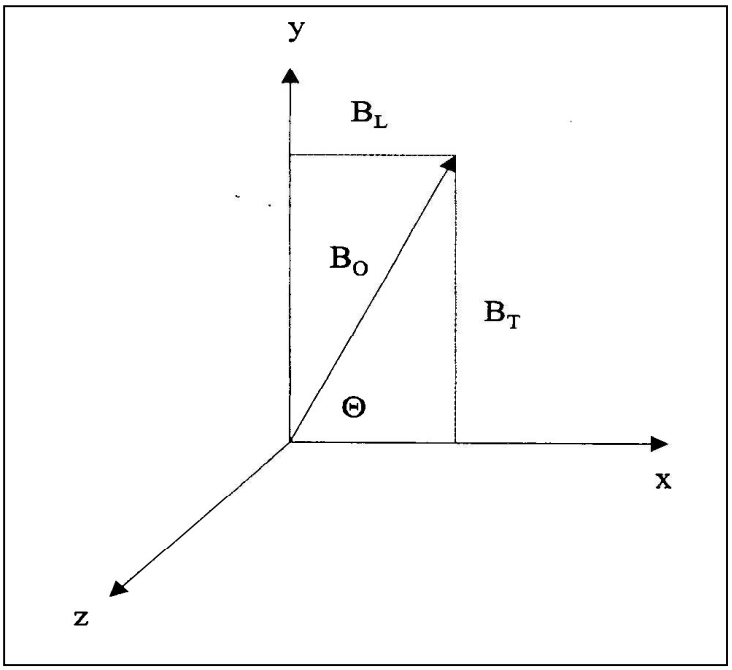

Figure 2.5: System of orthogonal axis x, y, and z after Davies (1990).

The Appleton-Hartree magneto-ionic theory applies to a medium that is electrically neutral with no resultant space charge, and an equal number of electrons and positive ions upon which a uniform magnetic field is imposed. The ion content is not of direct consequence to electromagnetic wave propagation, since the relative size of the ion means that it will not be excited by passing energy of this level to any significant extent (e.g. Steward, 1997). The electron density encountered by the signal is of importance to this study.

2.6.1 Phase refractive index

At radio wave frequencies, the ionosphere may be regarded as a dispersive medium (Ratcliffe, 1957). That is, the refractive index is a function of the radio wave frequency, the electron density, and to some lesser extent, the intensity of the Earth's magnetic field. In order to derive the phase refractive index, let us consider a plane polarized electromagnetic wave traveling in the x direction of the orthogonal coordinate system depicted in Figure 2.5. Let us also consider a uniform magnetic field that lies in the x-y plane and which makes an angle Θ with the direction of propagation. The complex refraction index n is given by the Appleton-Hartree magnetoionic dispersion equation (Langley, 1996; Davies 1966; 1990; Hunsucker, 1991):

$$n^2 = 1 - \frac{X}{(1 - jZ) - \left[\frac{Y_T^2}{2(1 - X - jZ)}\right] \pm \left[\frac{Y_T^4}{4(1 - X - jZ)^2} + Y_L^2\right]^{1/2}} \tag{2.1}$$

where n is the complex refractive index $(\mu - j\chi)$ with μ the real part and χ the imaginary part. The values of X, Y, and Z are dimensionless, defined as:

$$X = \frac{\omega_N^2}{\omega^2} = \frac{f_N^2}{f^2}, \tag{2.2}$$

$$Y = \frac{\omega_H}{\omega} = \frac{f_H}{f}, \tag{2.3}$$

$$Y_L = \frac{\omega_L}{\omega},\ Y_T = \frac{\omega_T}{\omega}, \tag{2.4}$$

$$Z = \frac{\omega_C}{\omega}, \tag{2.5}$$

where ω (radian.s^{-1}) is the angular frequency of the propagated electromagnetic wave $f\left(\mathrm{Hz}\right)$, and ω_c(radian.s^{-1}) is the angular collision frequency between electrons and heavier particles. Furthermore, ω_N is the angular plasma frequency with $\omega_N^2 = \frac{Ne^2}{\varepsilon_0 m}$ with N the electron density (m^{-3}), electron charge e (1.6×10^{-19} Coulomb), permittivity constant of free space ε_0 (8.8542×10^{-12} farad.s^{-1}) and electron mass m (9.1095×10^{-31}kg). Here ω_H is the angular frequency expressed as $\omega_H = \frac{B_0|e|}{m}$ (radian.s^{-1}) with electromagnetic field strength B_0 (Wb.m^{-2}). However, ω_L is the longitudinal angular frequency given by $\omega_L = \frac{B_0|e|}{m}\cos\Theta$ (radian.s^{-1}), and ω_T is the transverse angular frequency given by $\omega_T = \frac{B_0|e|}{m}\sin\Theta$ (radian.s^{-1}), respectively.

When collisions are negligible (i.e. $Z = 0$), the equation (2.1) takes the form:

$$n^2 \cong \mu^2 = 1 - \frac{2X\left(1-X\right)}{2\left(1-X\right) - Y_T^2 \pm \left[Y_T^4 + 4\left(1-X\right)^2 Y_L^2\right]^{1/2}}. \tag{2.6}$$

According to magneto-ionic theory, a plane polarized electromagnetic wave will split into two characteristic waves: that is, an ordinary wave which approximates the behaviour of a wave propagating without an imposed magnetic field displayed with a sign "+" in equation (2.6), and the wave with the sign "-" is called an extraordinary wave.

The expansion of equation (2.6) into a series up to the 4th inverse power of frequency $\left(1/f^4\right)$ according to Bassiri and Hajj (1993) and Brunner and Gu (1991) yields:

$$n \cong 1 - \frac{1}{2}X \pm \frac{1}{2}XY\left|\cos\Theta\right| - \frac{1}{8}X^2 - \frac{1}{4}XY^2\left(1+\cos^2\Theta\right), \tag{2.7}$$

where it is evident that the 2nd and the 4th terms are functions of the maximum electron density and frequency, whereas the 3rd and 5th are a function of the maximum electron density, the Earth `s magnetic field strength and the frequency. However, Komjathy (1997) showed that the contribution of the 3rd, 4th and 5th terms to the error budget of the determination of the refractive index are 3, 5, and 6 orders of magnitude less than the second term when assuming $\Theta = 0,$ and the typical values for F2 layer maximum electron density ($N = 10^{12}$ m^{-3}) and typical value for the Earth's magnetic field strength ($B_0 = 5.0 \times 10^{-5}$ $Wb.m^{-2}$) respectively.

When both collisions and the magnetic field are negligible, only the 1st and 2nd terms in equation (2.7) are considered. However, to enable calculating the phase refractive index of the ionosphere, appropriate for the carrier phase observations, we obtain:

$$n_\varphi \cong 1 - \frac{40.3 \cdot N}{f^2}. \tag{2.8}$$

2.6.2 Group refractive index

According to Langley (1996), the group refractive index is defined as:

$$n_g = n + f\frac{dn}{df}. \tag{2.9}$$

By invoking the value of phase refractive index $n = n_\varphi$ in equation (2.8),

$$\begin{aligned} \frac{dn}{df} = \frac{dn_g}{df} &= \frac{d}{df}\left(1 - \frac{40.3 \cdot N}{f^2}\right), \\ &= -40.3 \cdot N \frac{d}{df}\left(\frac{1}{f^2}\right), \\ &= 2(-40.3 \cdot N)\left(\frac{1}{f^3}\right), \end{aligned} \tag{2.10}$$

and therefore the equation (2.9) takes the form:

$$n_g = 1 - \frac{40.3 \cdot N}{f^2} + 2\frac{40.3 \cdot N}{f^2} = 1 + \frac{40.3 \cdot N}{f^2}, \tag{2.11}$$

which is the group refractive index (see also Stewart, 1997).

2.6.3 Ionospheric group delay and phase advance

Since the ionosphere is a dispersive medium, it exerts significant influence on the propagation of electromagnetic waves such as GNSS signals. In particular, the signal experiences a time delay and phase advance when traversing the ionosphere due to the interaction with free electrons. By integrating equation (2.8) and (2.11) along the line of sight of the signal, the ionospheric delay is obtained as:

$$d_{ion} \cong \pm 40.3 \cdot \frac{TEC}{f^2}, \tag{2.12}$$

where TEC is the Total Electron Content in TEC Units (TECU=10^6 electrons.m^{-2}) along the signal path. The sign "+" in equation (2.12) indicates that the modulated code range shows a delay in time of reception and hence an increase in the apparent range and is referred to as group delay, whereas "-" indicates that the phase measurements are shorter than the true range and thus it is advanced by an amount controlled by the signal frequency and electron density, and this is termed phase advance.

2.6.3.1 Phase and group velocity

By invoking equation (2.8), it follows that the phase velocity v_P (m.s^{-1}) is given by:

$$v_p = \frac{c}{n_\varphi} \cong \frac{c}{1 - \frac{40.3 \cdot N}{f^2}} \cong c \cdot \left(1 + \frac{40.3 \cdot N}{f^2}\right), \tag{2.13}$$

where c is the speed of light in free space (3.0×10^8 m.s^{-1}). By applying a similar approach using equation (2.11), the group velocity is given by:

$$v_g = \frac{c}{n_g} \cong \frac{c}{1 + \frac{40.3 \cdot N}{f^2}} \cong c \cdot \left(1 - \frac{40.3 \cdot N}{f^2}\right). \tag{2.14}$$

Using equation (2.8), the vertical incident reflection which take place when $n = 0$ is defined as:

$$1 - \left(\frac{f_N^2}{f^2} \right) = 0, \tag{2.15}$$

where f_N (Hz) is the plasma frequency at which a slab of neutral plasma with density N naturally oscillates after the electrons have been displaced from the ions and are allowed to move freely. However, f_N can also be expressed as:

$$f_N^2 = \frac{Ne^2}{4\pi^2 \varepsilon_0 m}, \tag{2.16}$$

where the parameter terms are as defined in Section 2.6.1. However, a condition for a wave to be reflected at vertical incidence is $f = f_N$ (Hundsucker, 1991). The electron density is related to frequency by the expression:

$$N / \mathrm{m}^{-3} = 1.24 \times 10^{10} \left(f / \mathrm{MHz} \right)^2 . \tag{2.17}$$

2.7. Ground based Ionosonde

An ionosonde or ionospheric sounder is a ground based instrument which operates by transmitting HF radio waves, sweeping from a low (~1 MHz) to high (~30 MHz) frequency, to measure the time required for the signal to travel and return from a refracting ionospheric layer (Breid and Tuve, 1926). Since radio waves travel more slowly in the ionosphere than in free space, the virtual height is recorded instead of the real height (Reinisch, 1986; Davies, 1990). Virtual height is what the height of reflection from the ionosphere would have been had the radio wave continued to travel at the speed of light through the ionosphere. In principle, each sounding produces an ionogram, a graph of virtual height versus frequency, which provides single site information about the characteristics and dynamics of the upper atmospheric layers discussed in Section 2.3. However, the process of interpreting the ionograms and recording the ionospheric parameters is termed scaling

(e.g. McKinnell, 2002). The ionogram can be converted into an electron density profile $N(h)$, were h represents the real height. Figure 2.6 depicts an example of a daytime ionogram and the corresponding electron density profile (McKinnell, 2002).

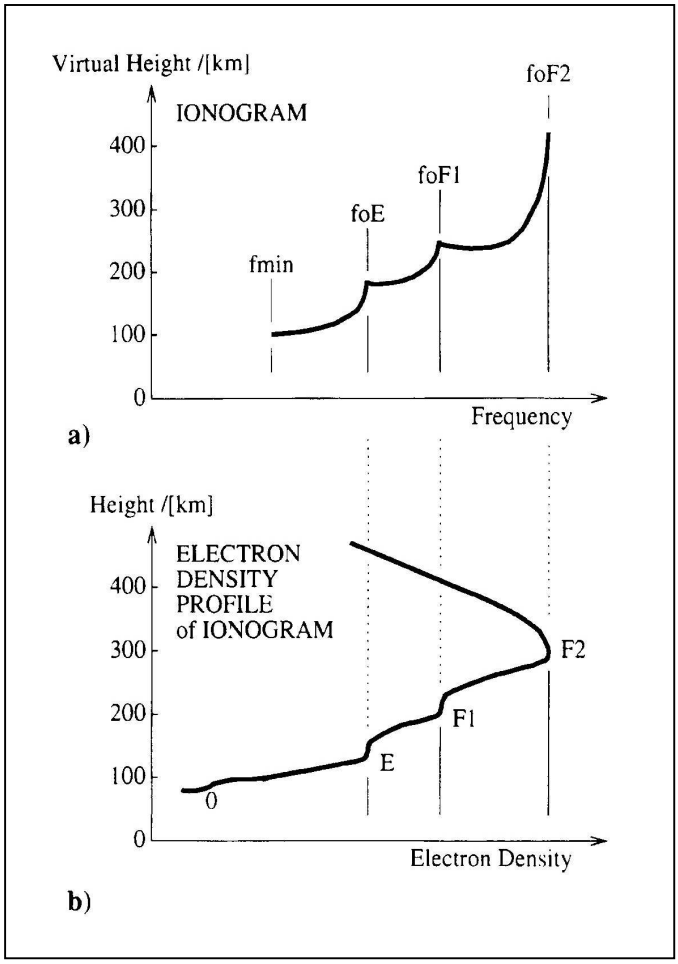

Figure 2.6: Panel (a) depicts daytime ionogram and (b) its corresponding electron density profile. The critical frequencies and electron densities for each layer are indicated (McKinnell, 2002).

A new technique has been introduced to determine ionospheric Total Electron Content (TEC) from ground based ionogram measurements (Reinisch and Huang, 2001). The ionogram provides the information to directly calculate the vertical electron density profile up to the peak of the F2 layer.

The profile above the peak is approximated by an $\alpha-$Chapman function with a constant scale height H_T derived from the bottomside profile shape at the F2 peak, according to the equation:

$$N_T = N_m F2 \exp\left[\frac{1}{2}\left(1 - z - e^{-z}\right)\right], \tag{2.18}$$

where $z = \frac{h - h_m F2}{H_T}$, $N_m F2$ is the maximum electron density, and $h_m F2$ the height of the F2 layer peak. Hence, the Ionosonde TEC can be calculated as an integral from 0 to ~1000 km over the entire profile. This technique is applied in Chapter 4 using the data from South African Ionosondes located at Madimbo (28.38°S, 30.88°E), Grahamstown (33.32°S, 26.50°E) and Louisvale (28.51°S, 21.24°E), respectively (McKinnell, 2002; McKinnell and Poole, 2004).

2.8 Satellite Missions

Since the main topic of this thesis is to investigate solar cycle effects on GNSS derived TEC over Southern Africa, this section will briefly discuss the GNSS system together with the instruments onboard the Solar Heliospheric Observatory (SOHO) and GOES satellites, which were used to record the data used in this work for investigation, analysis and interpretation of results.

2.8.1 Global Navigation Satellite System

GNSS is a generic name used by the International Global Navigation Satellite System Services (IGS) community referring to the US GPS, Russian GLONASS, and the future European GALILEO satellite system. The principles and everyday applications of GNSS are described in e.g. Hoffman-Wellenhof et al. (1993), Kaplan (1996), Langley (1997a;b), and Komjathy (1997). In this work the main focus is on GPS, due to the instrumental limitation in receiving signals from GLONASS and GALILEO over South Africa, therefore discussions will be limited to GPS. The future plan of HartRAO is to install GNSS receivers over the Southern Africa Development Community (SADC) region that will be capable of receiving signals from all the GNSS constellations.

GPS is a satellite-based system for positioning, navigation, and timing purposes developed by the US Department of Defense (DoD). The system can be separated into three components: the space component, the control component and the user segment. The space segment consists of 24 satellites, which are placed in six orbital planes (four satellites in each plane), each inclined by 55° with respect to the ecliptic plane. The satellites orbit at altitudes of ~20 200 km above the Earth's surface. Each satellite transmits a navigation signal composed of two carriers (dual frequency) L1=1575.42 MHz and L2=1227.60 MHz, two binary pseudorandom noise (PRN) codes which modulates the carriers at chipping rates of 10.23 MHz (The P, or precision, code) and 1.023 MHz (the C/A, or coarse/acquisition, code), and a navigation message formatted into frames of 1500 bits with a transmission rate of 50 bps. The C/A-code is modulated onto the L1 carrier, whereas the P-code is transmitted on both L1 and L2 (Langley, 1990). Future GPS modernization includes the introduction of a new frequency, L5 = 1176.45 MHz, with a civil code superimposed.

The control segment is composed of five ground-stations within a tracking network, geographically spread in longitude around the world, belonging to the Operational Control System (OCS). One of the stations acts as the Master Control Station (MCS). The MCS, based on tracked data, calculates and predicts orbits and satellite clock errors. It can also maneuver the satellites and upload, along with the four other sites, the ephemerides and clock correction to be broadcast by the satellites (dos Santos, 1995).

The user segment consists of antennas and receivers providing positioning, velocity and precise timing (Hoffman-Wellenhof et al., 1993; Kaplan, 1996).

Although the use of GNSS is extensive in defense, navigation and surveying applications, it is also used in geo-science, ionospheric and tropospheric studies, global climate change studies, observing polar and Earth rotation rate, mapping the gravitational field, detecting earthquake effects on the

ionosphere, transport and communications, environmental management and space weather monitoring (e.g. Lui et al., 2007; Skone and Yousuf, 2007).

2.8.2 SOHO CELIAS/SEM

The Solar and Heliospheric Observatory (SOHO) spacecraft, launched on 2 December 1995 and injected in 1996 into its halo orbit around the first Lagrangian point of the Sun-Earth System, performs global investigations of the Sun and Heliosphere. Since then, the Charge, Element, and Isotope Analysis System/Solar Extreme Ultraviolet Monitor (CELIAS/SEM) instrument onboard the spacecraft has continuously been monitoring solar X-Ray and EUV fluxes up to date. A detailed description of the instrument is given in Hovestadt et al. (1995) and Judge et al. (1998).

Figure 2.7: Image of SOHO Charge, Element, and Isotope Analysis System/Solar Extreme Ultraviolet Monitor instrument (http:///.www.usc.edu/dept/space_science/intrument_pages).

The SOHO CELIAS/SEM instrument is a transmission grating spectrometer, as shown in Figure 2.7, which utilises highly stable photodiode detectors designed and fabricated for high efficiency and stability especially in EUV wavelength ranges. This spectrometer continuously measures the full disk absolute solar flux at the prominent and important HeII 30.4 nm line as well as the absolute

solar flux between 0.1 to 50 nm. The dispersing element is a freestanding 5000 bar/mm gold transmission grating. Two thin film aluminium filters are utilized to reduce out of band stray light, resulting in a background diode current. This instrument has been at a near temperature of 3°C throughout the mission (Judge et al., 2002). The precision of the SEM is ~0.5% and is primarily to log compression of the CELIAS database. Integration period for CELIAS is 15s and data values are continuously transmitted.

The CELIAS/SEM EUV data have provided scientists with a wealth of information to better understand the connections within the solar-magnetosphere-ionosphere system (e.g.Tsurutani et al., 2005), and used in this study to investigate effects of solar flares on TEC over South Africa.

2.8.3 GOES Satellite Solar Environment Monitor

A geostationary satellite experiment began in 1966 with the launch of the first satellite of the Applications Technology Satellite (ATS) series. These satellites carried an instrument capable of providing continuous images of the Earth, and instrumentation that enabled the transmission of data to and from ground stations. The Geostationary Operational Environmental Satellite (GOES) program formally began in 1975 as a joint effort of the National Oceanic and Atmospheric Administration (NOAA) and NASA with the launch of SMS-1 and SMS-2 satellites. Thereafter, a series of generations of GOES satellites were launched. The recent launch included GOES 8, GOES 10 and GOES 12 which carried the Space Environment Monitor (SEM). The GOES 12 satellite was the first to carry Solar X-ray Imager (SXI) type instruments.

The SEM consists of three instrument groups: an energetic particle sensor (EPS), two magnetometer sensors and a solar X-ray sensor which monitors space weather at ~35,000 km altitude. These instruments provide the real-time data to the Space Environment Center (SEC) in Boulder, Colorado. The SEC is the USA's space weather center and receives, monitors, and interprets a wide variety of solar terrestrial data and issues reports, alerts, warnings, and forecasts for special events

such as solar flares and geomagnetic storms. This information is crucial for military and civilian, radio communication, satellite communication and navigation systems, electric power networks, geophysical exploration, shuttle and space station astronauts, high-altitude aviators, and scientific researchers. A detailed description of the GOES mission can be found at NOAA's website (http://www.ngdc.noaa.gov/stp/goes_mission.htm).

Of interest to this work is the X-ray Sensor telescope that observes and measures solar X-ray emissions in two ranges (0.3 nm and 0.1 to 8 nm). In real-time it measures the intensity and duration of the solar flares in order to provide alerts and warning of potential geophysical responses, such as changes in the ionospheric conditions that can disrupt radio communication and GNSS signals. The EUV sensor provides a direct measure of the solar energy that heats the upper atmosphere and creates the ionosphere.

2.9 Summary

In this chapter, background theory was presented about the Sun and its activity cycle, the Earth's ionosphere and its structure and subsequent effects on propagation of electromagnetic waves as related to this work. A brief description was also presented of ground based Ionosondes related to the southern Africa network. Furthermore, important satellite missions such as GNSS, SOHO Charge, Element and Isotope Analysis System/Solar Extreme Ultraviolet Monitor (CELIAS/SEM) sensor and GOES Solar Environment Monitor (SEM) instrument used to collect the data utilised in this study for validation, investigation and analysis of results were briefly discussed.
The next chapter discusses the Ionospheric TEC Model used in this study.

Chapter 3

THE IONOSPHERIC TOTAL ELECTRON CONTENT MODEL

3.1 Introduction

This chapter is dedicated to providing a brief description of the University of New Brunswick Ionospheric Modelling Technique (UNB-IMT) (Komjathy, 1997) used as a main tool in this study. It begins with a brief overview of modelling ionospheric TEC using GNSS and highlights recent development and efforts undertaken by South Africa to model the ionosphere using GPS. It proceeds with a description of the UNB ionospheric modeling technique covering discussions on the GNSS ionospheric observable, TEC estimation strategy, concept of ionospheric shell height, mapping function, and the interpolation technique used to create TEC maps. Furthermore, it proceeds by discussions on modification of global UNB-IMT used as a regional TEC model to study the solar cycle effects on GNSS-derived TEC over South Africa. Finally, a brief description is given on the International Reference Ionosphere (IRI) Model (Bilitza, 2001) used later for comparison with UNB-IMT TEC results of southern Africa.

3.2 Overview of modelling ionospheric TEC using GNSS

Early studies of ionospheric Total Electron Content (TEC) were carried out using measurements from geostationary radio beacon satellites using the Faraday rotation technique (e.g. Garriott et al., 1965; Titheridge, 1973; Davies, 1980). These studies were based mainly on measurements obtained either from single frequency receivers or a ground network of instruments. Due to the declining number of special experiments onboard Faraday satellites and the advent of GNSS such as the

Russian GLONASS and the US GPS in the last two decades, it became possible to use the GPS-technique for a comprehensive monitoring of the ionosphere.

The ionosphere affects electromagnetic waves such as GNSS signals that traverse through it, by inducing additional transmission time delays and phase advances (Langley, 1996). The magnitude of this delay is determined by the electron content and the frequency of the electromagnetic waves. Single frequency users have to correct for this delay in applications such as GPS positioning, navigation and communication. Early ionospheric correction models using GPS include the Klobuchar broadcast regional model (Klobuchar, 1987). This model is based on a function-fitting approach and could only correct for about 50% of the total ionosphere effects (e.g. Gao and Liu, 2002). Other function-based models were later developed, such as the polynomial function-fitting techniques (e.g. Coster et al., 1992; Komjathy, 1997) and spherical harmonics (e.g. Walker, 1989; Schaer, 1999). On the other hand, the grid-based technique (El-Arini et al., 1995; Gao et al., 1994), has demonstrated its capabilities for higher modelling accuracy compared to the function-based algorithms. All the current grid and function-based models are two dimensional in nature, which assumes that the ionosphere is condensed on a single shell at a fixed altitude above the Earth's surface. This assumption is only an approximation to reality and is not physically true (Gao and Liu, 2002). However, these ionospheric modelling methods, using the IGS GPS networks, have been extensively used for global and regional modelling of the ionosphere during the past several years (e.g. Jakowski and Paasch, 1984; Klobuchar, 1991; Komjathy and Langley, 1996; Komjathy, 1997; Jakowski et al., 1998; Manucci et al., 1998; Fedrizzi et al., 2001)

In recent years, efforts have been undertaken to improve modelling of the ionosphere using tomography techniques (e.g. Raymund et al., 1990; Raymund et al., 1994; Raymund, 1995; Howe, 1997; Liu et al., 2001). The ionospheric tomographic model can describe the ionospheric field in a three-dimensional frame instead of a two-dimensional frame as used by the other techniques discussed earlier. All these studies are carried out using GNSS data, which have densely distributed networks in the northern hemisphere. The network in southern Africa is more sparsely populated

although efforts are continuously in process to densify the network. Most recently, efforts have been undertaken in South Africa to adopt and modify some of these models to characterise the dynamics and variations of the ionospheric TEC over the Southern Africa region. In particular the Multi-Instrument Data Analysis System (MIDAS) algorithm used for ionospheric tomographic inversion developed at the University of Bath (Mitchell et al., 1997; Cilliers et al., 2004) and the spherical harmonic model, now referred to as a variable degree adjusted spherical harmonic (ASHA) model (Opperman et al., 2007, McKinnell et al., 2007) and the University of New Brunswick Ionospheric Modelling Technique UNB-IMT (Komjathy, 1997; Fedrizzi et al., 2005; Ngcobo et al., 2005; Moeketsi et al., 2007a,b; Shetti, 2007) have been developed. The latter is adopted for the purpose of this study and is described in the following section.

3.3 The UNB ionospheric modelling technique

A Unix-compatible UNB Ionospheric Modelling Technique was developed in 1997, at the Department of Geodesy and Geomatics Engineering at the University of New Brunswick. The main purpose was to compute global and regional TEC using the IGS network of dual-frequency GNSS receivers in order to provide ionospheric corrections to communications, surveillance and navigation systems operating at a single frequency (Komjathy and Langley, 1996; Komjathy, 1997; Komjathy et al., 1998). Comparison of UNB-IMT TEC results with TOPEX/Poseidon TEC measurements during medium and low solar activity conditions, showed a good level (~5 TECU) of agreement (Komjathy, 1997; Komjathy et al., 1998). Recently, Fedrizzi et al. (2001, 2005) also applied the same model to study the ionospheric TEC response during perturbed geomagnetic conditions of the Southern American Sector and this model is adopted as the main tool in this thesis to study the solar cycle effects of GNSS-derived ionospheric TEC over South Africa.

3.3.1 GNSS ionospheric observables

The basic measurements carried out on the L1 and L2 frequencies by a GNSS receiver are the signals travel time from the GPS satellite to the receiver on the Earth's surface. This time multiplied

by the speed of light c, yields the range between the satellite and the receiver antenna. Since the range has several errors and biases lumped into it, it is called pseudorange (e.g. Langley, 1993). The pseudorange observation equation can be expressed as (Komjathy, 1997):

$$P_1 = \rho + c \cdot (dT - dt) + d_{ion,L1} + d_{trop} + b^{s_i,L1} + b_{r_j,L1} + mp_{P_1} + \varepsilon_{P_1}, \tag{3.1}$$

$$P_2 = \rho + c \cdot (dT - dt) + \gamma \cdot d_{ion,L1} + d_{trop} + b^{s_i,L2} + b_{r_j,L2} + mp_{P_2} + \varepsilon_{P_2}. \tag{3.2}$$

Here

P_1, P_2 are pseudorange measurements on L1 and L2 in units of distance,

ρ is the geometric range between the satellite and the receiver,

dT, dt the receiver and satellite clock offsets from GPS time,

$d_{ion,L1}$ is the ionospheric delay on L1,

$\gamma = \left(\frac{f_1}{f_2}\right)^2 = \left(\frac{L_1}{L_2}\right)^2$ is the frequency ratio squared,

d_{trop} is tropospheric delay,

$b^{s_i,L1}, b^{s_i,L2}$ are the satellite instrumental delays on P_1 and P_2 respectively for satellite s_i,

$b_{r_j,L1}, b_{r_j,L2}$ are the receiver instrumental delays on P_1 and P_2 respectively for satellite r_j,

mp_{P_1}, mp_{P_2} are the multipaths on P_1 and P_2 measurements, and

$\varepsilon_{P_1}, \varepsilon_{P_2}$ are the receiver noise on P_1 and P_2 respectively.

By subtracting equation (3.2) from equation (3.1) and rearranging the terms we obtain:

$$P_1 - P_2 = (1 - \gamma) \cdot d_{ion,L1} + \left[b^{s_i,L1} - b^{s_i,L2} + b_{r_j,L1} - b_{r_j,L2} \right] + \nu_p, \tag{3.3}$$

where

$$\nu_p = mp_{P_1} - mp_{P_2} + \varepsilon_{P_1} - \varepsilon_{P_2}. \tag{3.4}$$

It is crucially important to note that the ionospheric term in equation (3.3) cannot be measured directly from pseudorange measurements due to the term in the square brackets on the right hand

side of the equation, which is slowly varying in time. However, since the ionospheric term cannot be measured directly, it needs to be estimated along with the term in the square brackets in equation (3.3).

The first order equation of the Appleton-Hartree formula (2.12) also gives an expression for the ionospheric delay in terms of TEC as:

$$d_{ion} = d_{ion,L1} = 40.3 \cdot \frac{TEC}{f_1^2}. \tag{3.5}$$

This equation gives centimeter-level accuracy for ionospheric delay (Komjathy, 1997). The equation (3.5) neglects terms higher than the 2nd order in the Appleton-Hartree formula as described in section 2.6.1.

After substituting equation (3.5) into equation (3.3) and doing some algebra, the expression for the TEC using pseudorange (*P*) observations in TECU is given by:

$$TEC_P = 9.52\left(P_2 - P_1\right). \tag{3.6}$$

Since electromagnetic waves such as GNSS signals also experience phase advances when traversing the ionosphere, the observation equations for carrier phase (Φ) measurements on L1 and L2 are:

$$\Phi_1 = \rho + c \cdot \left(dT - dt\right) + \lambda_1 N_1 - d_{ion,L1} + d_{trop} + b^{\varphi,s_i,L1} + b_{\varphi,r_j,L1} + mp_{\varphi 1} + \varepsilon_{\varphi 1}, \tag{3.7}$$

$$\Phi_2 = \rho + c \cdot \left(dT - dt\right) + \lambda_2 N_2 - \gamma . d_{ion,L1} + d_{trop} + b^{\varphi,s_i,L2} + b_{\varphi,r_j,L2} + mp_{\varphi 2} + \varepsilon_{\varphi 2}, \tag{3.8}$$

where

Φ_1, Φ_2 are the carrier phase observations on L1 and L2 respectively in distance units,

λ_1, λ_2 are the wavelengths of the L1 and L2 carriers respectively,

N_1, N_2 are the unknown L1 and L2 integer carrier phase ambiguities,

$b^{\varphi,s_i,L1}, b^{\varphi,s_i,L2}$ are the satellite instrumental delays on L1 and L2 carrier phase for satellite s_i,

$b_{\varphi,r_j,L1}, b_{\varphi,r_j,L2}$ are the receiver instrumental delays on L1 and L2 carrier phase for receiver r_j,

$mp_{\varphi_1}, mp_{\varphi_2}$ are the multipaths on L1 and L2 carrier phase measurements,

$\varepsilon_{\varphi_1}, \varepsilon_{\varphi_2}$ are the noise on L1 and L2 respectively, and the terms are defined in equation (3.1) and (3.2) respectively.

Now, after subtracting carrier phase observation equation (3.8) from equation (3.7), and re-arranging the terms we obtain:

$$\Phi_1 - \Phi_2 = (\gamma - 1) \cdot d_{ion,L1} + \left[b^{s_i} + b_{r_j} \right] + N_1\lambda_1 - N_2\lambda_2 + \nu_\varphi, \tag{3.9}$$

where

$$\nu_\varphi = mp_{\varphi_1} - mp_{\varphi_2} + \varepsilon_{\varphi_1} - \varepsilon_{\varphi_2}, \tag{3.10}$$

and

b^{s_i} is the satellite differential delay corresponding to $b^{\varphi,s_i,L1} - b^{\varphi,s_i,L2}$ for satellite s_i,

b^{r_j} is the receiver differential delay corresponding to $b_{\varphi,r_j,L1} - b_{\varphi,r_j,L2}$ for receiver r_j, and the sum of the satellite and receiver differential delays is referred to in this thesis as the satellite-receiver differential delays.

After combining equation (3.9) and (3.5) and some algebraic manipulation, we obtain an expression similar to equation (3.6) for TEC using carrier phase observations in TECU:

$$TEC_\varphi = 9.52 \cdot (\Phi_1 - \Phi_2), \tag{3.11}$$

which is very precise but results in an ambiguous observable.

By taking advantage of the very precise but ambiguous $\Phi_1 - \Phi_2$ carrier and the unambiguous but less precise $P_1 - P_2$ observable, the two can be combined by phase levelling as:

$$TEC_{comb_i} = TEC_{\varphi_i} - \frac{\sum_{j=-\frac{n}{2}}^{\frac{n}{2}} p_j \left[TEC_{\varphi_j} - TEC_{P_j} \right]}{\sum_{j=-\frac{n}{2}}^{\frac{n}{2}} p_j}, \tag{3.12}$$

where i and j are indices for ionospheric observable to be levelled starting at the beginning of an arc, $i = 1, 2, ..., n$ with the total number of observations n in an arc. However, in the case where n is an even number $j = -\frac{n}{2}, ..., \frac{n}{2}$ as in equation (3.12), and $j = -\frac{n-1}{2}, ..., \frac{n+1}{2}$ for the scenario where n is an odd number. For each phase-connected data arc, the level of the L1 minus L2 carrier phase observable TEC_{φ_i} were set using all $P_1 - P_2$ pseudo range observables TEC_{P_j} in the same phase-connected arc. In order to implement this approach, a minimum arc length of 20 minutes was used resulting in a minimum of 40 observations needed to set the level of TEC_{φ_i} (Komjathy, 1997). The simple weighting scheme with individual weights $p_j = \frac{1}{j^2}$, is used when setting the level of TEC_{φ_i} for each arc. The highest weight is placed on the data in the middle of the arc and the lowest to the observations at the both ends of the arc corresponding to the lowest satellite elevation angles thereby minimising the effects of multipath and noise.

To detect bad points and cycle slips, repair cycle slips and adjust phase ambiguities, a modified version of PhaseEdit version 2.0 software was used (Komjathy, 1997; Fedrizzi, 2005). UNB-IMT uses a Kalman filter algorithm, described in the next section to estimate ionospheric parameters and satellite-receiver differential delays.

3.3.2 Estimating Strategy

The UNB ionospheric modelling technique uses the single-layer ionospheric (shell) model to compute TEC from ionospheric measurements obtained using dual frequency GPS receivers, according to the following observation equation (Komjathy, 1997):

$$I_{r_j}^{s_i}(t_k) = M\left(e_{r_j}^{s_i}\right)\cdot\left[a_{0,r_j}(t_k) + a_{1,r_j}(t_k)\cdot d\lambda_{r_j}^{s_i} + a_{2,r_j}(t_k)\cdot d\varphi_{r_j}^{s_i}\right] + b_{r_j} + b^{s_i}, \tag{3.13}$$

where $I_{r_j}^{s_i}(t_k)$ is the L1 minus L2 phase levelled ionospheric observations in units of TECU, generated by equation (3.12) at each epoch t_k made by receiver r_j observing satellite s_i. $M\left(e_{r_j}^{s_i}\right)$ is the thin-shell elevation angle mapping function projecting the line-of-sight measurement to the vertical, with $e_{r_j}^{s_i}$ representing the satellite s_i elevation angle viewed by receiver r_j at the sub-ionospheric point. Furthermore, $a_{0,r_j}, a_{1,r_j}, a_{2,r_j}$ are parameters for spatial linear approximation of TEC to be estimated per station r_j, assuming a first-order Gauss-Markov stochastic process (Gail et al., 1993), $d\lambda_{r_j}^{s_i} = \lambda_{r_j}^{s_i} - \lambda_0$ is the difference between the longitude of a sub-ionospheric point and the longitude of the mean Sun, $d\varphi_{r_j}^{s_i} = \varphi_{r_j}^{s_i} - \varphi_{r_j}$ is the difference between the geomagnetic latitude of the sub-ionospheric point and the geomagnetic latitude of the station, and b_{r_j}, b^{s_i} refer to the receiver and satellite differential delays or biases respectively.

The parameters $a_{0,r_j}, a_{1,r_j}, a_{2,r_j}$ in equation (3.13) are estimated for each station using a Kalman filter algorithm. The prediction and update equations for the state estimation are described by Coster et al (1992) and van der Wal (1995). For a detailed explanation of the Kalman filter algorithm, the reader is referred to Komjathy (1997) and dos Santos (1995).

Because of the ionospheric dependence on solar radiation and the Earth's geomagnetic field, a solar-geomagnetic reference frame is used to compute TEC. The TEC values change much more slowly in

this reference frame compared to the Earth-fixed one (Langley, 1996; Komjathy, 1997; Fedrizzi et al., 2005). However, the use of such a reference frame results in more accurate ionospheric delay estimates when using Kalman filter updating (Mannucci et al., 1995).

3.3.3 Ionospheric shell height and mapping function

The single layer ionospheric model assumes that a spherical thin shell can approximate vertical TEC, which is located at a specified altitude above the Earth's surface. This altitude is often assumed to correspond to the maximum electron density of the ionosphere. In this case, it is assumed that the ionospheric shell height has no temporal or geographical variation and therefore it is set to a constant value regardless of the time or location of interest. A sensitivity analysis has been conducted using different ionospheric shell heights in Komjathy (1997), which included a variable height component in the UNB-IMT model. It was shown that the predicted shell height can vary with geographical location, time of the day, season and solar activity.

It has been reported that one of the major error sources in ionospheric modelling using GNSS is the ionospheric mapping function that projects line-of-sight TEC (slant TEC) into vertical TEC. An investigation into the accuracy of various mapping function was conducted in Komjathy (1997). It was found that the standard geometric mapping function performed marginally better than the other mapping functions investigated. However, in this work the standard mapping function (Mannucci et al., 1993) given by:

$$M\left(e_{r_j}^{s_i}\right) = \left[1 - \frac{r_E \cos^2 e_{r_j}^{s_i}}{r_E + h}\right]^{-\frac{1}{2}} \tag{3.14}$$

is used in equation (3.13). Here, r_E is the mean radius of the Earth and h is the mean value for the assumed height of the thin spherical shell, located at a fixed height of 400 km, slightly higher than the average maximum electron density (Komjathy, 1997). The elevation cutoff angle was set to 10°. Equation (3.14) computes the secant of the zenith angle of the signal geometry and projects the line-

of-sight measurements to the vertical of the sub-ionospheric point. It should be noted that recent studies comparing techniques for mapping TEC, reported an improvement in the accuracy of mapping TEC compared with the thin shell approach (Meggs et al., 2004; Meggs and Mitchell, 2006).

3.3.4 Interpolation scheme to create TEC maps

In order to compute the 15 minute regional TEC maps using a 5 degree by 5 degree grid spacing, equation (3.13) was evaluated for four GNSS stations closest to the grid node at which the TEC value is computed. Then the inverse distance squared weighted average of the individual TEC data values corresponding to the four GNSS stations was computed as (Komjathy, 1997):

$$TEC_i = \frac{\sum_{j=1}^{4} \frac{1}{d^2 j} \cdot TEC_{\mathrm{GNSS}_j}}{\sum \frac{1}{d^2 j}}, \tag{3.15}$$

where TEC_i is the computed TEC value for grid node i, TEC_{GNSS_j} is the computed TEC value based on the estimated ionospheric model parameters for the GNSS station j, and d_j is the distance between station j and the grid node i. This particular weighting function scheme (equation 3.15) is used to take into account the spatial decorrelation of the ionosphere (Komjathy, 1997). The closer a particular grid node is to a GNSS station, the more weight is placed on the TEC computed by evaluating the ionospheric model describing the temporal and spatial variation of the ionosphere above the particular station. Each fifteen minute TEC map produced reflects the observations obtained from 7.5 minutes before to 7.5 minutes after the respective quarter hour (Fedrizzi et al., 2005).

A standard interpolation scheme was used to compute TEC between grid nodes, produced by equation (3.15), in order to provide ionospheric corrections for single frequency users (Komjathy,

1997). For more information about this algorithm, the reader is referred to Junkins et al. (1973) and Komjathy (1997).

3.4 Modification of UNB-IMT for application over southern African region

The global UNB-IMT algorithm was used to compute TEC using the IGS GPS data densely distributed in the northern hemisphere, with a few such stations over southern Africa (Komjathy, 1997; Fedrizzi et al., 2005). Due to the South African efforts to increase installation of GNSS receivers over the Southern African Development Community (SADC) region (Combrinck et al., 2003), it became profound to test performance of GPS TEC model such as the UNB-IMT over the southern Africa region with more local GPS data than before.

As a consequence, efforts were undertaken by the Space Geodesy Programme at HartRAO to modify the global UNB-IMT Unix version to compile and execute on a Linux platform in order to compute ionospheric TEC over southern Africa using more data from the IGS and Southern African GPS network (Ngcobo et al., 2005; Moeketsi et al., 2007a,b). The software module "EditObs" developed, was used to edit the Receiver Independent Exchange Format (RINEX) GPS observation file, and create a new RINEX file, which contains GPS observables used by the UNB-IMT Linux version during computations (Ngcobo et al., 2005).

Figure 3.1 is an example of a regional TEC map produced by the HartRAO Space Geodesy Programme using the UNB-IMT Linux version with data from the South African GPS network at 12:00 UT on 31 December 2004. Evidently, TEC values increase towards ionospheric equatorial region, as expected.

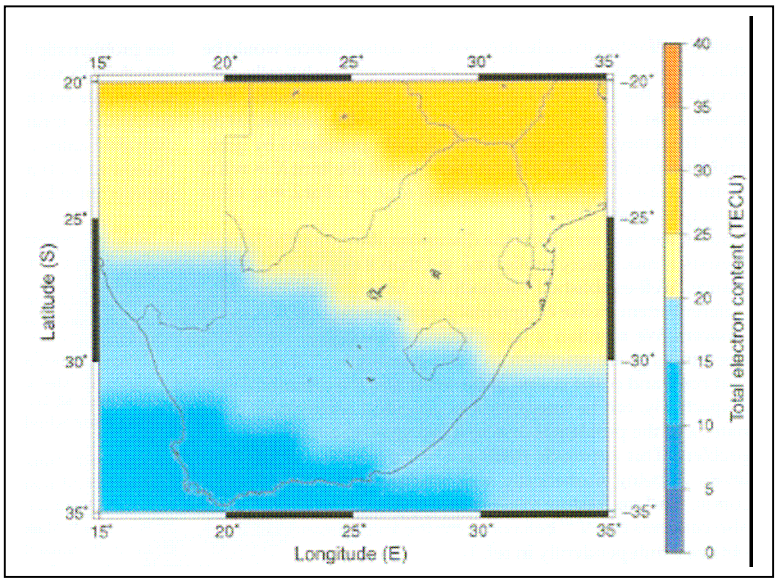

Figure 3.1: South African regional TEC map produced using UNB-IMT Linux version at 12:00 UT on 31 December 2004. The orange colours correspond to higher TEC values (Ngcobo et al., 2005).

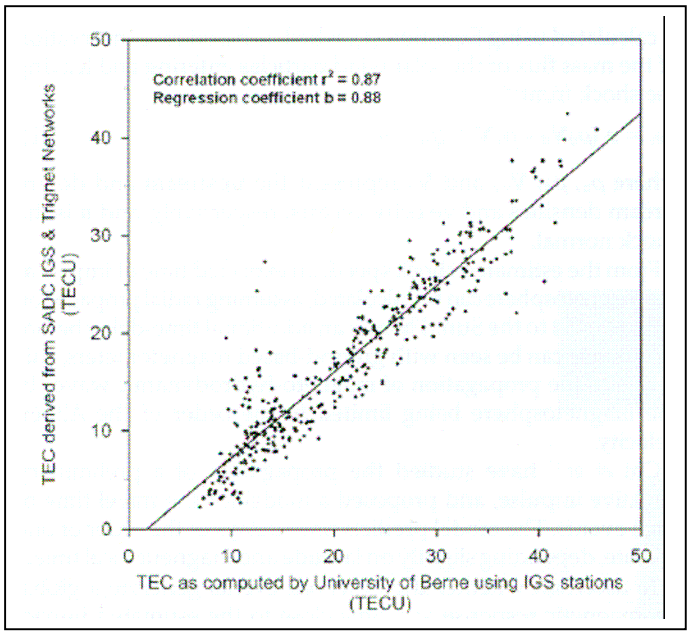

Figure 3.2: Comparison of UNB-IMT with the CODE IGS analysis center (University of Berne, Switzerland) EC over HartRAO, South Africa for December 2004. The straight line is a result of a linear regression fit to the observations (Ncobo et al., 2005).

As first validation, Figure 3.2 illustrates comparison of the month of December 2004 over HartRAO IGS station with TEC determined by CODE IGS analysis center at University of Berne, Switzerland, using global IGS stations. There is a good correlation ($r^2 = 0.87$) between the two sets of results, with r.m.s. residual of 5.2 TECU (Ngcobo et al., 2005). A detailed validation of UNB-IMT TEC results over South Africa with Ionosonde TEC measurements is performed in Chapter 4, in order to provide ground truth for the use of this model in this study.

3.5 International Reference Ionosphere

The International Reference Ionosphere (IRI) is an international project jointly sponsored by the Committee on Space Research (COSPAR) and the International Union of Radio Science (URSI). These organisations formed a Working Group in the late nineteen sixties to produce an empirical standard model of the ionosphere, based on all available data sources. This Working Group meets on an annual basis to discuss and implement improvements to the IRI model.

For a given location, time and date, IRI estimates: the electron and ion densities; electron, ion and neutral temperature; equatorial vertical ion drifts and ion composition in the middle altitude range from about 50 km to about 2000 km, and can also provide predictions of TEC up to 2000 km. The IRI model is the most commonly used global ionospheric model providing monthly averages in the non-auroral ionosphere for magnetically quiet conditions. Since its inception several improvements on the IRI model have been made (Bilitza, 1990; Bilitza, 1997; Bilitza, 2001).

Although IRI is based on all major ionospheric data sources, it is well known that it is not well represented over southern Africa due to historic lack of data (Mckinnell, 2002). As a consequence, IRI does not perform well in predicting the ionospheric conditions over South Africa. Efforts have been undertaken using the Neural Network technique to develop ionospheric models, which could be used to improve performance of IRI in predicting ionospheric parameters over South Africa (e.g. McKinnell and Poole, 2000; McKinnell, 2002; Oyeyemi, 2005; Oyeyemi et al., 2007). In this thesis

the IRI 2001 model TEC prediction is compared with the UNB-IMT TEC determined over southern Africa. Results from this comparison appear in Chapter 5.

3.6 Summary

This chapter has provided a brief description of the University of New Brunswick Ionospheric Modelling Technique (UNB-IMT) (Komjathy, 1997), used as a main tool in this study. It started with a brief description of ionospheric TEC modeling using GNSS, and some highlights of recent development in South African related to this research topic. The strategy behind the UNB ionospheric modelling technique was discussed, including how GNSS pseudorange and carrier phase observables are used to compute ionospheric TEC. A brief description of the modifications made to UNB-IMT was given as related to modeling TEC over the Southern Africa region. Comparison of UNB-IMT with CODE analysis center TEC predictions for December 2004 showed a good level of agreement. It was followed by a brief discussion of the International Reference Ionosphere (IRI) Model (Bilitza, 2001), which as the most commonly used global model will be used later as a comparison tool.

The next chapter compares UNB-IMT TEC with Ionosonde TEC measurements over South Africa, to provide the ground truth for use of this model as main tool in this study.

Chapter 4

VALIDATION OF UNB-IMT USING IONOSONDE TEC MEASUREMENTS OVER SOUTH AFRICA

4.1 Introduction

For more than a decade, ionospheric research over South Africa has been carried out using data from three ionospheric sounders located at Grahamstown (33.32˚S, 26.50˚E), Louisvale (28.51˚S, 21.24˚E) and Madimbo (28.38˚S, 30.88˚E) respectively. These three ionosondes are all digital pulse sounders, manufactured by the University of Massachusetts Lowell Center for Atmospheric Research (ULMCAR). The area of interest has been modelling bottomside ionospheric parameters using neural networks (e.g. Willicroft and Poole, 1996; McKinnell and Poole, 2000; Poole and McKinnell, 2000; McKinnell, 2002; Oyeyemi and Poole, 2004; McKinnell and Poole, 2004; Oyeyemi et al., 2007). Recently, efforts have been undertaken to use the Global Navigation Satellite System (GNSS) as a new technique to monitor the dynamics and variations of the ionosphere over South Africa as discussed in Chapter 3 (Cilliers et al., 2004; Ngcobo et al., 2005, Moeketsi et al., 2007a,b; Opperman et al., 2007; McKinnell et al., 2007). The dual frequency (L1 = 1572.42 MHz and L2 = 1227.60 MHz) signals transmitted by GNSS, and received by the worldwide network of GPS receivers, can be used to provide a technique to determine high resolution spatial and temporal ionospheric Total Electron Content (TEC) at regional and global level (e.g. Klobuchar, 1991; Komjathy and Langley, 1996; Jakowski, 1996; Komjathy, 1997; Mannucci et al., 1998). Decades of ionospheric research showed that TEC is highly variable and depends on several factors such as local time, geographical location, season and solar cycle (e.g. Jakowski, 1996; Jakowski et al., 1999; Warnant and Pottiaux, 2000; Tsurutani et al., 2005; Mannucci et al., 2005; Fedrizzi et al., 2005,

Moeketsi et al., 2007a,b). Recently, Jakowski et al. (2001, 2002) illustrated that TEC monitoring using the GNSS network can contribute to space weather monitoring.

A new technique described in Chapter 2 has been proposed by Reinisch and Huang (2001), which estimate the topside ionospheric electron density profile from ground-based Ionosonde measurements. This technique provides another tool to determine TEC by calculating the integral from 0 to ~ 1000 km over the entire ionospheric electron density profile. However, it is crucial to note that this technique has limitations in terms of geographical location of ionospheric sounders and spatial coverage in determining TEC. The GNSS technique provides more detailed information and is not limited in geographical and spatial coverage and, therefore, should complement the ionosonde but not replace them. It has been demonstrated recently that comparisons between Ionosonde-derived TEC (ITEC) and GPS-derived TEC (GTEC) and other techniques (e.g. Incoherent Scatter Radar, Geostationary Satellite Beacons and TOPEX) at lower and mid-latitudes shows, in general, a very good level of agreement (Reinisch and Huang, 2001; Belehaki and Tsagouri, 2002; Belehaki et al., 2003; Zhang et al., 2006; and McKinnell et al., 2007).

In this Chapter, the midday GTEC determined using the UNB-IMT (Komjathy, 1997; Ngcobo et al., 2005; Moeketsi et al., 2007a,b), primed with data from the South African GPS network are compared with ITEC measurements over the three Ionosonde locations in South Africa. The residual of GTEC and ITEC, which is believed to correspond to the plasmaspheric electron content is computed and further discussed. The ionospheric and total slab thickness parameters (e.g. Forster and Jakowski, 2000; Belehaki et al., 2003; Miro et al., 1999) are also computed and comprehensively discussed. The study is performed for two selected periods during the descending phase of solar cycle 23; the year 2002 for near-solar maximum, and 2005 for near solar minimum conditions respectively. The ITEC values are derived from ionograms using the technique described in Reinisch and Huang (2001). The main aim of this chapter is to investigate midday TEC variability over South Africa during different periods of solar cycle 23 and further to validate UNB-IMT TEC

results using ITEC measurements as one of the tools to be used for future related ionospheric physics research and application over South Africa.

4.2 Observations and data analysis

Observations and data analysis from the South African network of GNSS stations and the Ionosonde network are discussed in this section.

Station Name	Station Code	Geograpical latitude (◦)	Geographical longitude (◦)	Geomagnetic latitude (◦)
Hartebeesthoek	HARB	-25.89	27.71	-27.13
Hartebeesthoek	HRAO	-29.89	27.69	-27.13
Ermelo	EMLO	-26.30	29.59	-27.87
Pietermaritzburg	PMBG	-29.36	30.23	-30.98
Phalaborwa	PBWA	-23.57	31.08	-25.46
Pietersburg	PTBG	-23.55	29.28	-25.12
Erasmia	ERAS	-23.41	27.41	-24.65
Kuruman	KMAN	-27.27	23.26	-27.70
Upington	UPTN	-28.24	21.15	-28.27
Springbok	SBOK	-29.40	17.52	-28.76
De Aar	DEAR	-30.39	23.59	-30.81
Sutherland	SUTH	-32.38	20.81	-32.26
Simonstown	SIMO	-34.19	18.44	-33.61
Graaf-Reinett	GFNT	-32.15	24.32	-32.66
Port Elizabeth	PELB	-33.98	25.61	-34.68
East London	ELDN	-33.02	27.49	-34.08

Table 4.1: Geographical coordinates and geomagnetic latitudes of Southern Africa dual frequency GNSS receivers used in this work.

4.2.1 Southern Africa GNSS networks

South African GNSS networks consist of two GPS networks: the Southern African Development Community (SADC) GPS Network, which forms part of the IGS network and is managed by

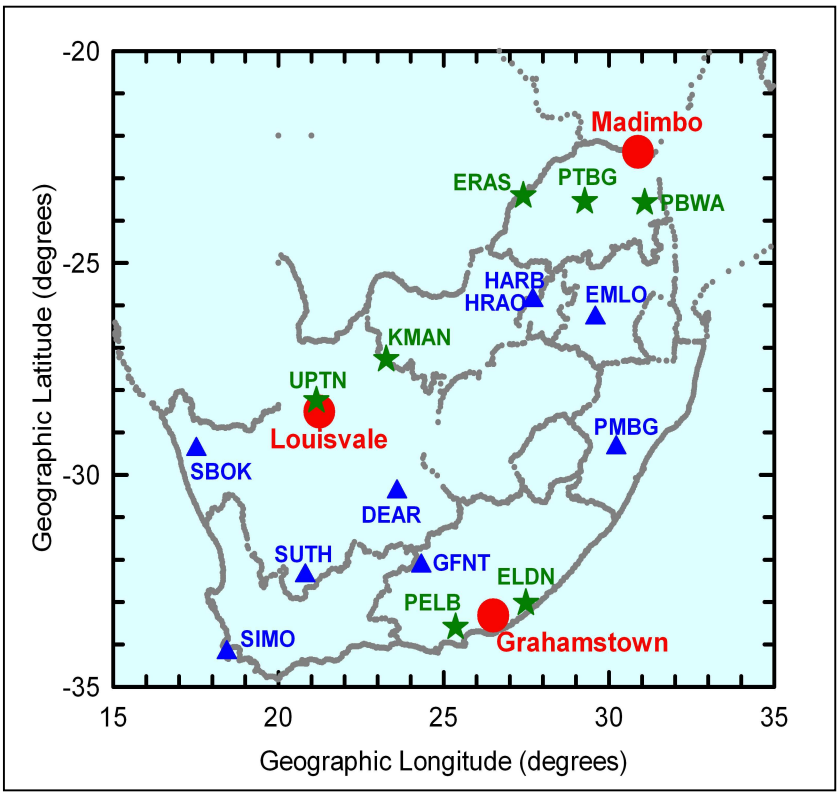

Figure 4.1: Geographic locations of Madimbo, Louisvale and Grahamstown (red circles) and South African GNSS network (blue triangles and green stars) of dual frequency receivers used during data processing in this work. The green stars denote the selected long time data record GNSS receivers located near Ionosondes used for the purpose of this study.

HartRAO and the Trignet Network which is managed by the Chief Directorate: Surveys and Mapping (Combrinck et al., 2003). Effort is undertaken by both agencies to increase installations of ground dual frequency GNSS receivers over Southern Africa. The data sampled at 30s from 16 South African dual frequency GNSS receivers, were used in this study as an input to the UNB-IMT

code described in Chapter 3 to compute TEC over the South African region. These station's geographical coordinates and geomagnetic latitudes are listed in Table 4.1 and depicted in Figure 4.1. The International GNSS data used were obtained from the HartRAO data server ftp://geoid.hartrao.ac.za and can also be obtained from ftp://lox.ucsd.edu/pub/rinex (see also Combrinck., et al., 2003), while the South Africa CDSM Trignet data were obtained from http://www.trignet.co.za (Cilliers et al., 2003). It was ensured that the quality of the GPS data was checked for all stations using the UNAVCO Translate/Edit/Quality Check (TEQC) software (Estey and Merteens, 1999). The software module "EditObs" developed locally (Ngcobo et al., 2005) was used to extract the GPS observables used by UNB code from the Receiver Independent Exchange format (RINEX) GPS observation file.

4.2.3 Southern Africa Ionosondes

The electron density profiles determined from the Grahamstown, Louisvale and Madimbo Ionosonde measurements over South Africa were used to determine ITEC by applying the Reinisch and Huang (2001) technique described in Chapter 2 (see Section 2.7). The Ionosonde stations geographic coordinates and geomagnetic latitudes are listed in Table 4.2 and shown in Figure 4.1. The electron density profile up to 1000 km is derived from a combination of the inverted bottomside ionograms and a modelled topside profile (Reinisch and Huang, 2001). All three ionosonde measurements have a time resolution of at least 30 minutes, and were automatically scaled using the Lowell scaling software ARTIST (McKinnell et al., 2007). To ensure data quality assurance, all recorded ionograms used for this work were manually edited for quality control before obtaining daily hourly ITEC data from the ionograms. The midday ITEC values for years 2002 and 2005 were determined for all three Ionosonde stations. There are some days for which ionogram data were not recorded, particularly for the period of near solar maximum conditions (2002) and this resulted in gaps in the ITEC data.

Station Name	Geograpical latitude (◦)	Geographical longitude (◦)	Geomagnetic latitude (◦)
Grahamstown	-33.32	26.50	-34.30
Louisvale	-28.51	21.24	-28.53
Madimbo	-22.38	30.88	-24.28

Table 4.2: Geographical coordinates and geomagnetic latitudes of southern Africa Ionosondes.

4.3 Comparison of GTEC with ITEC

Two years (2002 and 2005) corresponding to the descending phase of solar cycle 23 were selected for this work, which compared the midday GTEC derived using the UNB-IMT algorithm with the ITEC measurements determined from the Madimbo, Grahamstown and Louisvale ionograms observed over South Africa. The results are discussed in this section.

4.3.1 Comparison of midday GTEC with ITEC measurements near solar maximum

Figures 4.2(a)-(c) depict a comparison of midday GTEC computed using UNB-IMT with ITEC measurements over the Madimbo, Grahamstown and Louisvale Ionosondes, for the period near solar maximum. Panels show TEC comparison computed from:

(a) Phalaborwa (PBWA), Pietersburg (PTBG) and Erasmia (ERAS) GNSS stations located near the Madimbo ionosonde,
(b) Port Elizabeth (PELB) and East London (ELDN) GNSS stations located near the Grahamstown ionosonde, and
(c) Kuruman (KMAN) and Upington (UPTN) GNSS stations near the Louisvale ionosonde.

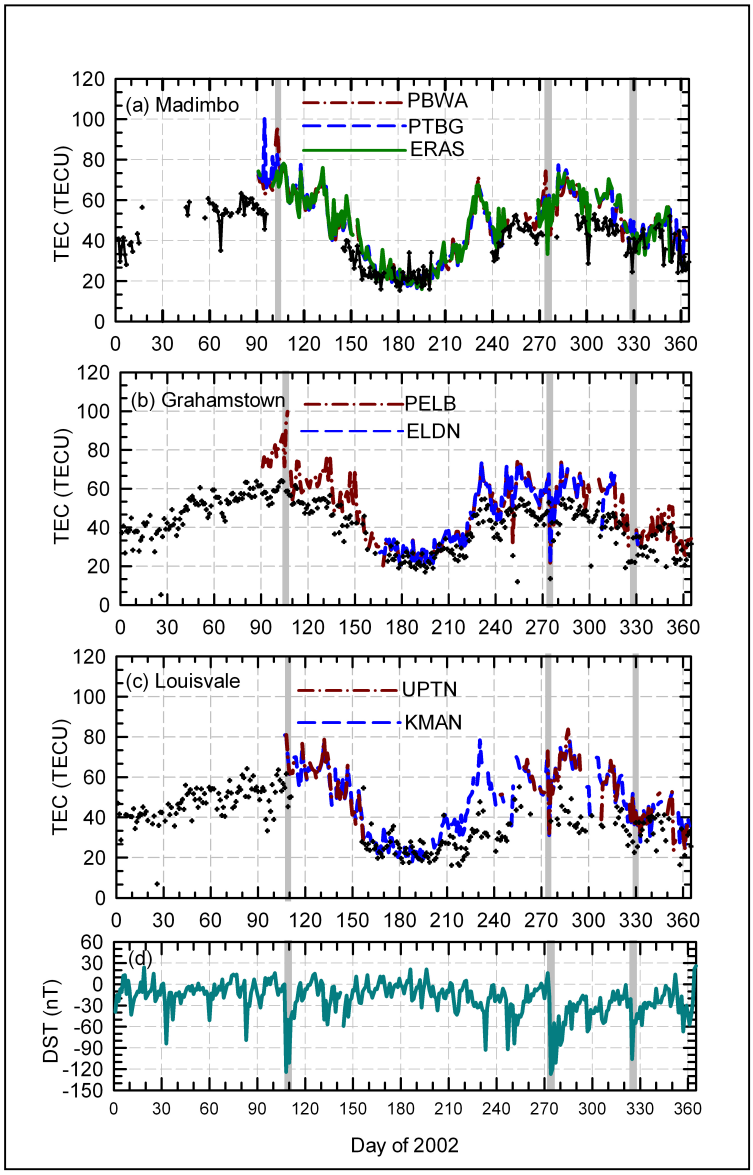

Figure 4.2: Comparison of daily midday TEC computed with UNB model with Ionosonde TEC measurements over South Africa for the period 2002 near solar maximum. Panels show TEC comparison computed from: (a) PBWA (dash-dot-dash line), PTBG (dashed line) and ERAS (solid line) GPS stations in the vicinity of the Madimbo ionosonde location, (b) PELB and ELDN GPS stations located in the vicinity of the Grahamstown Ionosonde, and (c) KMAN and UPTN stations located near the Louisvale Ionosonde. Black scatter points denote the Ionosonde TEC measurements. The Panel (d) shows midday DST values for year 2002.

The midday GTEC values are computed from Day 91 of 2002 due to a lack of GPS data recorded earlier in 2002, while ITEC values were determined for the whole period, except for the days where the ionogram data were not recorded. However, it is inferred from the panels that the variation trend of GTEC and ITEC over all stations are generally in good agreement and show pronounced seasonal variations with maximum values (~80 TECU) around autumn and spring equinoxes and minimum values (~22 TECU) around winter and summer. The short-term (~27 days) TEC variations presumably due to solar rotation are evident from both techniques, and are more pronounced around autumn and spring equinoxes and less significant around winter and summer (Bhonsle et al., 1965). Of particular interest is the significant TEC depletions and enhancement observed from both techniques over all stations as shown by the grey-shaded bands. These observations were investigated by analysing the midday, 2002 Disturbance Storm Time (DST) index of geomagnetic activity as shown in Fig.2 (d). In particular, a closer analysis (not shown) indicated that TEC enhanced spikes occurred on Day 108 around the autumn equinox with a DST value of -124 nT during the recovery phase of the geomagnetic storm, and TEC depletions occurred on Day 274 around spring equinox with a DST value of -127 nT during the negative phase of the geomagnetic storm. This TEC behaviour is consistent with the interpretation that during geomagnetic storms, the response of the ionosphere depends on the interplay of various physical phenomena responsible for the occurrence of different phases of the storm. In particular, during the;

(a) Initial phase: the TEC is expected to be greater than the background values before the onset of the storm due to an upliftment of the dayside ionosphere as a result of the existence of an effective interplanetary electric field (Jakowski et al., 1992; Prölss, 1993; Fuller-Rowellet al., 1994; Tsurutani and Gonzalez, 1997; Basu et al., 2001; Tsurutani et al., 2004; Foster and Rideout, 2007). As a consequence, photoionisation of the lower F region produce new plasma, which replaces the uplifted plasma leading to an overall increase in the TEC,

(b) Main phase: the TEC is expected to be reduced below the normal values due to a downdraft of the ionosphere, which is mostly related to compositional changes in the atmosphere. These changes increase the number of molecular constituents, which enlarge recombination (Fuller-Rowell et al., 1997; Jakowski et al., 1999; Forster and Jakowski, 2000; Fedrizzi et al., 2005; Mendillo, 2006),

(c) Recovery phase: the TEC gradually recovers from (b) to normal values during a geomagnetically quiet day. Sub-storm activities are possible during this period, which may be responsible for TEC perturbations (Fedrizzi et al., 2005).

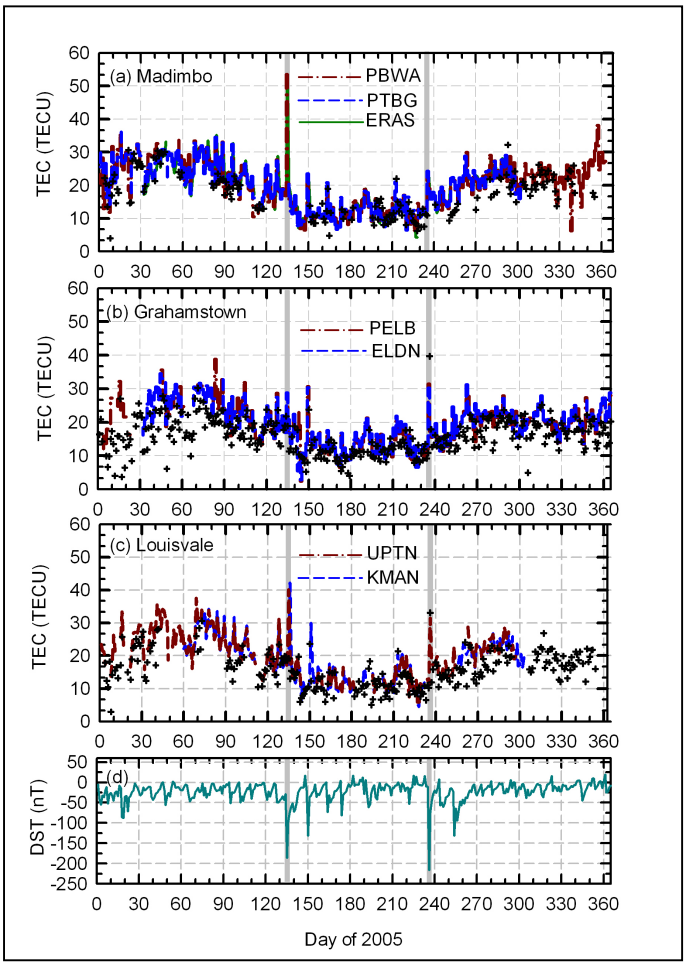

Figure 4.3: Similar to Figure 4.2, but shown for 2005 near solar minimum conditions.

4.3.2 Comparison of midday GTEC with ITEC measurements near solar minimum

The response of TEC on Day 325 with a DST value of -106 nT during the recovery phase of the geomagnetic storm was not well captured by either technique. However, this could be due to problems with data recordings by either technique. Interestingly, geomagnetic storm activitities seem to be increasing around equinoxes for period 2002 near solar maximum with the subsequent evidence of TEC perturbations from both techniques over all the stations. Further analysis and discussion on these observations is beyond the scope of this study, and require high temporal resolution data in order to study effects of geomagnetic storm phases on ionospheric TEC in great detail.

Figure 4.3 (a)-(c) is similar to Figure 4.2 (a)-(c), but is shown for the period 2005 near solar minimum conditions. It is clear that the variation trend of GTEC and ITEC are generally in good agreement. A less pronounced seasonal variation of TEC is evident from both techniques with maximum values (~30 TECU) around autumn and spring equinoxes and minimum values (~ 10 TECU) around winter and summer as compared to the year 2002 for the solar maximum as discussed in Section 4.1.

Short-term (~27 days) variations of TEC presumably attributed to the solar rotation period are also evident and pronounced around autumn and spring equinoxes and less enhanced around winter and summer. Of interest is the enhanced TEC spikes observed from both techniques over all stations as shown by shaded-grey bands. These observations were investigated by a closer analysis of the midday 2005 DST index shown in Figure 4.3 (d). In particular, TEC enhanced spikes occur on Day 135 around autumn equinox and Day 236 around spring equinox during the recovery phase of geomagnetic storms exhibiting values of DST = - 186 nT and -216 nT respectively. However, these observations are consistent with the interpretation that during the recovery phase of a geomagnetic storm, sub-storms are possible, which could be the cause of the observed TEC perturbations

(Fedrizzi, et al., 2005). Further investigation of the latter is beyond the scope of this study and should be left for future works where larger data sets are available. Of interest is the evidence of increased geomagnetic disturbances around equinoxes, which are not as frequent for the period 2002 near solar maximum. These observations seem to indicate that space weather activities occur frequently around equinoxes, particularly towards solar maximum.

4.4 The difference between midday GTEC and ITEC

In order to compute the difference between midday GTEC and ITEC for both the period 2002 near solar maximum and the period 2005 near solar minimum, the mean GTEC $= \frac{1}{n}\sum_{i}^{n} TEC_i$ (where *i =1 ...n,* represents the number of GNSS stations used*)* was calculated for the selected GNSS stations located near each Ionosonde station for the days where data was available. For illustration, Figure 4.4 shows the scatter plot of midday average GTEC against the corresponding ITEC values over Madimbo, Grahamstown and Louisvale stations for the year 2002 near solar maximum (Panels (a) – (c)) and the year 2005 near solar minimum (Panels (d) – (f)) respectively. In general, the scatter plots show a good correlation between both techniques over all sites. The lines drawn correspond to the best-fit line. However, a closer examination of the intercept of the best-fit lines reveals that the midday GTEC values exceed those of ITEC by ~1.96 TECU, ~0.73 TECU and ~0.32 TECU over Madimbo, Grahamstown, and Louisvale respectively for the year 2002 near solar maximum. For the year 2005 near solar minimum, the midday GTEC values exceed those of ITEC by ~0.58 TECU, ~1.18 TECU and ~1.88 TECU over Madimbo, Grahamstown, and Louisvale respectively. The latter values, particularly over Grahamstown and Madimbo (~ 1.18 TECU and ~0.58), are significantly lower than the ~3.6 TECU recently reported by McKinnell et al. (2007). A reason could be that for this study we only considered the midday (10:00 UT) TEC values from both techniques while the McKinnell et al. (2007) study used diurnal TEC data from March to June 2005. Nevertheless, these results are comparable with related studies performed using data in the Northern Hemisphere (Lunt et al., 1999; Belehaki et al., 2003; Zhang et al., 2006).

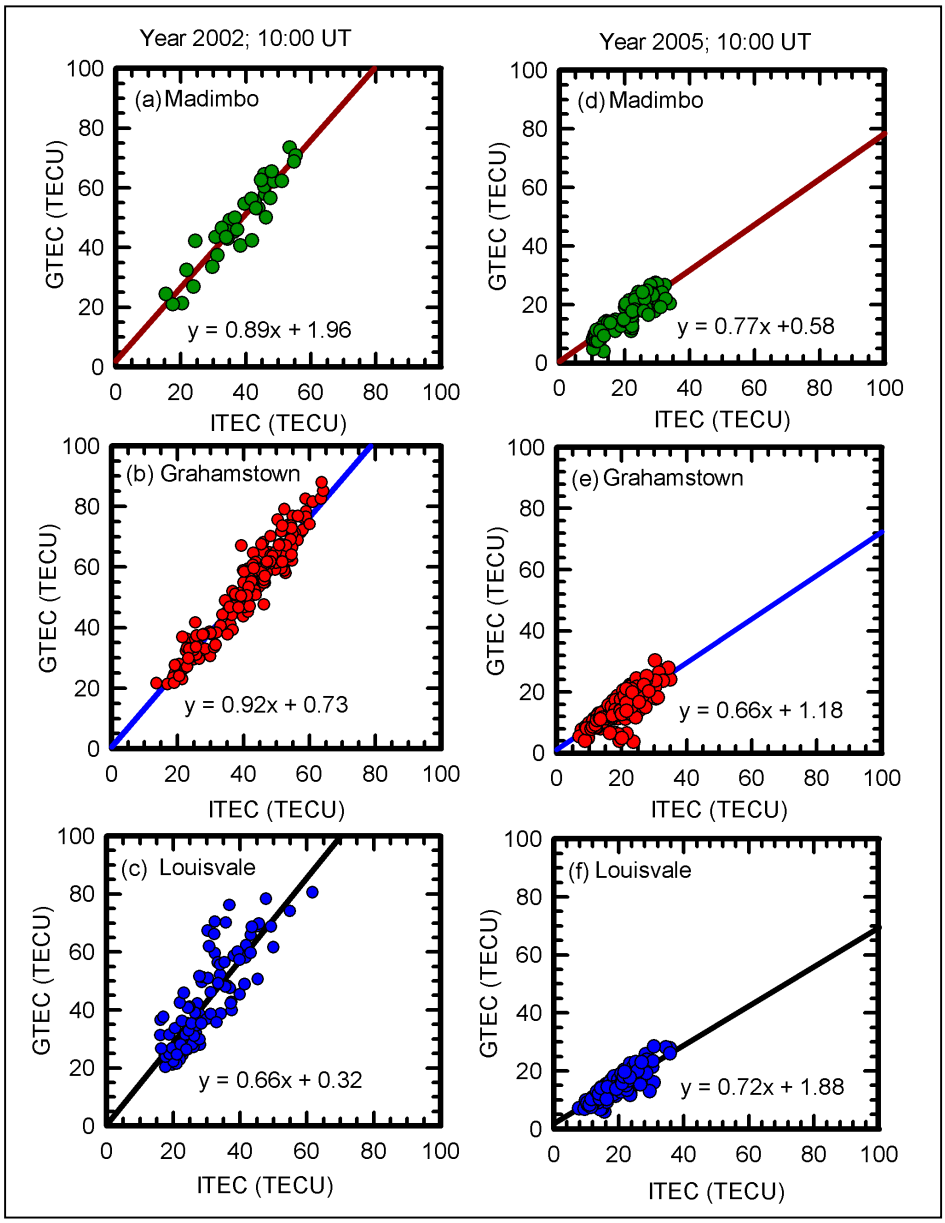

Figure 4.4: The scatter plot of midday (10:00 UT) GTEC against the corresponding ITEC over Madimbo, Grahamstown and Louisvale stations. Panels (a), (b) and (c) correspond to the period 2002 near solar maximum and (d), (e) and (f) represent period 2005 near solar minimum. The lines drawn correspond to the best-fit line.

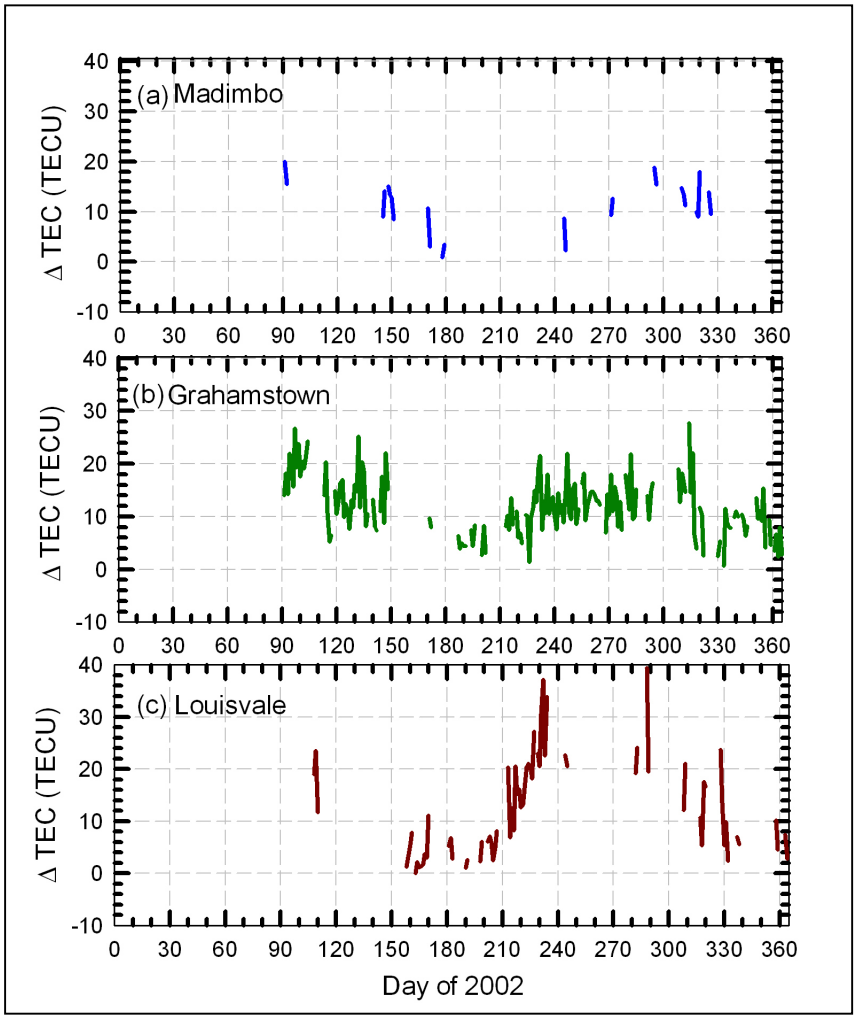

Figure 4.5: Computed difference ΔTEC between mean GPS TEC and Ionosonde TEC measurements over (a) Madimbo, (b) Grahamstown, and (c) Louisvale for period 2002 near solar maximum conditions.

Furthermore, the residual $\Delta TEC = GTEC - ITEC$, which corresponds to plasmaspheric electron content (e.g. Reinisch and Huang, 2001; Belehaki et al., 2003), was computed over (a) Madimbo, (b) Grahamstown and (c) Louisvale stations and is shown in Figure 4.5 and Figure 4.6 for the year 2002 near solar maximum and the year 2005 near solar minimum conditions, respectively. It is

evident that midday ΔTEC trends over all stations show pronounced seasonal variations for the period around 2002 with large values (~ 20 TECU) around autumn and spring equinoxes and small values (~ 4 TECU) around winter and summer solstices. For the year 2005, plasmaspheric electron content is highly variable with a minimum value of ~2 TECU and a maximum value of ~10 TECU over all stations.

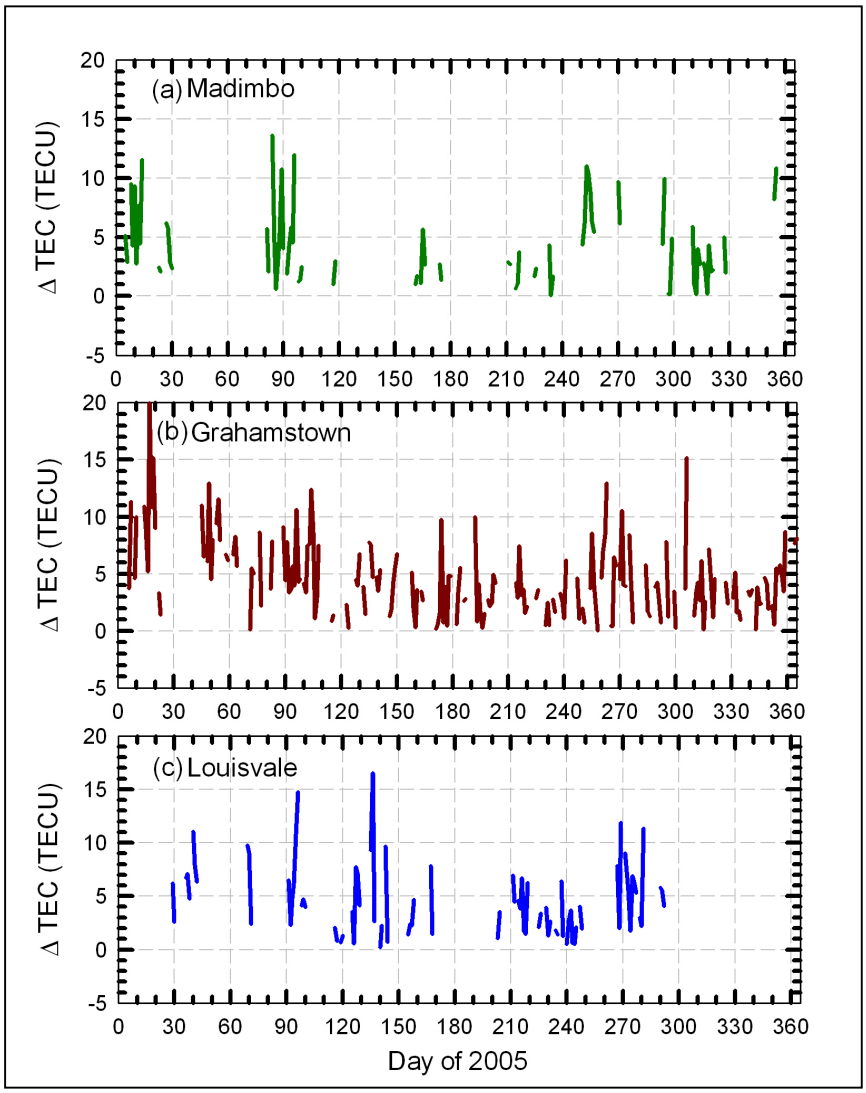

Figure 4.6: Similar to Figure 4.5, but is shown for the period 2005 near solar minimum conditions.

The seasonal variation is difficult to trace considering plasmaspheric electron content trends. This could be an indication of the reduction of the seasonal variation trend of the plasmaspheric electron content towards solar minimum conditions. However, noting that there was a lack of data recorded for some days by both techniques, more data is required in future to further investigate the dynamics and variations of plasmaspheric electron content over South Africa so that its contribution to TEC can be understood.

4.5. Variations of equivalent midday ionospheric total slab thickness parameters

The slab thickness may be regarded as the depth of an imaginary ionosphere, which has the measured TEC and uniform electron density equal to the maximum electron density of the actual ionosphere (Breed and Goodwin, 1997; Forster and Jakowski, 2000; Belehaki et al., 2003). For a given foF2 value, the slab thickness depends on the electron density versus height profile, the sharper the peak electron density the smaller is the slab thickness. The slab thickness is calculated using both GTEC and ITEC parameters according the formulae:

$$\tau_t = \frac{GTEC}{N_m F2} = \alpha \cdot \frac{GTEC}{f_o F2^2} \ , \tag{4.1}$$

and

$$\tau_i = \frac{ITEC}{N_m F2} = \alpha \cdot \frac{ITEC}{f_o F2^2} . \tag{4.2}$$

Here α is a coefficient equal to 806.45 and is determined according to the relation between the electron density NmF2 and the critical frequency foF2:

$$N_m F2 / 1\ \mathrm{m}^{-3} = \frac{1}{80.6}\left(\frac{f_o F2}{1\ \mathrm{Hz}}\right)^2 , \tag{4.3}$$

and foF2 is units of MHz, and τ in km respectively. The τ_t includes the electron content of both the ionosphere and the plasmasphere up to ~20 200 km while τ_i provides electron contents of the

bottomside and topside ionosphere up to ~1000 km (Breed and Goodwin, 1997; Belehaki et al., (2003).

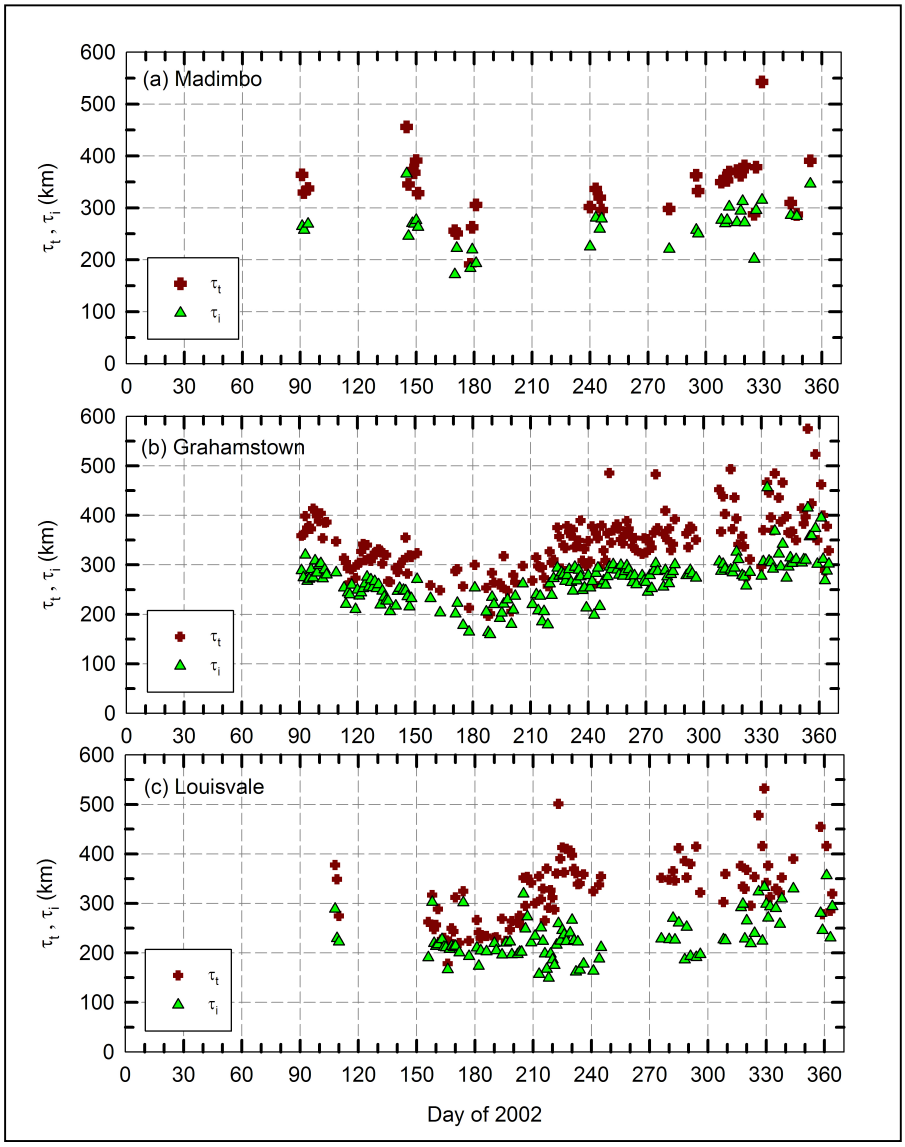

Figure 4.7: Variation of the midday ionospheric slab thickness parameters τ_t (red cross) and τ_i (green triangles) over (a) Madimbo, (b) Grahamstown, and (c) Louisvale for the year 2002 near solar maximum conditions.

Figure 4.7 (a)-(c) depicts the midday variation of slab thickness parameters τ_t and τ_i over (a) Madimbo, (b) Grahamstown, and (c) Louisvale for the year 2002 near solar maximum conditions. It is inferred from the panels that variation trends of τ_t and τ_i are in good agreement over all stations and show a pronounced seasonal variation with maximum values (~200 km to ~500 km) around summer and minimum values (~200 km to ~ 300 km) around winter. These results are consistent with the Miro et al. (1999) results obtained over EL Arenosillo (37.1° N, 6.7° W) middle latitude station. The seasonal variation trends are in phase with the near midday plasma temperature or plasma scale height (Miro et al., 1999; Belehaki et al., 2003). A noticeable difference between τ_t and τ_i is also evident in all panels which is attributed to the plasmaspheric electron content contributions in determining the total slab thickness particularly towards the year 2002 (high solar activity). It is important to mention that under a quiet-day time the ionosphere is mainly controlled by diffusion (e.g. Forster and Jakowski, 2000).

Figure 4.8 (a)-(c) is similar to Figure 4.7, but shown for the year 2005 near solar minimum conditions. The variation trends of τ_t and τ_i over all stations are in good agreement and show a less pronounced seasonal variation, which maximises (~200 km to ~ 500 km) around summer and minimises around winter (~150 km to ~300 km). Of interest is the small difference between τ_t and τ_i over all the stations compared to year 2002 of high solar activity. This could be indicating a state close to diffusion equilibrium between the ionosphere and the plasmasphere as reported in Belehaki et al., 2003.

By comparison, it is evident that the midday total slab thickness parameters τ_t and τ_i computed for year 2002 near solar maximum and year 2005 near solar minimum conditions over all the stations, maximises around the summer season. This is in contrast with midday GTEC and ITEC, which maximises around equinoxes as discussed in Section 4.1 and 4.2. However, these results are

consistent with Bhonsle et al., 1965 findings for the mid-latitude seasonal variation of the slab thickness and total electron content derived using beacon satellite measurements.

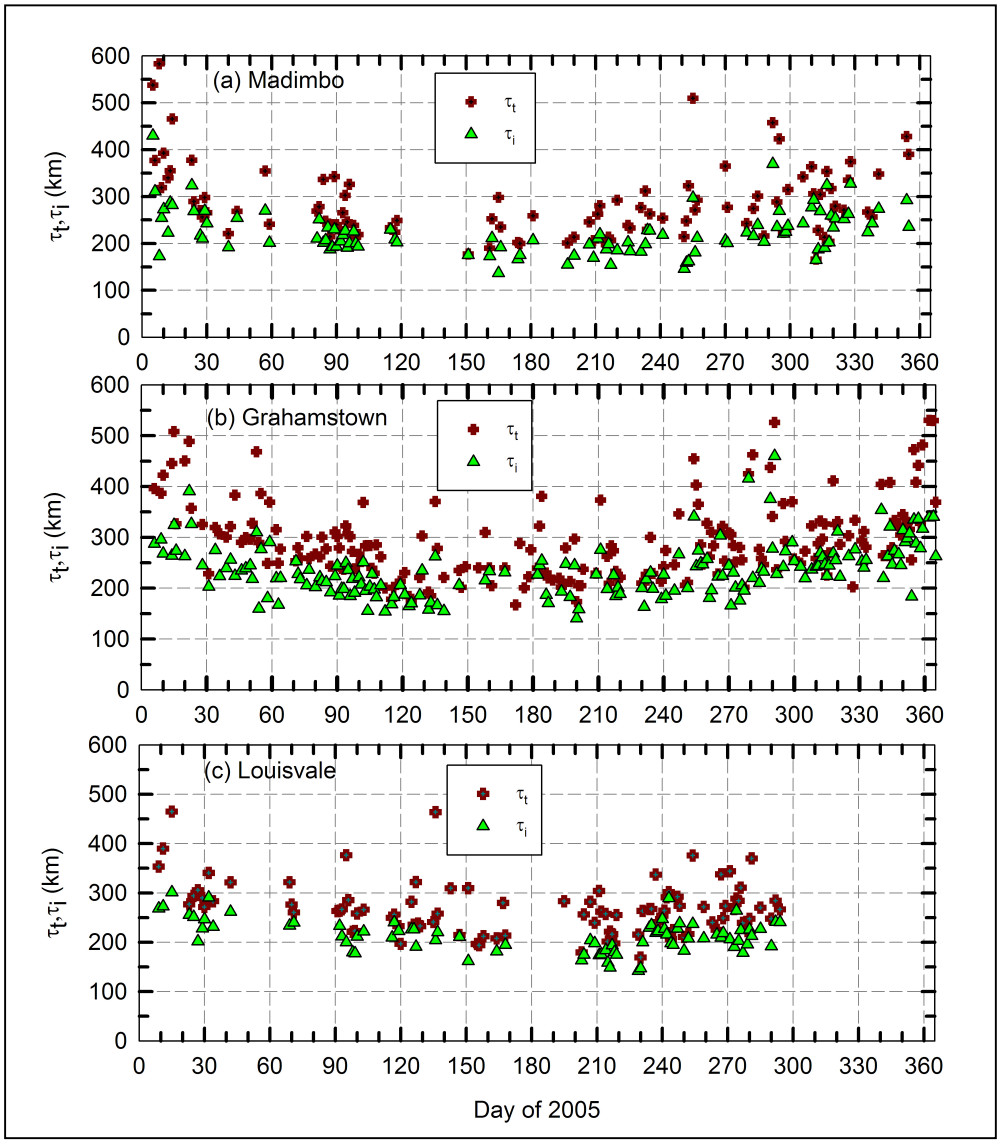

Figure 4.8: Similar to Figure 4.7, but shown for the period 2005 near solar minimum conditions.

5. Summary and Conclusions

This work reports on the validation of UNB-IMT midday GTEC results using the ionosonde-derived total electron content (ITEC) measurements over South Africa during the years 2002 and 2005, corresponding to solar maximum and minimum conditions respectively. It was found that in general both techniques showed a good degree of agreement. In particular, the variation trends of GTEC and ITEC over all stations showed a pronounced seasonal variation for the period near solar maximum, with maximum values (~ 80 TECU) around autumn and spring equinoxes, and minimum values (~22 TECU) around winter and summer solstices. For the period near solar minimum, the seasonal variation trends were found to be less pronounced with maximum values (~30 TECU) around equinoxes and minimum (~10 TECU) values around summer and winter. Short-term variations of TEC (presumably due to solar rotations) were evident from both techniques and were more pronounced during the autumn and spring equinoxes near solar maximum than solar minimum. Of interest were the signature of TEC depletions and enhanced spikes revealed by both techniques, occurring more frequently around equinoxes particularly near solar maximum conditions. These observations were investigated by an analysis of the midday DST index of the geomagnetic activities. It was found that geomagnetic storm activity was forcing the observed TEC perturbations. In particular, the observed TEC depletions and enhanced spikes were due to an interplay of various phenomena occurring during different phases of geomagnetic storms and are consistent with the findings of the related studies reported (Jakowski et al., 1992; Tsurutani and Gonzalez, 1997; Fuller-Rowell et al., 1997; Jakowski et al., 1999; Fedrizzi et al., 2005).

A comparison between GTEC and ITEC values found that in general good inter-technique correlations exist during solar maximum and minimum periods respectively. Finally, the residual $\Delta TEC = GTEC - ITEC$ was computed for the Ionosonde stations. It was evident that ΔTEC, which corresponds to plasmaspheric electron content, showed a pronounced seasonal variation with maximum values (~ 20 TECU) around equinoxes and minimum (~ 5 TECU) around winter near solar maximum. For the period 2005, plasmaspheric electron content was found to be highly

variable with a minimum value of ~2 TECU and a maximum value of ~10 TECU over all stations. The variation trend of plasmaspheric electron content near solar minimum was found to display a complicated picture. This could be an indication of the reduction of seasonal variation trends towards solar minimum conditions.

The ionospheric and total slab thickness parameters were also computed. It was evident that the ionospheric and total slab thickness over all stations maximises around summer, which is in contrast with the seasonal variation of midday GTEC and ITEC, which maximises around equinoxes. These results are consistent with earlier studies of TEC using beacon satellites (Bhonsle et al., 1965) and, therefore verified the use of UNB-IMT as one of the tools for current and future ionospheric TEC research and applications.

The next Chapter, The UNB-IMT is applied to study the variations of GNSS-derived TEC maps over South Africa during different epochs of solar cycle 23.

Chapter 5

MAPPING GNSS-DERIVED TEC OVER SOUTH AFRICA DURING DIFFERENT EPOCHS OF SOLAR CYCLE 23

5.1 Introduction

The current trend in ionospheric physics research has proven that the dual frequency (L1 = 1575.42 MHz and L2 = 1227.60 MHz) signals transmitted by the GNSS, and received by the network of GPS receivers distributed worldwide provide a unique opportunity to determine the higher resolution spatial and temporal ionospheric TEC at regional and global level (e.g. Jakowski and Paasch, 1984; Klobuchar, 1991; Komjathy and Langley, 1996; Jakowski, 1996; Komjathy, 1997; Mannucci et al. 1998). The magnitude of TEC is highly variable and depends on several factors such as local time, geographical location, season and solar activity cycle (e.g. Jakowski, 1996; Jakowski et al. 1999; Jakowski, et al. 2002; Immel et al. 2003; Tsurutani, et al. 2004, Skoug et al. 2004; Jee, et al. 2005; Mannucci et al. 2005; Fedrizzi, et al. 2001). Recent studies (Jakowski et al. 2001; Jakowski et al. 2002) illustrate that TEC monitoring using the GNSS network can contribute to space weather monitoring.

Based on the validation of UNB-IMT results with Ionosonde TEC measurements over South Africa presented in Chapter 4, it is possible to adopt and use this model as a tool to characterise variations and dynamics ionospheric TEC over southern Africa. In this Chapter, UNB-IMT is applied to study the solar cycle variations of TEC maps over the South African region using data from the Southern African GNSS networks described in Chapter 4. For this task, the monthly averaged sunspot number was used as a proxy for solar activity cycle 23 as shown in Figure 5.1. From these monthly averaged values, it is well established that the Sun has a quasi-periodic ~11 year activity cycle (e.g. Smith and

Marsden, 2003). Approximately every 11 years the Sun moves through a period of fewer sunspots that is termed 'solar minimum' followed by a period of maximum activity that is termed 'solar maximum'.

TEC observations around a selected day and hour during an extreme solar maximum period display interesting features which could be associated with frequent solar activity events. These observations are further investigated by analyzing the GOES 8 X-ray flux (0.1 – 0.8 nm) data and the SOHO Charge, Element and Isotope Analysis/Solar Extreme Ultraviolet Monitor (CELIAS/SEM) 26.0 – 34.0 nm higher resolution data. These instruments are briefly discussed in Chapter 2.

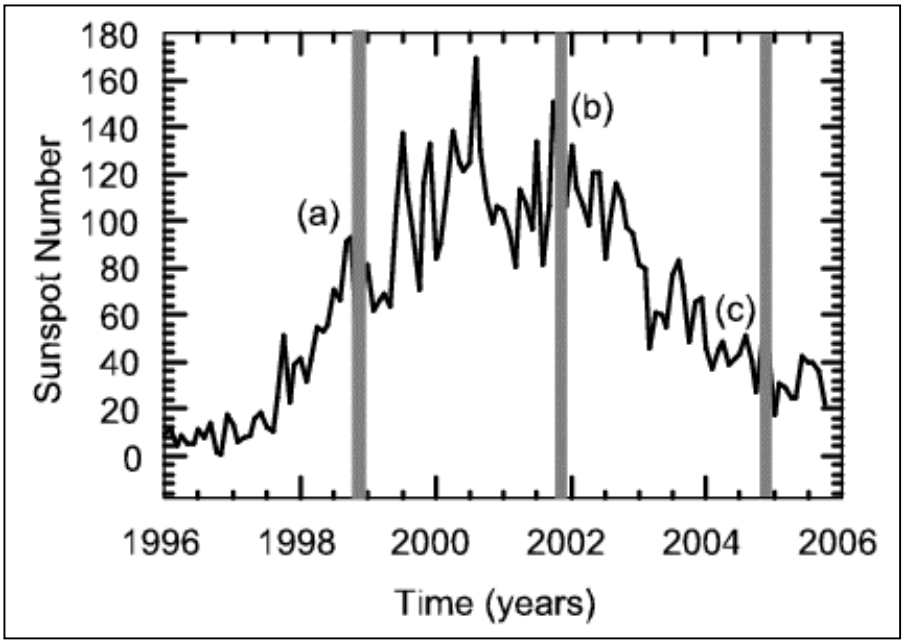

Figure 5.1: Monthly averaged sunspot number for solar cycle 23. The shaded regions depict selected day 345 at 14:00 UT for different epochs of solar cycle 23. Epoch "(a)" represents intermediate solar activity conditions during the ascending phase; "(b)" represents extreme solar maximum conditions during the peak; and "(c)" represents the descending phase of the solar cycle.

A detailed description of CELIAS/SEM 26.0 – 34.0 nm sensor can be obtained from Hovestadt et al. (1995) and Judge et al. (1998, 2001; 2002). Comparisons of the TEC derived from the collocated HRAO and HARB receiver during the solar X17 and X9 flares events, which occurred on day 301, 2003 during moderate solar activity conditions and day 339, 2006 during solar minimum conditions respectively was done by comparing the TEC difference between these stations. Furthermore, the daytime TEC computed with the UNB-IMT algorithm are comprehensively compared with TEC values computed with the IRI 2001 model predictions described in Chapter 3, to further test the reliability of the UNB-IMT results over southern Africa. Extracts from this chapter have been published in Moeketsi et al. (2007a; b).

5.2 Observations and data analysis

The data sampled at 30 s from 11 International GNSS Services and 10 Southern African Development Community (SADC) of dual frequency GPS receivers were used in this chapter as an input to the UNB-IMT software described in Chapter 3. The geographical coordinates and geomagnetic latitudes of stations used are listed in Table 5.1 and illustrated on the map shown in Figure 5.2. The International GNSS data used is obtained from ftp://lox.ucsd.edu/pub/rinex and can also be obtained from HartRAO data server ftp://geoid.hartrao.ac.za, while the CDSM Trignet were obtained from ftp://www.trignet.co.za (Combrinck et al., 2003). The quality of GPS data was checked for all stations using the UNAVCO Translate/Edit/Quality Check (TEQC) software (Estey and Merteens, 1999).

International GNSS stations	Geographical Latitude (°)	Geographical Longitude (°)	Geomagnetic Latitude (°)
SOYG	-69.58	39.58	-70.88
VESL	-71.67	357.16	-66.06
GOUG	-40.38	350.13	-35.00
MALI	-2.99	40.19	-6.77
DAV1	-68.58	77.97	-74.60
ASC1	-7.95	345.59	-2.35
NKLG	0.35	9.67	1.86
MAW1	-67.60	62.87	-73.22
SEY1	-4.67	55.48	-10.81
REUN	-21.21	55.57	-27.18
KERG	-49.35	70.23	-56.93
SADC GNSS			
HRAO	-25.89	27.69	-27.13
HARB	-25.89	27.71	-27.13
RBAY	-28.80	32.08	-30.76
SUTH	-32.38	20.81	-32.26
S121	-25.74	28.22	-27.09
ZAMB	-15.43	28.31	-16.97
UPTN	-28.41	21.26	-28.46
EMLO	-26.50	29.50	-28.05
SIMO	-34.19	18.44	-33.61
TDOU	-23.08	30.38	-24.85
PELB	-33.98	25.61	-34.68

Table 5.1. Geographic coordinates and geomagnetic latitudes of international GNSS and SADC GPS stations used in this study.

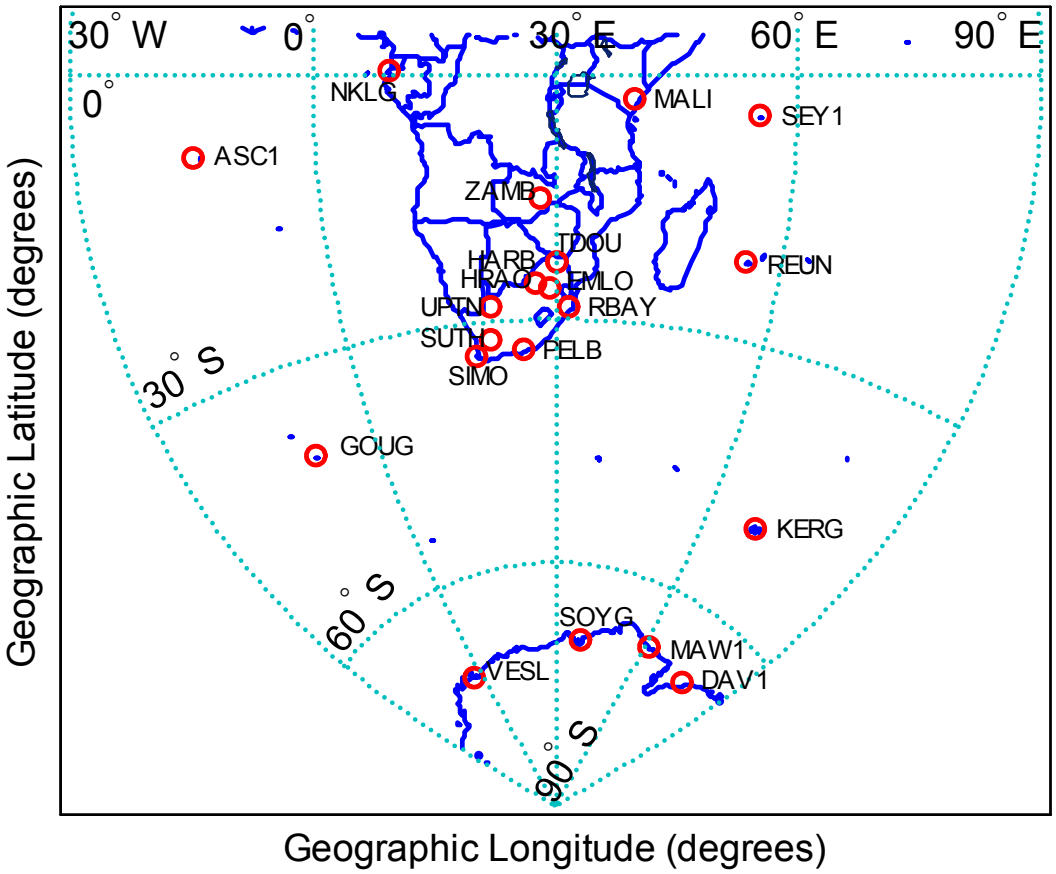

Figure 5.2: Southern African geographical map showing the distribution of the ground based International GNSS and SADC network of dual frequency GPS stations (red cycles).

The software module "EditObs" developed locally (Ngcobo et al., 2005) as discussed in Chapter 3, was used to edit RINEX GPS observation file and create a new RINEX file, which contains GPS observables used by UNB-IMT software during the computations. The station HRAO was chosen as a reference station based on its central location and the good quality data for the period of interest to this study. Furthermore, the sunspot number and DST index data used in this study as proxies for solar cycle and geomagnetic activity were obtained from http://www.spaceweather.com and http://swdcwww.kugi.kyoto-u.ac.jp. The SOHO CELIAS/SEM and GOES X-ray data used in the

analysis were obtained from http:www.usc.edu/dept/space_science/semdata and http://goes.ngdc.noaa.gov/data respectively.

5.3 Mapping TEC during different periods of Solar Cycle 23

A common day and time (Day 345, 14: 00 UT) was selected during different epochs of solar cycle 23. The epochs selected are indicated as (a), (b) and (c) in Figure 5.1 and refer to:

"(a)" the moderate solar activity conditions around 1998 during the ascending phase of the solar cycle;

"(b)" the extreme solar maximum conditions around 2001; and

"(c)" the moderate solar activity conditions around 2004 during the descending phase of the solar cycle as discussed in section 5.1 for the purpose of this study.

Figure 5.3 (a), (b) and (c) display the TEC maps computed with the UNB-IMT software over South Africa for the different selected epochs of solar cycle 23. Evidently, TEC values computed for epochs "(a)" and "(c)" are comparable and increase towards low latitudes as expected. Furthermore, TEC values computed for epoch "(b)" are significantly higher than for epochs "(a)" and "(c)" respectively. These observations are possible because of the high rate of production of solar EUV and X-ray radiation during the period of maximum solar activity conditions, which causes significant photoionisation within the daytime ionosphere resulting in relatively high TEC values compared to moderate and low solar activity. Of particular interest on the TEC map for epoch "(b)" is the double peak display with enhanced TEC values near mid-latitudes comparable with values observed towards the lower latitudes. An attempt was undertaken to investigate possible causes of this midlatitude enhanced TEC peak anomaly by analyzing the disturbance storm time (DST) index shown in Figure 5.4(a). It is evident from this approach that day 345 of the year 2001 was geomagnetically quiet with DST > -20 nT, which implies that the observed TEC anomaly near mid-

latitudes is not associated with geomagnetic activity. It should be noted that the DST value for day 345, in both 1998 and 2004 was also found to be > -42 nT.

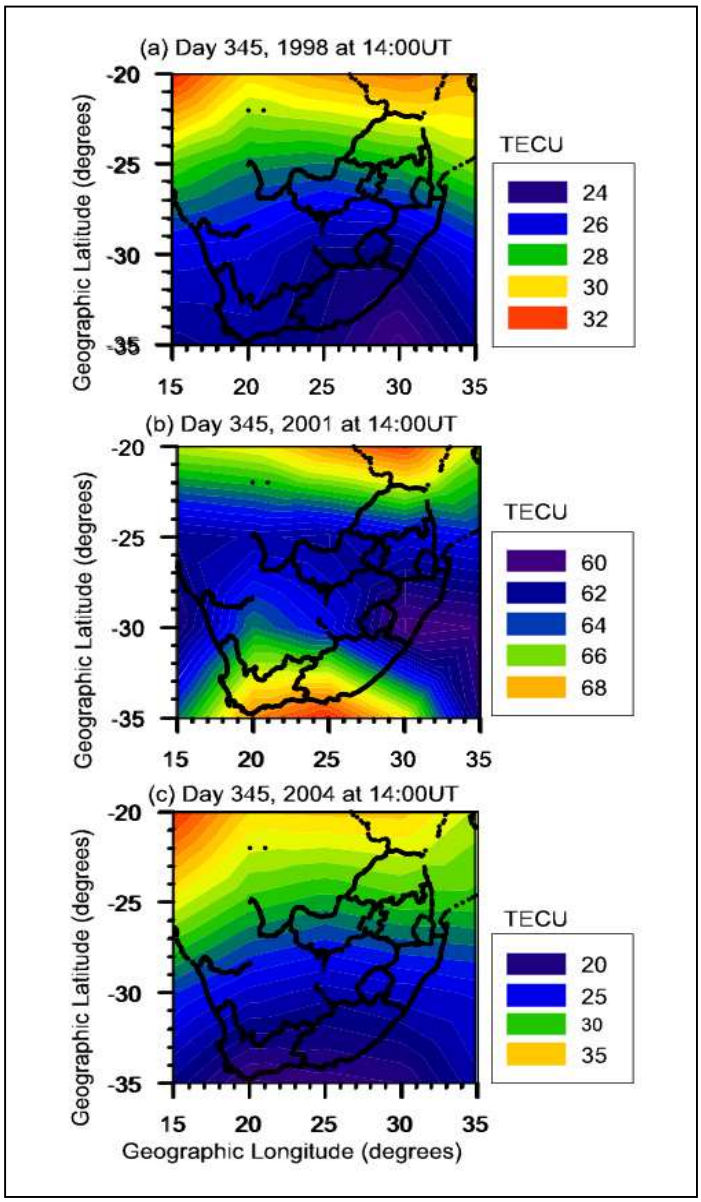

Figure 5.3: South Africa TEC maps computed using the UNB-IMT code for day 345 at 14:00 UT for the different epochs of solar cycle 23 indicated in Figure 5.1.

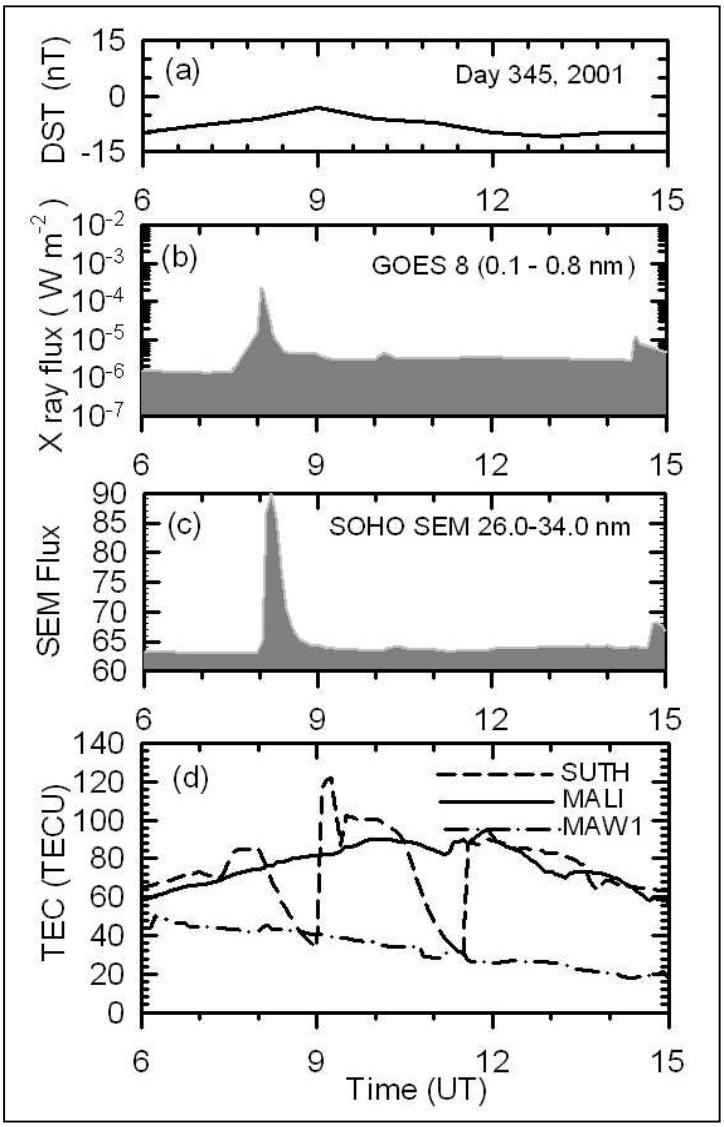

Figure 5.4: The day 345, 2001 solar X28 flare. The different panels depict: (a) Disturbance Storm Index (DST) measurements, (b) GOES 8 five minute average X-ray fluxes on the 0.1 – 0.8 nm wavelengths band, (c) SOHO SEM five minute average EUV fluxes on the 26.0 – 34.0 nm wavelength band and (d) UNB-IMT five minute TEC observed over MALI (Solid line), SUTH (dashed line), and MAW1 (dash-dot-dash line) respectively. The SEM EUV fluxes are in units of (photons/cm^2/s$\times$ 10^9).

However, a further investigation was conducted by analyzing the five minute averaged GOES 8 satellite X-ray (0.1 – 0.8 nm) flux and SOHO CELIAS/SEM (26.0-340 nm) measurements for day 345, 2001 shown in Figure 5.4(b) and (c) respectively. It should be noted that CELIAS/SEM 26.0 - 34.0 nm channel time series data has shown that this channel is not sensitive to X-rays as reported in Tsurutani et al. (2005). It became clear from this analysis that GOES 8 recorded an X-ray flare of magnitude X28 at ~ 8.05 UT. Interestingly, the SEM EUV instrument onboard SOHO also observed a EUV flare event associated with the recorded X ray flare. The X-ray fluxes show that the flare occurred at ~7:50 UT and reached a peak intensity at ~8:05 UT. The EUV flare seems to have occurred later at ~8:00 UT and reached maximum peak intensity at ~8:05. The decay phase of both flares took much longer (~45 minutes) to reach the inertial background before the onset of the flares.

To investigate the effects of these flares on TEC, Figure 5.4 (d) shows the UNB-IMT five minute averaged TEC between 6:00 UT and 15:00 UT. TEC are shown over GPS stations at low latitudes (MALI), midlatitudes (SUTH) and higher latitudes (MAW1) respectively. For the SUTH midlatitude station, a simultaneous increase in TEC was evident at the onset of the X-ray flare reaching a maximum enhancement value of ~20 TECU above the background just before the onset of the EUV flare, at which, the TEC over SUTH decreased abruptly to a minimum value of ~ 32 TECU around 9:00 UT and suddenly increased sharply to ~124 TECU within 20 minutes and decreased instantly to have a minimum value of ~ 28 TECU around 11:45 UT. Furthermore, TEC values suddenly increased again to reach a maximum value of ~ 84 TECU around 12:00 UT and decreased gradually without large variations after noon as expected. No such TEC perturbations were observed over the MALI and MAW1 GPS stations. Of interest is that the TEC values over SUTH located in the vicinity of the observed TEC peak anomaly seems to be comparable with TEC values over MALI. However, TEC values over MALI seem to be averaged compared to those observed over SUTH after the decay phase of the flares, while TEC over MAW1 remained significantly lower and gradually decreased throughout this period.

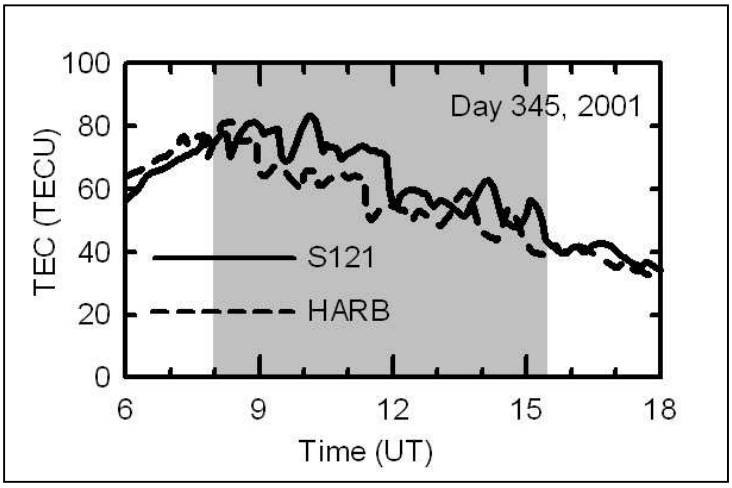

Figure 5.5: The S121 (solid line) and HARB (dashed line) TEC response due to the day 345, 2001 solar X28 flare.

Figure 5.5 depicts the UNB-IMT five minute averaged TEC between 6:00 UT and 18:00 UT for midlatitude GPS station HARB and S121 located not far from SUTH. Evidently, pronounced TEC variation occurs over both stations at the onset of the EUV flare. TEC variation took longer (shaded period) than the duration of the flare. The ionospheric TEC response due to this flare seems to be localized, however, more data and further investigations is required to explore this possibility. The observed high sharp intensity (90×10^9 photons/cm^2/s) peak of EUV could be the cause of the ~3 hr TEC variation over SUTH and the subsequent lengthy TEC variation over HARB and S121. However, the near mid-latitude peak anomaly (enhanced ionisation) on the TEC map during extreme solar maximum conditions may be due to particle precipitation from the outer radiation belt at latitude > 30 degrees South as a result of this flare or problem related to the TEC calibration, possibly caused by non-detected cycle slips in the phase data. Although this explanation is likely, more data is required to substantiate it.

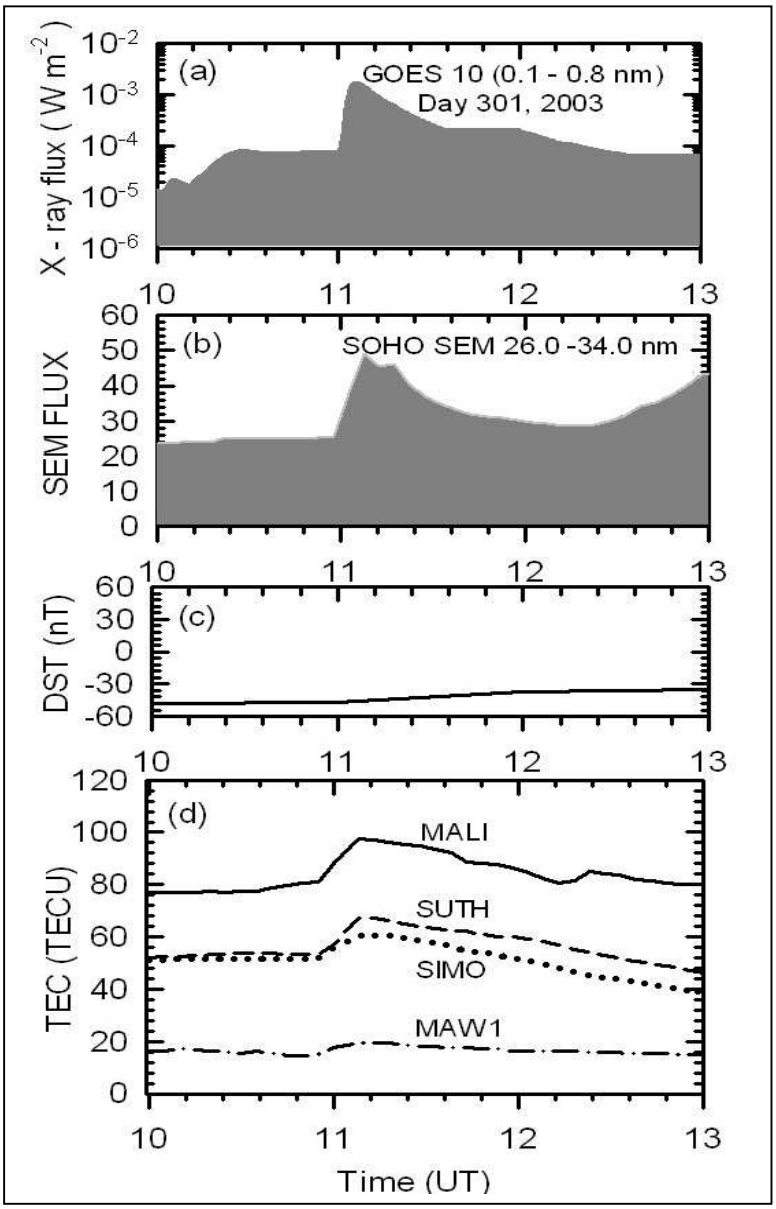

Figure 5.6: The day 301, 2003 solar X17 flare. The different panels show: (a) GOES 10 five minute average X-ray fluxes on the 0.1 – 0.8 nm wavelength band, (b) SOHO SEM five minute average EUV fluxes on the 26.0 – 34.0 nm wavelength band, (c) Disturbance Storm Index (DST) measurements, and (d) UNB-IMT five minute TEC observed over MALI (solid line), SUTH (dashed line), SIMO (dotted line) and MAW1 (dash-dot-dash line) respectively. The SEM EUV fluxes are in units of (photons/cm^2/s$\times$ 10^9).

Earlier studies of the solar flare effects on the ionosphere have identified sudden ionospheric disturbances (Thome and Wagter, 1971; Mitra 1974; Donelly, 1976). However, to further investigate the effects of flares on GPS derived TEC over southern Africa, Figures 5.6 (a) and (b) show the GOES 10 satellite 0.1 – 0.8 nm X-ray fluxes and SOHO SEM 26.0 – 34.0 nm fluxes observed between 10:00 UT and 13:00 UT on day 301, 2003 during the recorded X17 flare event. The global effects of this flare on ionospheric TEC derived from the worldwide GPS network were recently studied (e.g. Tsurutani et al. 2005; Zhang and Xiao, 2005). The X-ray flux measurements show that the flare occurred at ~11:00 UT and reached a peak at ~ 11:10. The decay phase of the flare took much longer (~1 hr 30 minutes) and reached the background level at ~ 12:40 UT. The EUV flare occurred simultaneously as the X-ray flare, but show a double peak at ~11:10 UT and at ~ 11:20 UT respectively. The decay period took almost the same time as the X-ray flare. The increase in SEM data after ~12:30 UT is not EUV flux, but it could be a contribution from the interaction of solar energetic particles (SEPs) with the SEM detector (*Jones, 2005; Private communication*). Figure 5.6 (c) shows that on day 301, 2003 geomagnetic activity was very low, with a DST > - 44 nT.

Figure 5.6 (d) depicts the ionospheric TEC response to the day 301, 2001 flare event over GPS stations MALI (near equatorial), SUTH and SIMO (mid-latitude) and MAW1 (high latitude) respectively. A sudden rapid increase in TEC over all GPS stations is evident from ~11:00 UT to ~11:10 UT and decreases gradually to reach values comparable to the values before the flare onset at ~ 12:40 UT. In particular, during the first rapid phase of the flares TEC over these locations was enhanced with respect to the background (prior) values as follows: MALI by ~20 TECU, SUTH by ~16 TECU, SIMO by ~ 8 TECU, and MAW1 by ~4 TECU.

It is evident from these results that TEC values were significantly enhanced for a near equatorial station (MALI), and the enhancement values decrease with increasing geographic latitudes of the GPS station to have lower values at MAW1. These results are consistent with Tsurutani et al. (2005)

who reported that the largest TEC enhancement occurred at the sub-solar region (Africa equatorial GPS station), with a TEC increase of ~22 TECU above the background. It is evident that the EUV flare associated with the X-ray flare causes photoionisation within the daytime ionosphere which results in significant TEC enhancements lasting longer (~3 hrs) than the duration of the flare.

Comparison of the two X-ray/EUV flares analyzed in this work indicates that the X28 flare was the largest and most intense in the 0.1 – 0.8 nm wavelength band, indicative of strong spectral variability between the two. The EUV flare event associated with this flare has a high intensity and a sharp peak. The high intensity ($\sim 90 \times 10^9$ photons/cm^2/s) sharp feature of the flare peak may lead to enhanced localized photoionisation within the daytime ionosphere. The latter possibility should be investigated in future work on the flare-ionosphere relationship. The EUV flare associated with the X17 flare has moderate intensity ($\sim 50 \times 10^9$ photons/cm^2/s) with a slightly broad peak. The broad sharp feature of this flare peak could be responsible for the global photoionisation within the daytime ionosphere. Further investigations on the characteristics of X-ray/EUV flares using more data sets is required to better understand their effects on the ionosphere (see Liu et al., 2006).

5.4 Comparison of TEC derived from two collocated GNSS receivers over HartRAO during solar flares

Two solar X-ray flare events which occurred on day 301, 2003 during moderate solar activity conditions and Day 339, 2006 during solar minimum conditions, are selected in this section to compare the behaviour of ionospheric TEC over two different collocated GNSS receivers, namely HRAO and HARB. The HRAO (ASHTECH X-ZII3) and the HARB (TRIMBLE 4000SSI) GNSS receivers are located ~3 km apart at Hartebeesthoek, South Africa. The classification and duration of these selected flare events are summarised in Table 5.2.

Flare Class	Onset time (UT)	Peak time (UT)	End time (UT)
X17	11:00	11:10	11:30
X9	10:18	10:35	10:45

Table 5.2: Summary of time duration of the X17 and X9 flares selected in this study.

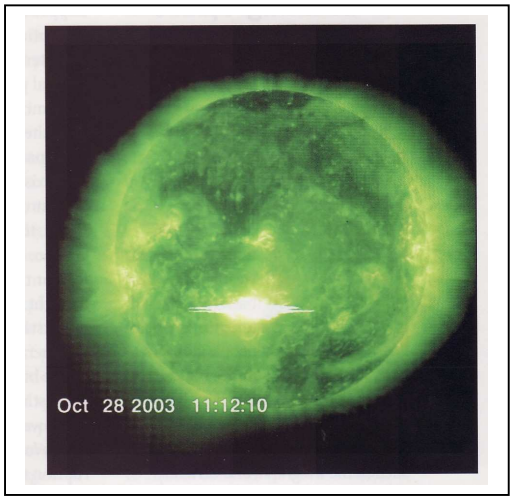

Figure 5.7: Day 301, 2003 at 11:12 UT Solar X17 flare (bright region) observed by Solar X-Ray Imager onboard GOES-12 Satellite (Liu, et al., 2007)

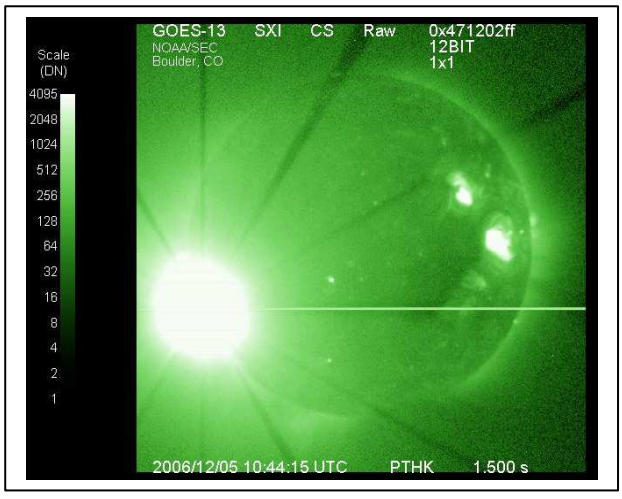

Figure 5.8: Day 399, 2006 at 11:44 UT Solar X9 flare (bright region) observed by Solar X-Ray Imager onboard GOES-13 Satellite (http://goes.ngdc.noaa.gov/data/plots/).

Figures 5.7 and 5.8 depict examples of the images recorded on day 301, 2003 at 11:12 UT and day 339, 2006 at 10:44 UT for solar X17 and X9 flares observed by the Solar X-ray Imager onboard the GOES 12 and GOES 13 satellites (http://sxi.ngdc.noaa.gov/images/; Liu et al., 2007).

The X17 is the most intense flare which occurred on day 301, 2003 around ~11:00 UT and reached peak intensity within 10 minutes, thereafter taking longer to decay as shown in Table 5.2. The X9 flare occurred on day 339, 2006 at ~10:18 UT and peaked at 10:35 UT and then decayed slowly back to the initial background values measured before the onset of the flare (http://goes.ngdc.noaa.gov/data/plots/). The ionospheric TEC response due to these flares over HRAO and HARB is discussed below.

5.4.1 The X17 flare on day 301, 2003

Figure 5.9(a) illustrates a comparison of the five minute averaged TEC over HRAO (dashed lines) and HARB (solid line) between ~6:00 and ~18:00 UT for the X17 flare. The TEC over these stations are compared by computing the TEC difference $\Delta TEC = HRAO_{TEC} - HARB_{TEC}$, as shown in Figure 5.9(b). It is evident that the TEC over HRAO ($HRAO_{TEC}$) is slightly (~5 TECU) higher than the TEC over HARB ($HARB_{TEC}$) during the early hours between ~6:00 and ~8:00 UT. However, the TEC value recorded between the (~8:00 – 10:00 UT) and (~13:00 – 15:00 UT) periods over both stations is comparable. The TEC over HARB and HRAO display a rapid increase from the onset of the X17 flare and reach the peak within ~ 10 minutes, after which it decreases gradually to reach the background values before the onset of the flare at ~ 13:00 UT. The difference between $HRAO_{TEC}$ and $HARB_{TEC}$ is large (~9 TECU) during the peak of the flare and after ~15:00 UT towards the night as shown in Figure 5.9(b).

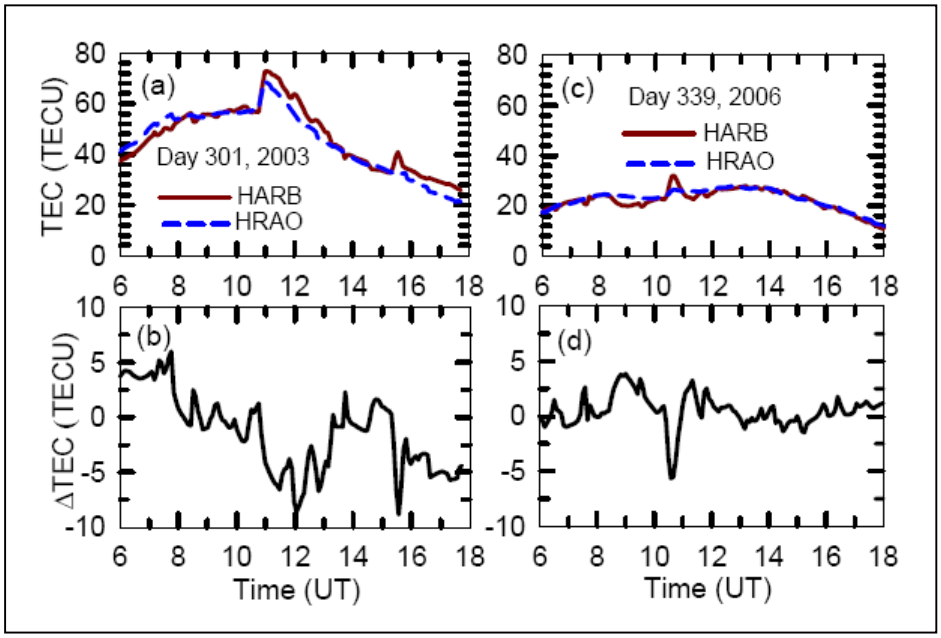

Figure 5.9: Panels (a) and (c) show comparisons of TEC over collocated HRAO and HARB GNSS stations during the solar X17 (day 301, 2003) and X9 (day 339, 2006) flares respectively. Panels (b) and (d) show the corresponding computed TEC difference between HRAO and HARB for (a) and (c), respectively.

5.4.2 The X9 flare on day 339, 2006

Figure 5.9(c) shows the comparison of ionospheric TEC over HRAO (dashed lines) and HARB during the X9 flare event which occurred on day 339, 2006. Coinciding with the flare onset (~10:18 UT), the TEC value rapidly increases over both stations and reaches a peak at ~10:35 UT, after which it decreases gradually as the flare decays. The TEC values over these stations for the X9 flare are compared by computing the TEC difference ΔTEC for the dayside ionosphere as shown in Figure 5.9(d). The $HRAO_{TEC}$ is slightly higher than the $HARB_{TEC}$ during the early hours (~8:00 – 10:00 UT). A significant difference (~6 TECU) between $HRAO_{TEC}$ and $HARB_{TEC}$ is evident around the peak.

Recent studies of the flare-ionosphere relations (e.g. Tsurutani et al., 2005; Zhang and Xiao, 2005; Moeketsi et al., 2007a; Liu et al., 2007) have shown that the daytime ionosphere responds

dramatically to the X – ray and Extreme Ultraviolet (EUV) flare inputs by an abrupt enhancement of TEC with respect to the prior flare background values. Furthermore, the EUV component of the flare is responsible for the TEC enhancement, which lasts far longer than the duration of the flare. This interpretation holds for the ionospheric TEC response to the two flares discussed in this work.

Of major interest is the pronounced difference of ~6 TECU and ~ 9 TECU between the collocated $HRAO_{TEC}$ and $HARB_{TEC}$ for the X9 and X17 solar flares. The two GNSS receivers are located ~3 km apart and the ionosphere is not expected to behave differently over such a short distance. However, possible causes for the TEC difference between the two could be due to the following:

(a) Two different types of collocated GNSS receivers (HRAO and HARB) used could possibly have different biases. It could also be probable that the calibration failed, e.g. due to some raw data errors which might even be linked to radiation burst because of receiver limitation in following very rapid changes.

(b) Some inaccuracy associated with the single-layer ionospheric model, as reported by Meggs et al. (2004) and Meggs and Mitchell (2006), could be expected in calculations.

(c) Some inaccuracies within the geometric mapping function in projecting the line-of-sight TEC into vertical TEC above each station particularly at high solar activity could be expected (e.g. Komjathy, 1998; Jakowski et al., 1998).

In order to investigate the TEC differences between the two collocated receivers, further studies using additional data are needed. Comparison of the TEC difference between the two flares indicates evidence of solar cycle dependence over South Africa (Moeketsi, 2007a). The TEC difference is larger for the X17 flare than for the X9 flare. The former occurred in 2003 during moderate solar activity conditions; the latter occurred in 2006 during solar minimum conditions.

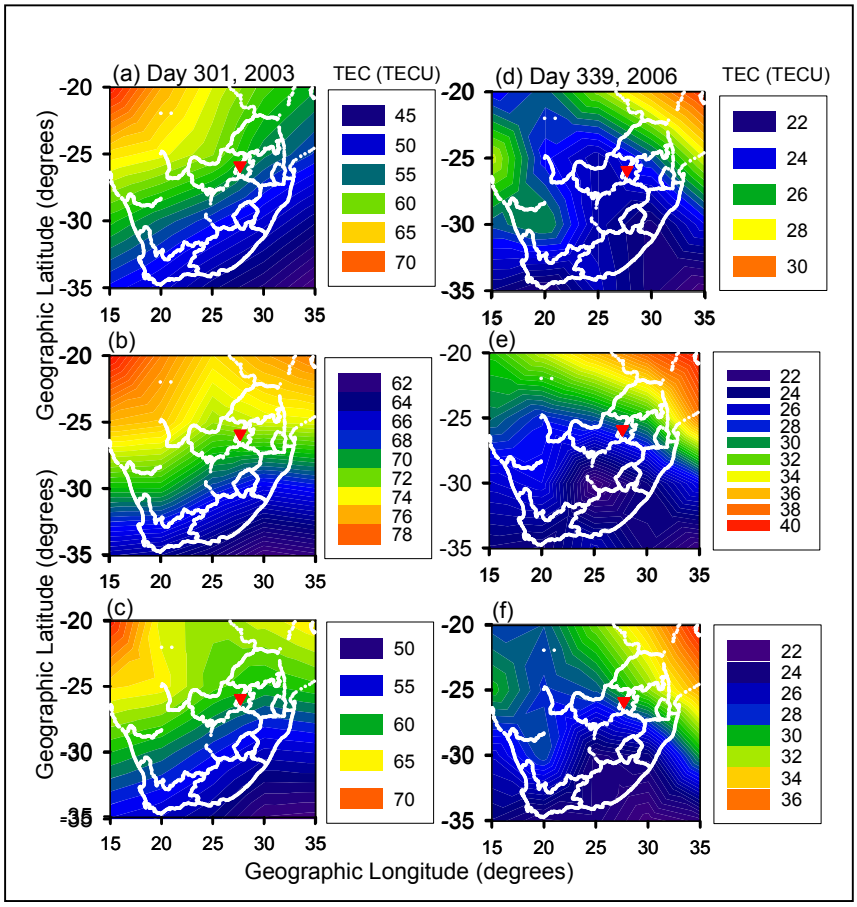

Figure 5:10: Panels (a), (b) and (c) show TEC maps over South Africa before (~10:15 UT), during (~11:15 UT) and after (~12:00 UT) the X17 flare which occurred on day 301, 2003. Panels (d) at ~10:15 UT, (e) at ~10:30 UT and (f) at ~11:15 UT show similar scenarios as panels (a), (b) and (c) for the X9 flare which occurred on day 399, 2006. The red triangles on the TEC maps indicate the geographical location of HRAO (27.69˚E, 25.89˚S) and HARB (27.71˚E, 25.89˚S).

5.4.3 TEC maps during X-ray flares

Shown in Figure 5.10 are the ionospheric TEC maps of South Africa computed with the UNB model for the two solar X- ray flares considered in this study. Panel (a), shows the TEC map at 10:15 UT before the onset, (b) near the peak (11:15 UT) and (c) after the decay phase (12:00 UT) of the X17 flare. The TEC values on the TEC map around the peak are significantly enhanced compared to the TEC map before and after the flare. Panel (d), shows the TEC map prior (10:15 UT) to the onset of

the X9 flare, (e) shows the TEC map during (10:30 UT) the flare and (f) shows the TEC map after the decay phase (11:15 UT) of the flare respectively. It is also evident that TEC values computed during this flare are enhanced compared to the period before and after the flare. The latter holds for both flares due to the high rate of solar radiation input causing photo-ionisation, which results in a sudden TEC enhancement within the daytime ionosphere during solar flares (Tsurutani et al., 2005; Moeketsi et al., 2007a). This provides direct evidence of space weather effects on the terrestrial ionosphere.

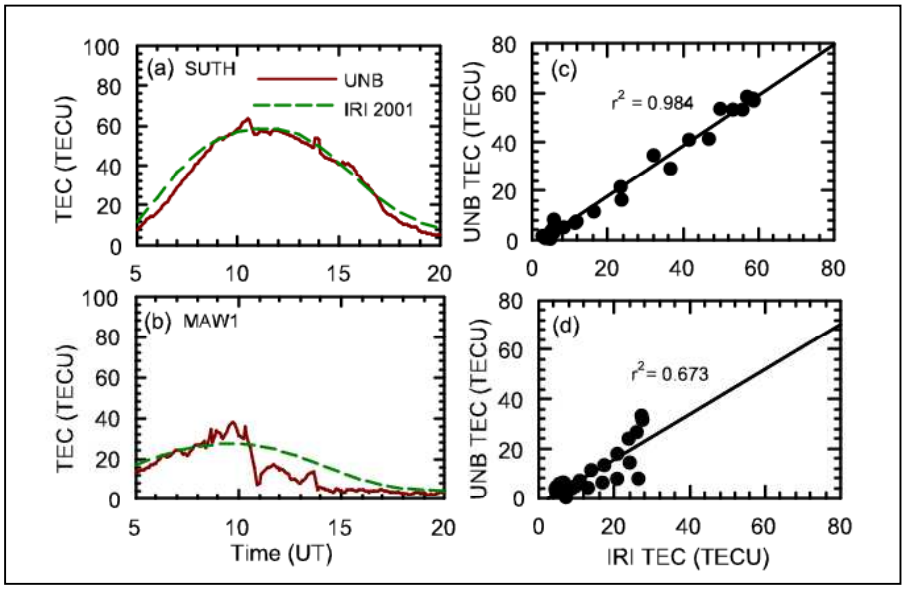

Figure 5.11: Comparison of UNB (solid line) and IRI (Dashed line) daytime TEC over the (a) SUTH and (b) MAW1 GPS stations for day 105, 2003. Panels (c) and (d) show the correlation coefficient computed by fitting a linear regression between the UNB-IMT and IRI TEC results over SUTH and MAW1 to provide an indication of the reliability of the UNB results.

5.5 Comparison of UNB-IMT TEC with IRI predictions

In Chapter 3, a comparison of the UNB-IMT algorithm and CODE analysis center TEC prediction was performed over South Africa, which showed a good level of agreement (Ngcobo et al., 2005). Validation of UNB-IMT with Ionosonde TEC measurements was conducted in Chapter 4 during

periods near solar maximum and near solar minimum. The results verified the use of UNB-IMT as a tool to study ionospheric TEC over South Africa. However, in this section, results from a further comparison of UNB-IMT with the commonly used IRI 2001 model (Bilitza, 2001) is presented to provide a further test of the reliability of this model over southern Africa.

Figure 5.11 shows the results from comparing daytime hourly average UNB-IMT TEC (solid line) and IRI 2001 TEC (dashed line) computed for day 105, 2001 over (a) SUTH and (b) MAW1 GPS stations. TEC computed over SUTH for both models is comparable and increases significantly from 5:00 UT to reach a maximum value of ~80 TECU at local noon (~10:00 UT), thereafter decreasing gradually as expected. There is a very good correlation ($r^2 = 0.984$) between the two models over SUTH as shown in Figure 5.11 (c). For MAW1, TEC computed from both models increases gradually to reach a maximum value of ~32 TECU at ~10:00 UT and decreasing after noon. However, there is a ~10 TECU difference between the UNB and IRI model results during the period ~10:00 UT to ~15:00 UT. A reason for this difference could be that the UNB-IMT algorithm underestimated TEC over the ocean because of a lack of data coverage. On the other hand, it could be that the IRI model is not accurate for predictions over southern Africa, where there is historically a lack of data coverage. As a result, a correlation coefficient of (r^2) of 0 .673 between the two models over MAW1 was obtained as shown in Figure 5.11(d). However, it is clear that in general both models show a good agreement during a geomagnetically quiet day at mid and higher latitudes.

5.6 Summary and Conclusions

This chapter reports on the effort being undertaken to study the solar cycle variations of GNSS-derived TEC observed over southern Africa by applying the UNB-IMT (Komjathy, 1997; Ngcobo et al., 2005; Moeketsi et al., 2007a,b). By using the sunspot number as a proxy for solar activity, TEC maps over South Africa were produced for day 345 at 14:00 UT during different epochs of solar cycle 23. It was found that the TEC values observed during extreme solar maximum conditions are significantly enhanced compared to the TEC values at different phases (epochs “a” and “c”) of the

solar cycle observed during moderate solar activity conditions. The enhancement of TEC from moderate to extreme solar activity conditions is associated with the increased rate of production of background Solar X-ray and EUV radiation causing high rates of photoionisation within the daytime ionosphere. Of particular interest was the observed midlatitude peak display on the TEC map at extreme solar maximum, which was noteworthy for the enhanced ionisation at midlatitudes. An analysis of the geomagnetic storm activity index was performed in an attempt to investigate the causes of the observed TEC anomaly at midlatitudes. It was found that day 345, 2001 was geomagnetically quiet.

A further investigation was conducted by analyzing the five minute average daytime GOES 8 satellite X-ray flux (0.1-0.8 nm) and SOHO SEM flux on 26.0-34.0 nm wavelengths. Comparison of these physical quantities revealed that there was a solar X-ray flare of magnitude X28 with an associated EUV flare event on day 345, 2001. Subsequent effects of these flares were investigated on the daytime TEC observed over GPS stations MALI (near equatorial), SUTH, HARB, S121 (midlatitude) and MAW1 (high latitude) respectively. It was found that the EUV flare associated with the X28 flare seems to have caused significant TEC variations at midlatitudes, whereas no such variations was evident at the lower and higher latitudes. The effects of this flare seem to be localized and the high TEC peak observed at midlatitudes may presumably be due to particle precipitation from the outer radiation belt that resulted from this flare at latitudes greater than 30 degrees South. Although the latter explanation is likely, more data is required to substantiate this possibility

Further investigations of solar flare effects on daytime TEC was pursued by selecting the X17 flare which occurred on the geomagnetically quiet day 301, 2003 over four GPS stations located at different latitudes. It was found that the EUV flare associated with this X-flare caused global photoionisation within the daytime ionosphere, which led to a sudden increase of TEC that lasted longer than the duration of the flare. It was also evident that the TEC enhancement, with respect to the background values, was significantly higher at lower latitudes near the equatorial region and

decreased towards the higher latitudes. This confirmed the TEC dependence on geographic locations and is consistent with the findings of Tsurutani et al. (2005) findings.

A comparison of the EUV flares associated with the solar X28 and X17 flares analyzed in this work was performed. It was found that the EUV flare associated with X17 caused a global ionospheric effect in contrast to the localized midlatitude ionospheric perturbations, which could be due to the EUV component of the X28 flare (Moeketsi et al., 2007a). A further investigation of the characteristics of EUV/X-ray flares and their relation to the ionosphere is required.

Comparison of TEC derived from HRAO and HARB GNSS receivers was performed during solar X17 and X9 flares which occurred on day 301, 2003 and day 339, 2006 respectively. It has been shown that considerable differences exist between the TEC observed by the two different but collocated receivers. This could presumably be attributed to the following reasons: (a) the instrumental differences in receivers or that the calibration failed, (b) inaccuracy associated with the single-layer ionospheric model as reported by Meggs et al. (2004) and Meggs and Mitchell (2006), and (c) inaccuracies of the geometric mapping function used in projecting the line-of-sight TEC into vertical TEC above each station particularly at high solar activity (e.g. Komjathy, 1997; Jakowski et al., 1998). In order to investigate TEC differences between the two collocated receivers, further studies using additional data are needed. However, a comparison of TEC for these flares showed evidence of a solar cycle dependence (Moeketsi et al., 2007a), and direct evidence of space weather effects on the ionosphere over South Africa. This is important for future application in high frequency radio communication, navigation, positioning, frequency management, space weather forecasting and long terms studies of impact of solar outputs on climate change over South Africa.

A comparison of the daytime UNB-IMT and IRI 2001 models was performed to further test the reliability of the UNB model results in reproducing the IRI 2001 predictions. It was found that the models show a good agreement during a geomagnetically quiet day at mid and higher latitudes. This

chapter demonstrated the capabilities of the UNB-IMT software for ionospheric research over the South African region. In particular, for short and long term studies of space weather impacts on the terrestrial magnetosphere-ionosphere system.

The next Chapter investigates the capabilities of TEC derived from geodetic VLBI over HartRAO for space weather monitoring over South Africa using the UNB-IMT results.

Chapter 6

INVESTIGATION ON CAPABILITIES OF GEODETIC VLBI DERIVED TEC FOR SPACE WEATHER MONITORING

6.1 Introduction

Since its development in the late 1960s (e.g. Clark et al., 1985), the Very Long baseline Interferometry (VLBI) technique has achieved significant improvement in precision and accuracy (e.g. Ros et al., 2000). The early geodetic VLBI measurements were carried out at single frequencies. As a consequence, ionospheric corrections have to be made using external techniques such as radio beacon satellites measurements. During the early 1980s, stations were equipped with dual-frequency (2.3 GHz and 8.4 GHz) receiving systems and the ionospheric effects on the observed group delay could be determined directly and applied in astronomical, astrometric and geodetic analysis. It is crucial to note that the ionospheric corrections that can be obtained from geodetic VLBI measurements have not been included in any model of the ionosphere (Hobiger, 2006).

However, dual frequency geodetic VLBI measurements provide a chance to obtain absolute ionospheric TEC over VLBI geodetic sites (Kondo, 1991; Hobiger, 2004). Because of the fact that VLBI is a differential technique, the computed ionospheric TEC depends on the difference in the propagation media over the stations. Recently, a method has been developed within project VLBIonos at the Institute of Geodesy and Geophysics, Vienna University of Technology, which estimate ionospheric parameters in terms of TEC from the world network of VLBI observations

(Hobiger et al., 2006). The main purpose behind the development of the Vienna TEC Model (VTM) was to determine ionospheric parameters from geodetic VLBI observations and provide ionospheric VLBI data for validation of global ionospheric models. In this Chapter the capabilities of VTM derived TEC for space weather monitoring is investigated over HartRAO collocated geodetic VLBI and GNSS antennae (25.89°S, 27.69°E) using the UNB-IMT (Komjathy, 1997; Moeketsi et al., 2007a,b) TEC results. The study is performed for the year 2002 near solar maximum and the year 2005 near solar minimum during the periods of the CONT02 and CONT05 campaigns.

6.2 The Vienna TEC Model

A method has been developed within project VLBIonos at the Institute of Geodesy and Geophysics, Vienna University of Technology, which estimates ionospheric parameters in terms of TEC from VLBI data (Hobiger et al., 2006). This section provides a brief description of this method which is referred to as the Vienna TEC Model (VTM). A more detailed description about VTM can be obtained from Hobiger et al. (2004; 2006).

Geodetic VLBI observations are carried out at 2.3 GHz (S band) and 8.4 GHz (X band) in order to compensate for dispersive delays caused by the ionosphere. Each ionospheric delay corresponds to the TEC along the ray path through the ionosphere. Because VLBI is a differential technique, each dual frequency provides the base line dependent ionospheric delay $\left(\tau_{measured}\right)$ expressed as:

$$\tau_{measured}\left(t\right)=\tau_{ion,1}\left(t\right)-\tau_{ion,2}\left(t\right)+\tau_{offset,1}+\tau_{0\,ffset,2}\,, \tag{6.1}$$

where $\tau_{offset,1}$ and $\tau_{offset,2}$ are instrumental offsets caused by the receiving system (Ray, 1991) which are assumed to be constant within a 24 hour geodetic VLBI session. The ionospheric delay at the X-band frequency measured at station i can be described using the relation:

$$\tau_{ion,i(t)}=\frac{1.34\times10^{-7}}{f_x^2}\cdot M_{f(\varepsilon_i)}\cdot VTEC_i\left(t\right), \tag{6.2}$$

where

$$MF\left(\varepsilon_i\right) = \frac{1}{\sqrt{1-\left(\frac{R_e}{R_e+H}\cos\varepsilon_i\right)^2}}, \tag{6.3}$$

is the appropriate mapping function for that mappig the slant TEC into vertical TEC corresponding to location of each VLBI station. In equation (6.3), R_e represents the radius of the Earth, ε_i is the elevation angle and H is the height of the ionospheric layer located at about the height of the F2 peak electron density (Schaer, 1999; Hobiger, 2006). For computations of VTEC in this chapter, the H is assumed to be 450 km for year 2002 and 400 km for year 2005 (Hobiger, 2007; *private communication*).

In order to compute VTEC above each VLBI station, the Vienna TEC Model (Hobiger et al., 2006) uses the following assumptions and simplifications that take into account the physical behaviour of the ionosphere:

(a) The instrumental offsets in equation (6.1) caused by the receiving system should remain constant within a 24 hours VLBI session. The sum of all station dependent offsets equals zero (Sekido et al., 2003).

(b) Uses the thin shell approximation of the ionosphere (Schaer, 1999), which takes into account that the diurnal variation of the ionosphere is mainly correlated with the position of the Sun. Since VLBI measurements are made at different elevation angle and azimuths, the VTEC value has to be assigned to the intersection of the ray path with the ionospheric shell that is not vertically located above the station.

(c) Apply assumption of linear north-south gradient for each station, which allows the determination of VTEC values above each station.

(d) Based on (a), (b) and (c), VTEC values for each station can be modeled by means of the least-square method. Different elevation angles for each station enable the separation of the station-dependent parameters.

(e) The ionospheric parameters are modelled with constant interval lengths in the form of piece-wise linear functions with only positive VTEC values allowed. Furthermore, a reflective Newton method is used to enable the unknown parameters under non-negative conditions to be obtained.

(f) For periods with no data, an adaptive piece-wise linear function is applied which shifts the interval boundaries so that every interval contains the same number of observations.

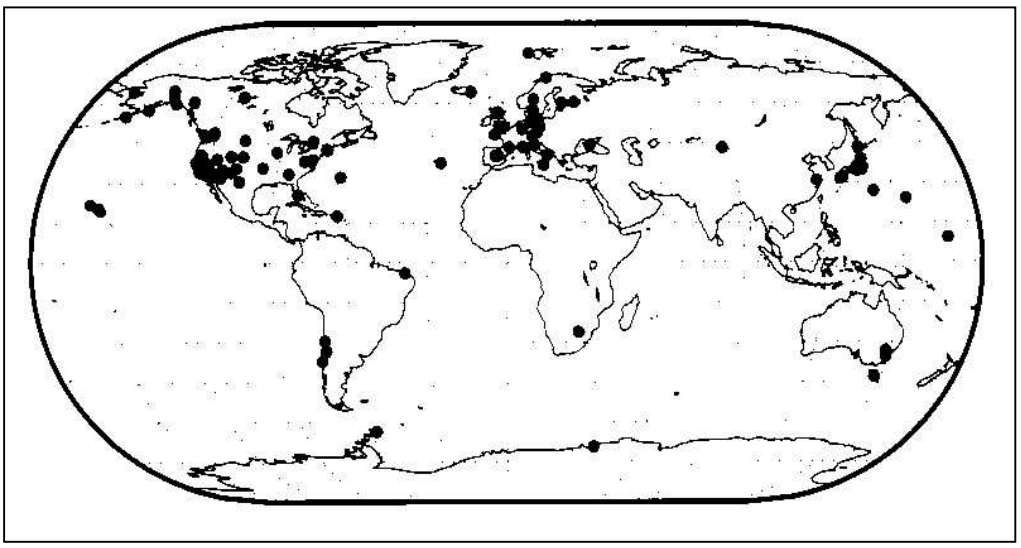

Figure 6.1: Map of VLBI stations for which VTEC time series were computed using VTM (Hobiger et al., 2006).

By applying VTM to the whole database of the International VLBI Service for Geodesy and Astrometry, a time-series of VTEC values for 143 worldwide geodetic VLBI network stations

depicted in Figure 6.1, were created spanning about two solar cycles depending on the availability of data (Hobiger et al., 2006). Some antennas contributed less than others, as they are not mainly dedicated to geodetic observations or not equipped permanently with dual frequency receivers. However, it has been shown by Hobiger et al. (2006) that the solar cycle dominates the general trend of VTEC, which is in good agreement with IGS Global Ionospheric Model results over Wettzell, Germany.

In the next section, effort is undertaken to investigate the potential for VTEC derived from the HRAO geodetic VLBI antennae (Hobiger, 2007; *private communication*) for space weather monitoring over South Africa using GTEC derived from UNB-IMT algorithm (Komjathy, 1997; Ngcobo et al., 2005; Moeketsi et al., 2007a;b) discussed in Chapter 3. The HRAO Space Geodesy Programme operates the three collocated main space geodetic techniques (VLBI telescope, Satellite Laser Ranging, GNSS receiver) depicted in Figure 6.2, which make it a very important geodetic site in the Southern African region (see http://www.hartrao.ac.za/geodesy). In addition, this collocation allows for cross validation and verifications of ionospheric information derived from GNSS and VLBI for tropospheric and ionospheric research over South Africa (Combrink, 2006; Moeketsi et al., 2007a,b).

Figure 6.2: The collocated GNSS dual frequency receiver and 25 meter diameter VLBI antenna over the Hartebeesthoek Radio Astronomy Observatory (HRAO) geodetic site geographically located at 25.89°S, 27.69°E.

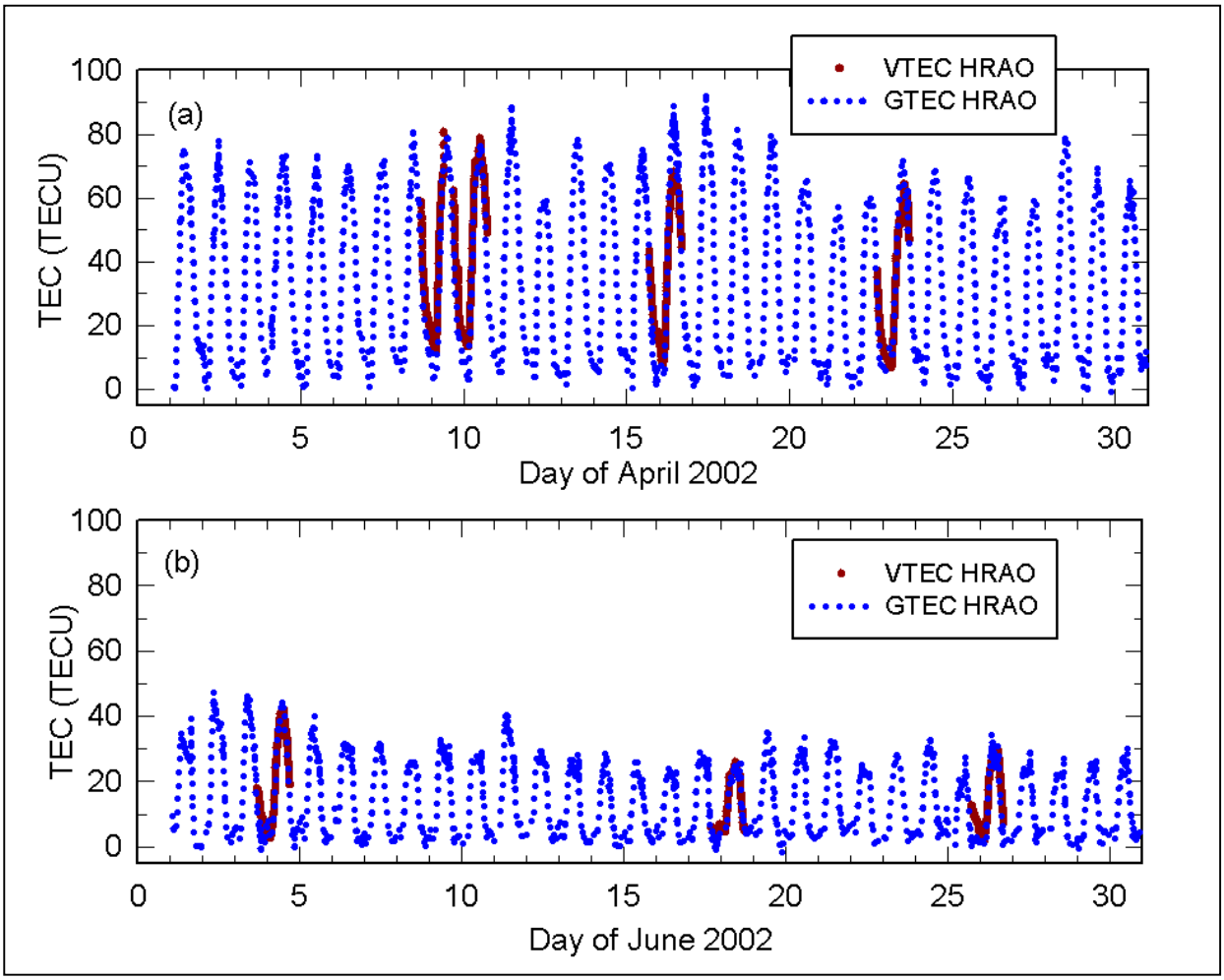

Figure 6.3: Comparison of VTEC (dark red line) with GTEC (blue dotted line) over HRAO for months of April and June 2002.

6.3 Diurnal and seasonal variations of VTEC and GTEC over HRAO

Figures 6.3 and 6.4 depict a comparison between the VTM VTEC (red dotted lines) obtained from project VLBIonos at the Institute of Geodesy and Geophysics, Vienna University of Technology (Hobiger, 2007; *private communication*) and GTEC (blue dotted lines) computed using UNB-IMT over the HRAO collocated geodetic VLBI and GNSS antennae. The results are for panels: (a) April

around autumn equinox, (b) June around winter solstice, (c) September around spring equinox and (d) December around summer equinox of the year 2002 (high solar activity). Evidently, there are numerous gaps in VTEC data compared to GTEC. This is due to the fact that HRAO antenna is not observing every day (only ~15% of telescope time is allocated to geodetic VLBI sessions) and data gaps in VTEC vary according to geodetic experiment scheduling, dedication and maintenance whereas the GNSS receiver records data in a real-time manner. As a result, the HRAO geodetic VLBI is restricted in providing near real-time data to the international scientific community.

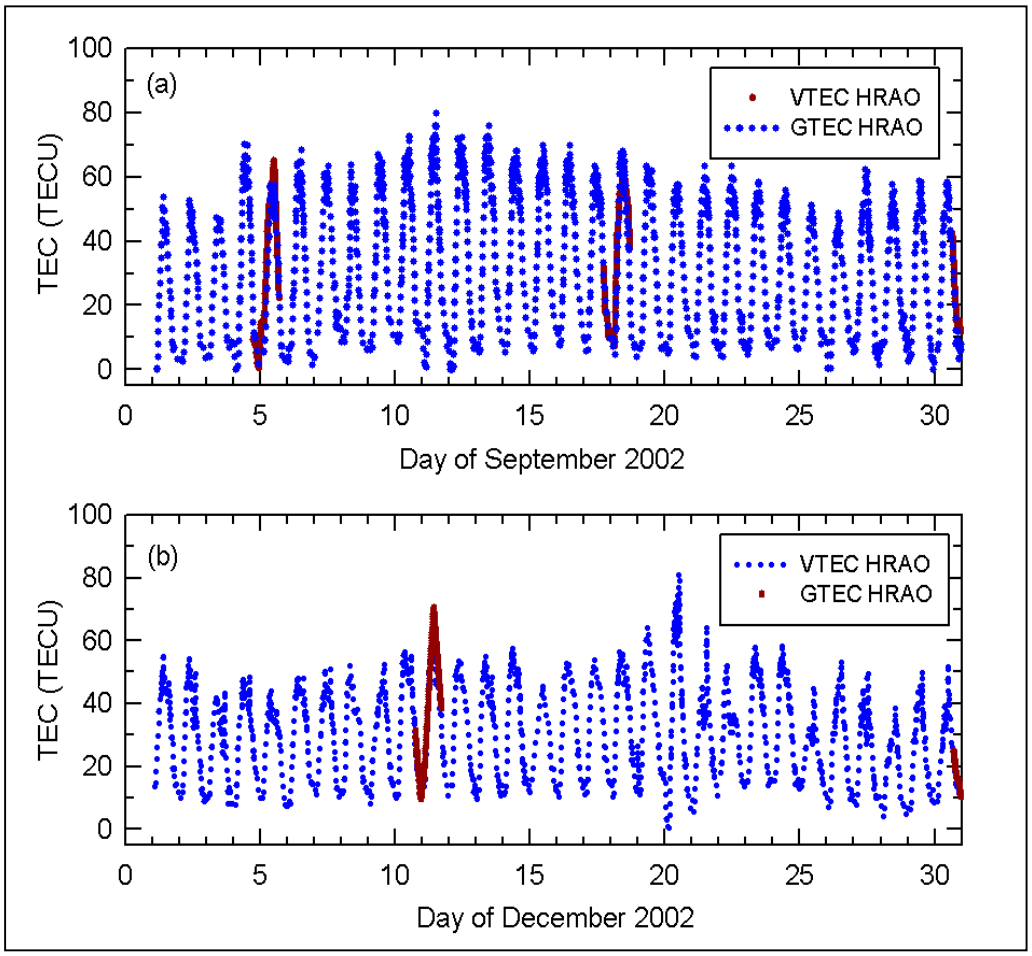

Figure 6.4: Similar to figure 6.3, but shown for months of September and December 2002.

However, for days in which data were recorded by both collocated techniques, the diurnal variation trend of VTEC and GTEC is generally comparable for all seasons. In particular, VTEC and GTEC exhibit semiannual variations with high values (~80 TECU) around months of equinoxes and small values (~40 TECU) around the winter solstice as expected (Bhonsley et al., 1965; Jee et al., 2005). Of interest is the evidence of high TEC values from both techniques during the summer (December) as opposed to the winter (June) month. This is an indication of the annual anomaly at the lower midlatitude station (HRAO) towards a year of high solar activity. It is consistent with results obtained by Jee et al. (2005), who after comparing IRI-2001 with TOPEX TEC reported that annual and semiannual anomalies mostly occur at low and lower midlatitude stations.

Comparing results from both techniques verifies that the HRAO VLBI antenna can be used as one of the instruments for monitoring the ionosphere over South Africa. The current challenge with the HRAO antenna is the fact that it is not currently dedicated for continuous geodetic VLBI sessions. There are only epochs during the planned CONT experiments were the antenna is dedicated to 15 days continuous geodetic measurements sessions. The CONT campaigns are discussed in the next section and provide the opportunity to study the ionosphere over a period of two weeks by means of VLBI.

6.4 Capabilities of VLBI TEC for space weather monitoring

Since the VLBI antenna at HRAO is not continuously dedicated to do geodetic observations, it only participates on 15 day 24 hour geodetic sessions during the CONT campaign experiments. The primary aim of these campaigns is the acquisition of the best possible VLBI data to demonstrate the high accuracy of which VLBI is capable (e.g. Hobiger et al., 2004). These campaigns provide the opportunity to monitor the ionosphere and troposphere for a continuous period of about two weeks. In this section, I investigate the capabilities of VTEC derived from the Vienna TEC Model (Hobiger et al., 2004; 2006) over HRAO for space weather monitoring during the CONT02 campaign run in

October 2002 (near solar maximum) and CONT05 campaign conducted in September 2005 (near solar minimum).

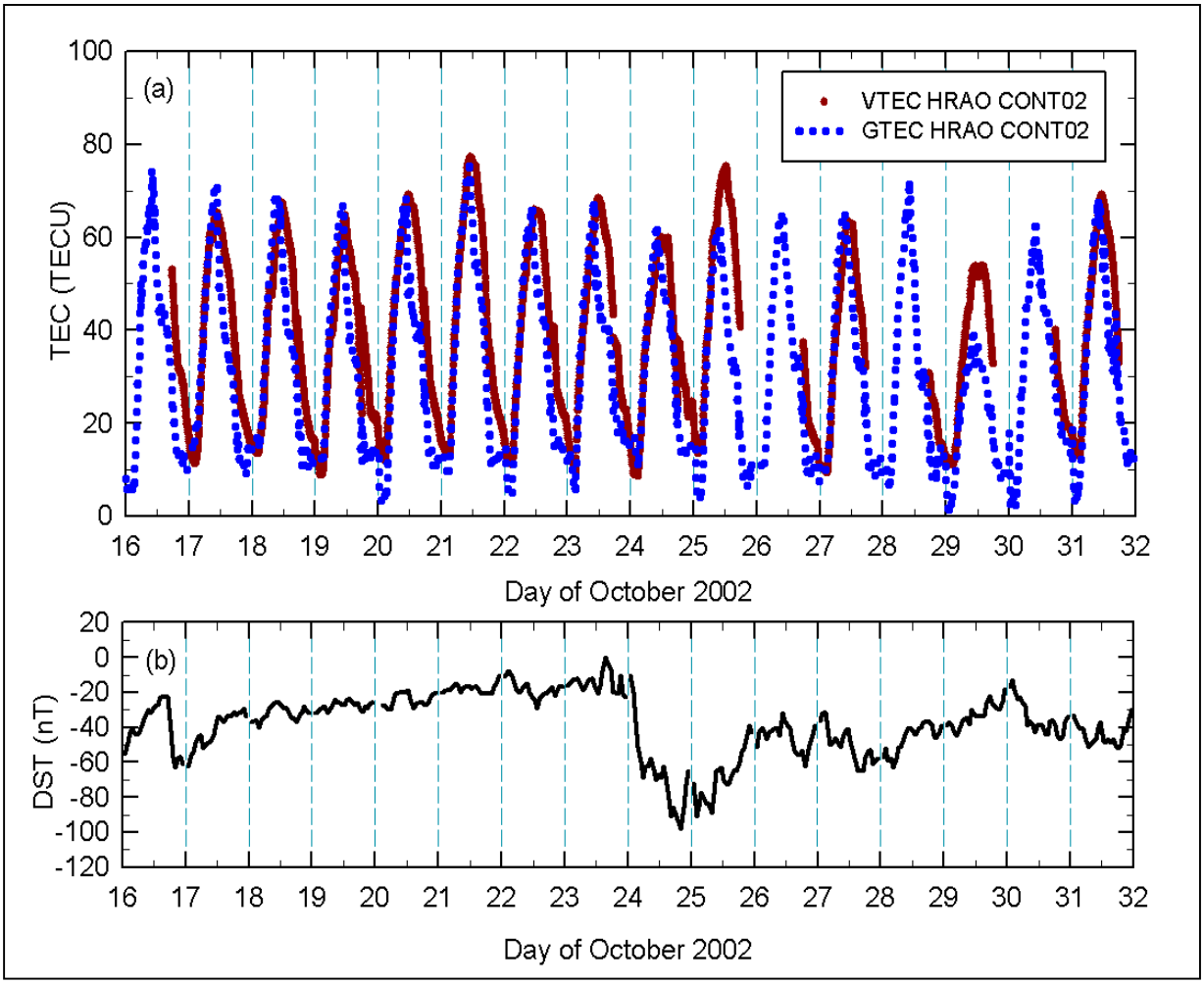

Figure 6.5: Panel (a) depicts the comparison of hourly VTEC (solid red line) computed using VTM and UNB-IMT GTEC (dotted blue line) values over HRAO during the CONT02 campaign. Panel (b) depicts the hourly DST values observed during the CONT02 (16 to 31 October 2002) campaign sessions.

6.4.1 CONTO2 Campaign

CONT02 was a two-week campaign of continuous VLBI sessions, scheduled for observing from 16 to 31 October 2002. The CONT02 campaign was the follow-on to the successful CONT94 (January

1994) and the follow-up to CONT95 (August 1995) and CONT96 (September 1996) campaigns. The main goal of the CONT02 campaign was to acquire the best possible state of the art VLBI data over a two week period to demonstrate the highest accuracy of which VLBI is capable. There were eight stations network who participated in observations during the CONT02 campaign (http://ivscc.nasa.gov/program).

Figure 6.5 (a) illustrates the comparison between the VTEC and GTEC computed using VTM (red solid line) and UNB-IMT (blue dotted line) over HRAO during CONT02 (16 to 31 October 2002). The diurnal variation trend from both techniques shows in general a good agreement, with minimum values (~10 TECU) around midnight and maximum values (~80 TECU) around midday. During the early hours to midday, the VTEC and GTEC values are highly comparable for all days. From about midday to midnight of all days, the VTEC slightly overestimates the GTEC.

In order to investigate the capability of VTEC for space weather monitoring, Figure 6.5 (d) depicts the hourly DST values for the period of CONT02 (16 to 31 October 2002). It is evident from the DST values that the level of geomagnetic activity was very low during most of the days of the CONT02 campaign, apart from the day 24 October 2002 when a minor geomagnetic storm occurred with a DST = -100 nT. The subsequent effect of this storm on VTEC and GTEC is not noticeable, indicating that the minor storm may not be the cause ionospheric TEC perturbations over the lower midlatitude station HRAO. Surprisingly, on 29 October 2002 there is a significant depletion on the diurnal variation trend of midday VTEC and GTEC. The cause of this TEC depletion could not be linked to the minor storm occurring on day 24 October 2002 since on 29 October 2002, the DST value was > -40 nT indicating a geomagnetically quite situation.

Figure 6.6 compares hourly GTEC against VTEC during the CONT02 campaign period. Evident from the best fit line to the scatter is that both techniques has a good correlation ($r^2 = 0.72$) with a – 0.84 TECU bias. The small biases between the two techniques can be attributed to the contribution

from the plasmasphere and mapping function mismodelling (Hobiger et al., 2004; Hobiger et al., 2006). The other possible explanation could be due to a contribution from interstellar and interplanetary plasma as the radio signal propagate from the radio source (e.g. quasar) to the ground antenna. The latter was ruled-out by Hobiger, (2007; *private communication*) since VLBI observe one common source with several antennae. Thus the rays appear to be parallel having a maximum separation by diameter of the Earth. This sets a limit to a plasma contribution from interstellar/interplanetary media.

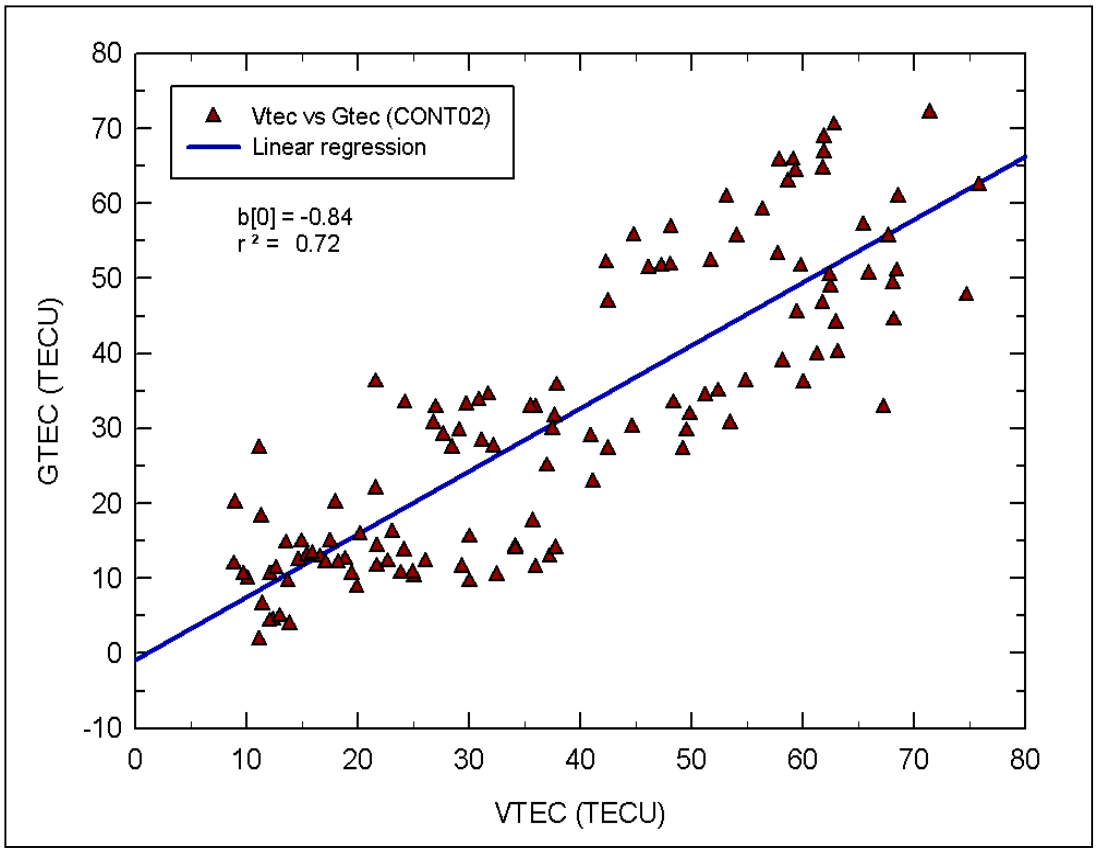

Figure 6.6: Scatter plots of hourly GTEC computed using UNB-IMT against VTEC computed using VTM over HRAO during the CONT02 campaign in October 2002. The straight line represents the best fit line to the TEC data.

6.4.2 CONT05 Campaign

CONT05 was a two-week campaign of continuous VLBI sessions, scheduled for observing from 12 to 26 September 2005. The CONT05 campaign was a follow-up to the successful CONT94, CONT96, and CONT02 campaigns discussed in Section 6.4.1. The main goal of the CONT05 campaign was to acquire state of the art solar minimum VLBI data over a two week period to demonstrate the high accuracy that VLBI is capable of. There were 11 observing network stations (including HRAO) who participated during the CONT05 campaign (http://ivscc.nasa.gov/program).

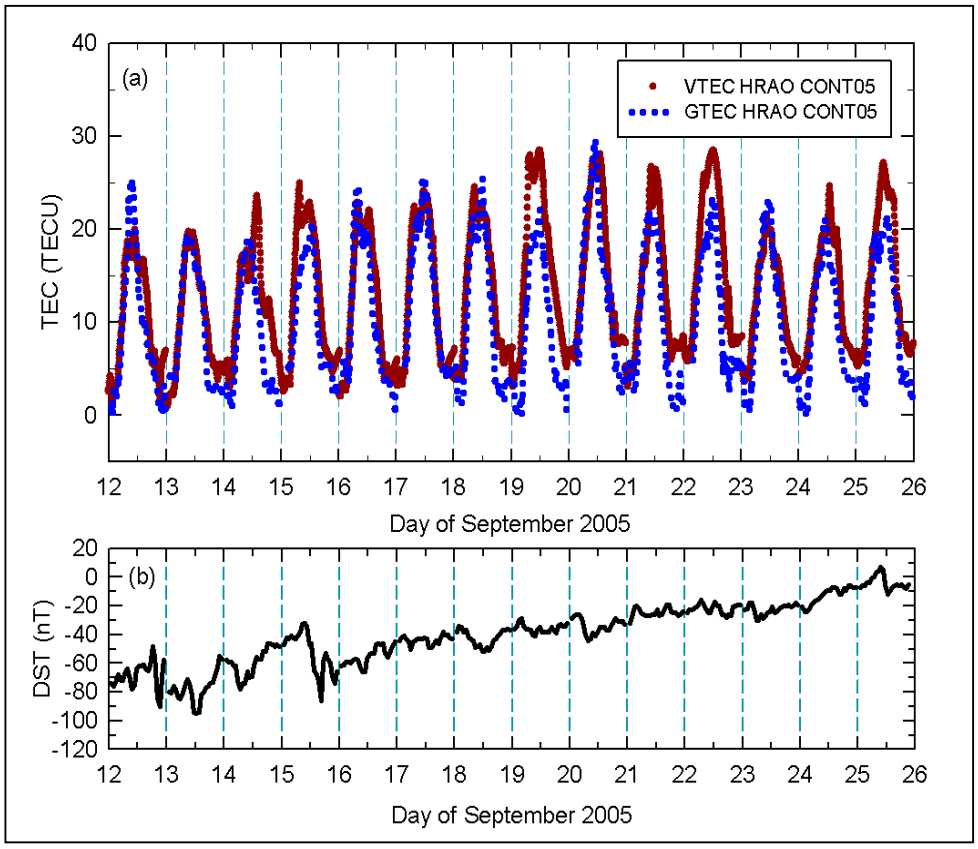

Figure 6.7: Panel (a) depicts the comparison of hourly VTEC (solid red line) computed using VTM and UNB-IMT GTEC (dotted blue line) values over HRAO during the CONT05 campaign. Panel (b) depicts the hourly DST values observed during the CONT05 (12 to 26 September 2005) campaign.

Figure 6.7 (a) illustrate comparison of the VTEC and GTEC computed using VTM (red solid line) and UNB-IMT (blue dotted line) over HRAO during CONT05 (12 to 26 September 2005). The diurnal variation trend from both techniques shows in general a good agreement, with minimum values (~2 TECU) around midnight and maximum values (~30 TECU) around midday. From midday to midnight of all days, the VTEC and GTEC values are highly comparable for all days. After midday to midnight of all days, the VTEC slightly overestimates the GTEC. Figure 6.8 compares hourly GTEC against VTEC during CONT05 campaign period. Evident from the best fit line to the scatter is that both techniques has a good correlation ($r^2 = 0.79$) with a -1.87 TECU bias. As discussed in section 6.4.1, the bias is unlikely to be the result of the contribution from interstellar and interplanetary plasmas.

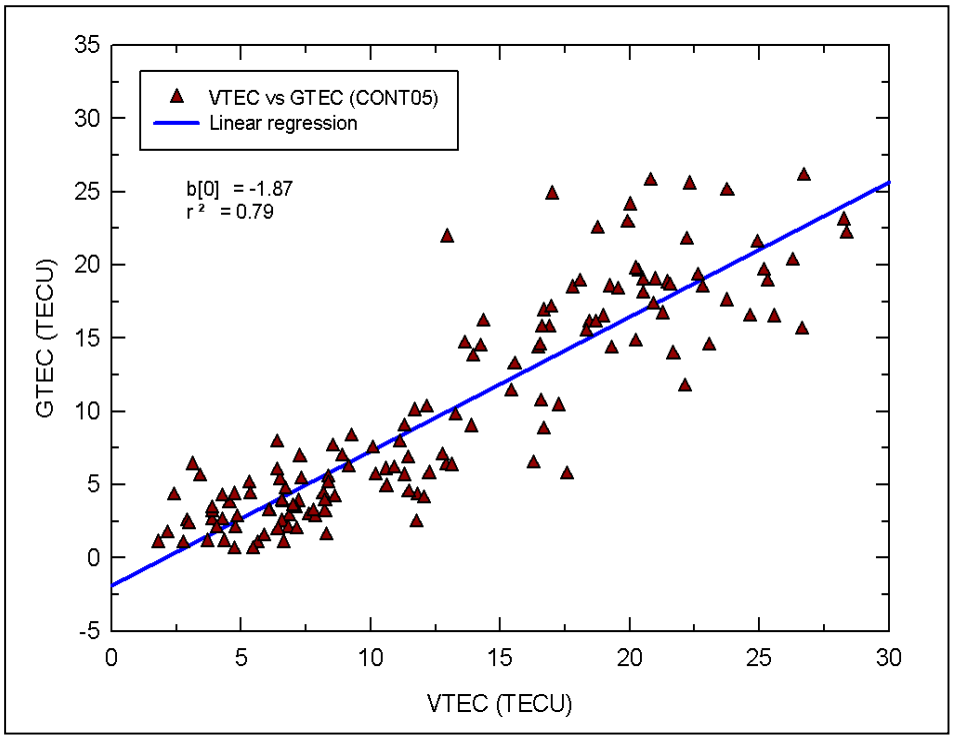

Figure 6.8: Scatter plots of hourly GTEC computed using UNB-IMT against VTEC computed using VTM over HRAO during the CONT05 campaign in September 2005 near solar minimum. The straight line represents the best fit line to the TEC data.

To further investigate the capability of VTEC for space weather monitoring, Figure 6.7 (b) depicts the hourly DST values for the period of CONT05 (12 to 26 September 2005). It is evident from the DST values that the geomagnetic activity was in process during the onset of CONT05 campaign. In particular, a magnetic storm was in the recovery phase from the 12 to 19 September 2005. The latter is evident from the diurnal variations seen in VTEC and GTEC for the 12 to 19 September 2005.

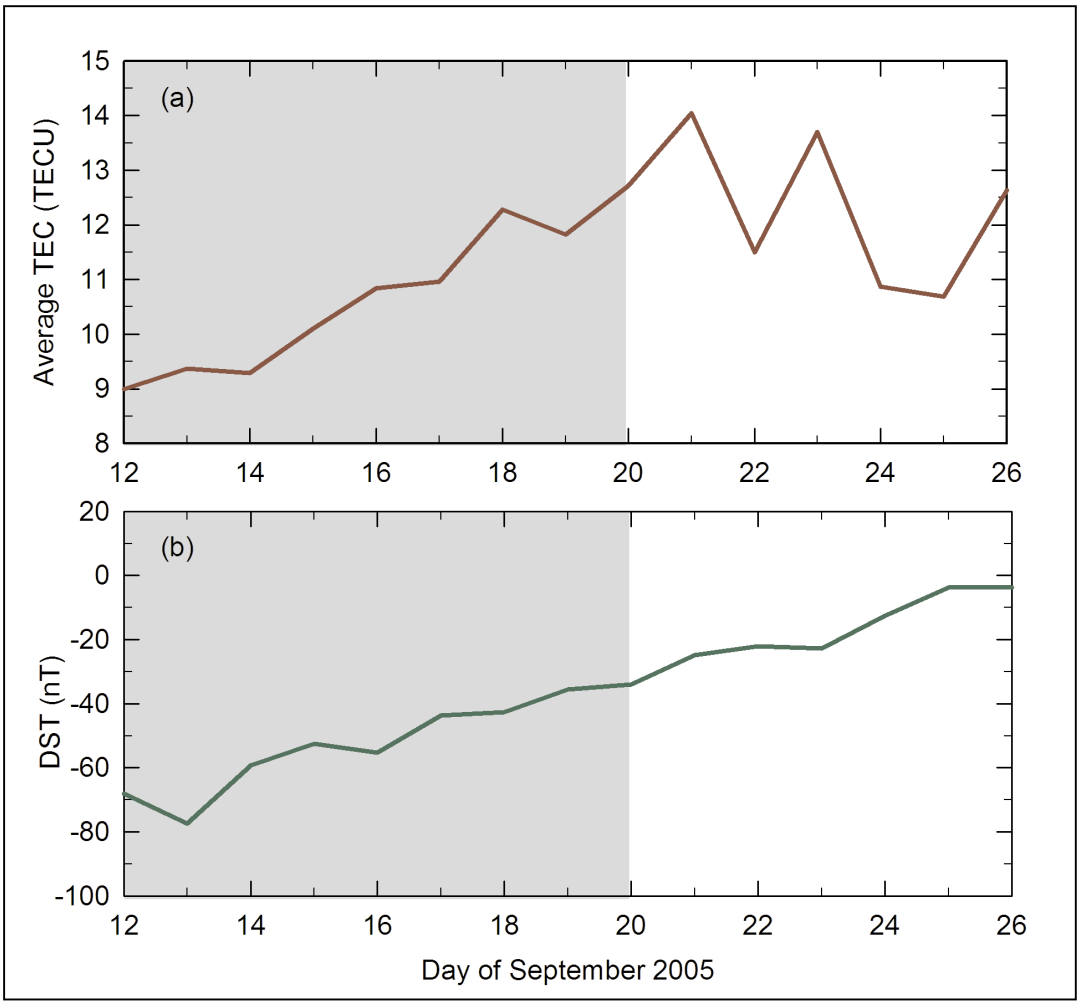

Figure 6.9: Panels (a) and (b) depict comparisons of the daily average TEC with corresponding daily DST values during the CONT05 campaign over HRAO. The shading indicates recovery phase of the geomagentic storm in process.

Figure 6.9 (a) and (b) illustrate the response of the daily average of combined VTEC and GTEC during the recovery phase of the geomagnetic storm. In particular, the average TEC trend increases from the 12 September 2005 at the beginning of CONT05 to ~ 20 September 2005, coinciding with recovery phase trend of the geomagnetic storm (Shaded area). This result verified the capabilities of VLBI derived TEC for monitoring space weather effects on the ionosphere over HRAO. However, since HRAO VLBI is not continuously dedicated for geodetic VLBI sessions, future verification of VLBI derived TEC for space weather monitoring requires dedicated 24 hour geodetic measurements. This is also a requirement for the current development in global Space Geodesy for the project VLBI 2010. VLBI 2010 will operate at the S, X, and Ka Bands of which the current HartRAO VLBI antenna cannot operate efficiently.

6.5 Summary and Conclusions

This Chapter reports on the capability of geodetic VLBI derived TEC computed with the Vienna TEC Model (Hobiger et al., 2006; Hobiger, 2007; *private communication*) for monitoring space weather effects on the ionosphere over HRAO, South Africa using the UNB-IMT TEC results. The study is conducted for a year (2002) near solar maximum and a year (2005) near solar minimum during the CONT02 and CONT05 geodetic VLBI campaigns. It has been shown that VTEC and GTEC show in general a good level of agreement. In particular, the TEC from both space geodetic techniques exhibits semiannual variations with higher values around the months of equinoxes and smaller values around the months of solstices as expected (Bhonsely et al., 1965). Evident also was the annual anomaly feature with high TEC values around the summer solstice compared to the winter solstice. The only shortcoming of VLBI technique for space weather purposes is that it is not a continuously observing technique. The latter resulted in VTEC data gaps within the seasonal variations trends. As a consequence, the capability of the Vienna TEC Model (Hobiger et al., 2006; Hobiger, 2007; *private communication*) for monitoring space weather effects on the ionosphere was investigated during the CONT02 and CONT05 campaigns, which provided a continuous 15 day, 24 hour geodetic VLBI measurements period. It was found that in general TEC derived from both

space geodetic techniques during the CONT02 and CONT05 campaigns is comparable and that diurnal and solar cycle dependence was evident. An investigation was performed on the effects of the geomagnetic storm that occurred during the CONT05 campaign on TEC derived from both techniques. It was found that the response of TEC correlate with the recovery phase of the storm. These results verified the use of VLBI derived TEC over HRAO for monitoring space weather effects on the ionosphere over South Africa.

However, since HartRAO VLBI is not continuously dedicated for geodetic VLBI sessions, future verification of VLBI derived TEC for space weather monitoring requires dedicated 24-hour geodetic measurements. This is also the requirement for the current development in global Space Geodesy for the project VLBI 2010. VLBI 2010 will operate at the S, X, and Ka Bands of which the current HartRAO VLBI antenna cannot operate efficiently. As a consequence, a proposal been submitted in South Africa to establish an International Institute of Space Geodesy and Earth Observations (IISGEO) (www.iissgeo.org). The IISGEO will be located at a new proposed site and will host four fundamental modern space geodetic techniques (VLBI antenna, GNSS receiver, Lunar Laser Ranging, and DORIS), which will disseminate data to the international community in near real time (continuous 24 hour geodetic VLBI measurements). These results can be used for characterising ionospheric parameters over the proposed Square Kilometer Array (SKA) site and also contribute to the development and validation of ionospheric TEC models over South Africa.

The next Chapter provides a concise summary, conclusions and recommendations for possible future spin-offs from this thesis.

Chapter 7

CONCLUSIONS

This chapter summarises the major conclusions of the thesis, and presents recommendations for future work based on the outcome of the study:

7.1 Summary and Conclusions

The main aim of this study was to investigate and develop an understanding of the solar cycle effects on GNSS derived ionospheric TEC over Southern Africa. For this purpose, the UNB-IMT UNIX compatible version developed at the University of New Brunswick, Canada was adopted, and modified to compile on a LINUX platform in order to be used as a regional TEC model for South Africa (Ngcobo et al., 2005; Moeketsi et al., 2007a;b). In particular, the modified UNB-IMT was applied to compute ionospheric TEC using the Southern Africa network of GNSS dual frequency receivers with more regional data sets. The results were validated using the CODE TEC analysis center, Ionosonde-derived TEC measurements and IRI 2001 model predictions over South Africa during the years 2002 and 2005, corresponding to solar maximum and minimum conditions respectively. It was found that all techniques showed a good degree of agreement. In particular:

(1) The variation trends of midday GTEC and ITEC over all stations showed a pronounced seasonal variation for the period near solar maximum, with maximum values around equinoxes and minimum values around solstices as expected.

(2) Short-term variations of TEC (presumably due to solar rotations) were evident from both techniques and were more pronounced during the autumn and spring equinoxes near solar maximum than solar minimum.

(3) There is evidence of a correlation between TEC depletions and enhanced spikes as revealed by both techniques with increased geomagnetic storm activities around equinoxes particularly near solar maximum conditions. In particular the observed TEC depletions and enhanced spikes were due to the interplay of various phenomena occurring during different phases of geomagnetic storms and are consistent with the findings of related studies reported in the literature (Jakowski et al., 1992; Tsurutani and Gonalez, 1997; Fuller-Rowell et al., 1997; Jakowski et al., 1999; Fedrizzi et al., 2005).

Furthermore, the residual $\Delta TEC = GTEC - ITEC$, which corresponds to plasmaspheric electron content was computed for the Ionosonde stations. It was evident that ΔTEC showed a pronounced seasonal variation with maximum value around equinoxes and minimum around winter near solar maximum. For the period 2005, the variation trend of plasmaspheric electron content was found to display a complicated picture. This could be an indication of the reduction of seasonal variation trends towards solar minimum conditions, which could be attributed to the state towards diffusion equilibrium between the ionosphere and plasmasphere (Forster and Jakowski, 2000).

The equivalent ionospheric F2 layer (foF2) and total slab thickness parameters were also computed. It was evident that foF2 and the total slab thickness over all stations maximises around summer, which is in contrast with the seasonal variation of midday GTEC and ITEC where maximum occurs around the equinoxes. These results are consistent with earlier studies of TEC using beacon satellites (Bhonsle et al., 1965).

The UNB-IMT algorithm was further applied to study the variations of GNSS-derived TEC maps during different epochs of solar cycle 23 (Moeketsi et al., 2007b). It was found that:

(1) The TEC values showed a direct correlation with the level of solar activity cycle.

(2) The observed midlatitude ionospheric TEC depletion at extreme solar maximum, was not associated with geomagnetic activities, but could presumably be due to particle precipitation from the outer radiation belt at latitudes greater than 30 degrees South that resulted from the solar flare X28 recorded by the GOES 8 satellite X-ray and SOHO SEM sensors.

Further investigations of solar flare effects on daytime TEC revealed that the EUV flares associated with X-flares could cause global photoionisation within the daytime ionosphere, which would then lead to a sudden increase of TEC lasting longer than the duration of the flare. This confirmed the TEC dependence on geographic locations and is consistent with the findings of Tsurutani et al. (2005). A further investigation of the characteristics of EUV/X-ray flares and their relation to the ionosphere is required (Moeketsi et al., 2007b).

Furthermore, comparisons of TEC derived from the HRAO and HARB GNSS receivers was also performed during the solar X17 and X9 flare events which occurred on day 301, 2003 and day 339, 2006 respectively. It has been shown that there exist considerable differences between TEC observed by the two different but collocated receivers, with strong solar cycle dependence, indicating the direct impact of space weather on the ionosphere over South Africa (Moeketsi et al., 2007a;b).

Finally, the UNB-IMT results were used to investigate the capability of geodetic VLBI derived TEC computed with the Vienna TEC Model (Hobiger et a., 2006; Hobiger, 2007; *private communication*) for monitoring space weather effects on the ionosphere over HRAO, South Africa. The study was

conducted for the year 2002 (near solar maximum) and year 2005 (near solar minimum) during the CONT02 and CONT05 geodetic VLBI campaigns. It has been shown from TEC results obtained with both space geodetic techniques that in general a good level of agreement exists. In particular:

(1) TEC exhibits semiannual variations with higher values around the months of equinoxes and small values around the months of solstices as expected (Bhonsely et al., 1965).

(2) Evidence of annual anomaly features with high TEC values around summer solstice compared to the winter solstice.

(3) Both techniques can be used in future for monitoring space weather impacts on the magnetosphere-ionosphere system over South Africa, in particular under the banner of the forthcoming VLBI2010.

These results verified that the modified UNB-IMT algorithm can be used to complement the ionosondes and geodetic VLBI techniques for ionospheric research and application in South Africa. This thesis contributed to understanding the solar cycle variations of Ionospheric parameters over South Africa and will be important for space weather studies, as well as local and international ionospheric research community.

7.2 Recommendation for future work

For future research and applications, the following topics can be addressed using UNB-IMT (Komjathy, 1997; Ngocbo et al., 2005; Moeketsi et al., 2007a,b):

(a) Monitoring space weather effects on the magnetosphere-ionosphere system over South Africa during solar cycle 24.

(b) Validations of ionospheric parameters from local and global ionospheric models, ground observations and satellite measurements over South Africa.

(c) Investigate solar cycle variations of plasmaspheric electron content over South Africa.

(d) Provide ionospheric corrections for single frequency users over South Africa.

(e) Provide near real time TEC maps for applications in communication, civil aviation, radio astronomy and frequency management over southern Africa.

(f) Monitoring ionospheric TEC over the South African Antarctica base during Solar Cycle 24.

(g) Monitoring ionospheric TEC over Africa.

REFERENCES

Bartels, J., Heck, N. H., Johnston, H. F. The three-hour-range index measuring geomagnetic activity. J. Geophys. Res., 44, 411, 1939.

Bassiri, S., Hajj, G. A. Higher order ionospheric effects on the Global Positioning System observables and means of modeling them. Manuscripta geodaetica, 18, 280-289, 1993.

Basu, S., Basu, Su., Goves, K. M., Yeh, H. C., Su, S. –Y., Rich, F. J., Sultan, P. J., Keskinen, M. J. Response of the equatorial ionosphere in South Atlantic region to the great magnetic storm of July 15, 2000. Geophys. Res. Lett., 28, 3577-3580, 2001.

Belehaki, A., Jakowski, N., Reinisch, B. W. Comparison of ionospheric ionization measurements over Athens using ground ionosonde and GPS-derived TEC values, Radio Sci. 38, 1105, doi:10.1029/2003RS002868, 2003.

Belehaki, A., Tsagouri, I. Investigation of the relative bottomside/topside contribution to the total electron content estimates. Ann. Geophys., 45, 73-86, 2002.

Biermann, L. The solar wind and the interplanetary media. In Space Astrophys., edited by W. Liller, McGraw-Hill, New York, pp.150, 1961.

Bhonsle, R. V., da Rosa, A. V., Carriot, O. K. Measurement of total electron content and equivalent slab thickness of the mid-latitude ionosphere, Radio Sci., 69D, pp. 929, 1965.

Bilitza, D. International Reference Ionosphere. National Space Science Data Center, 1990.

Bilitza, D. The E- and D- region in IRI. Adv. Space Res., 21, 871-874, 1998.
Bilitza, D. International Reference Ionosphere 2000. Radio Sci., 36, 261-275, 2001.

Breed, A. M., Goodwin, G. L. Ionospheric slab thickness and total electron content determined in Australia. Radio Sci., 32(4), 1635-1643, 1997.

Breit, G., Tuve, M. A. A test of the existence of conducting layer. Phys. Rev., 28, 554-561, 1926.

Brunner, F. K., Gu, M. An improved model for the dual frequency ionospheric correction of GPS observations, Manuscripta Geodaetica, 16, 205-214, 1991.

Carpenter, D. L. Whistler evidence of the dynanic behavior of the duskside bulge in the plasmasphere. J. Geophys. Res., 75, 3837, 1970.

Cilliers, P. J., Gouws, D., Opperman, B., Wonnacott, R. T., Combrinck, L. The southern African network of dual frequency global positioning system satellite receiver base stations: A national asset with many applications and research opportunities., S. Afr. J. Sci., 37820, 112-120, 2003.

Cilliers, P. J., Opperman, B. D. L., Mitchell, C. N., Spencer, P. J. Electron density profiles determined from tomographic reconstruction of total electron content obtained from GPS dual frequency data: first results from South African network of dual frequency GPS receiver stations. Adv. Space Res., 34, 2049-2055, 2004.

Clark, T. A., Corey, B. E., Davis, J. L., Elgered, G., Herrig, T. A., Hintergger, H. F., Knight, C. A., Levine, J. I., Lu, G., Ma, C., Nesman, E. F., Phillips, R. B., Rogers, A. E. E., Ronnang, B. O., Ryan, J. W., Schupler, B. R., Shaffer, I., Shapiro, I. I., Vandenberg, N. R., Webber, J. C., Whitney, A. R.

Precision Geodesy using the Mark-III Very Long Baseline Interferrometry System. Geosci. and remote Sensing, IEEE transactions, GE-23, 438-449, 1985.

Coco, D. GPS-Satellite of opportunity for ionospheric monitoring. GPS world, October 1991, 47-50, 1991.

Combrinck, L., Merry, C. L., Wonnacott, R.T. South African research in Geodesy: 1999 – 2003. S. Afr. J. Sci., 99, 398-400, 2003.

Combrink, A. Z. A. Sensing atmospheric water vapour using the Global Positioning System. Ph.D. Thesis, University of Cape Town, South Africa, pp1-127, 2006.

Combrink, A. Z. A., Combrinck, W. L., Moraal, H. Near real-time detection of atmospheric water vapour using SADC GPS network. S. Afr. J. Sci., 100, 436-442, 2004.

Coster, A. J., Gaposchkin, E. M., Thompson, L. E. Real time ionospheric monitoring using GPS. J. Inst. Nav., 39, 191-204, 1992.

Davies, K. Ionosphere Radio Propagation. Dover Publications, Inc., New York, 1966.

Davies, K. Recent progress in Satellite Radio Beacon Studies with particular emphasis on the ATS-6 Radio Beacon Experiment. Space Sci. Rev., 25, 357-430, 1980.

Davies, K. Ionosphere Radio. Peter Peregrinus Ltd., London, United kingdom, 1990.

Donnelly, R. F. Empirical models of solar flare X-ray and EUV emissions for use in studying the E and F region effects. J. Geophys. Res., 81, 4745, 1976.

dos Santos, M. C. Real-time orbit improvement for GPS Satellites. PhD dissertation, Department of Geodesy and Geomatics Engineering, Technical Reports No. 178, University of New Brunswick, Fredericton, New Brunswick, Canada, pp. 125, 1995.

El-Arini, M. B., Conker, R. S., Albertson, T. W., Reagan, J. K., Klobuchar, J. A., Doherty, P. H. Comparison of real time ionospheric algorithms for a GPS wide area augmentation system (WAAS). J. Inst. Nav., 41, 393-412, 1995.

Estey, L. H., Merteens, C. M. TEQC: The multi-purpose toolkit for GPS/GLONASS data. GPS Solutions, 3, 42-49, 1999.

Fedrizzi, M., de Paula, E. R., Kantor, I. J., Langley, R. B., Komjathy, A., Batista, I. S. Study of the March 31, 2001 magnetic storm effects on the ionospheric GPS data. Adv. Space Res., 36(3), 534-545, 2005.

Fedrizzi, M., Langley, R. B., Komjathy, A., Santos, M.C., de Paula, E. R., Kantor, I. J. The low-latitude Ionosphere: Monitoring its behaviour with GPS. Institute of Navigation. Proceedings of ION GPS-2001, Salt lake City, pp. 2468-2475, 2001.

Forster, M., Jakowski, N. Geomagnetic storm effects on the topside ionosphere and plasmasphere: A compact Tutorial and new results. Surveys in Geophys., 21(1), 47-87, 2000.

Foster, J. C., Rideout, W. Storm enhanced density: magnetic conjugate effects. Ann. Geophys., 25, 1971-1979, 2007.

Fuller-Rowell, T. J., Codrescu, M. V., Moffett, R. J., Quegan, S. Response of the thermosphere and ionosphere to geomagnetic storms. J. Geophys. Res., 99, 3893-3914, 1994.

Fuller-Rowell, T. M., Godrescu, M. V., Roble, R. G., Richmond, A. D. How does the thermosphere and ionosphere react to a geomagnetic storm? In Magnetic storm, Geophys. Monogr. Ser. 98, edited by Tsurutani et al., p. 203, AGU, Washington D. C., 1997.

Gail, W. B., Prag, A. B., Coco, D. S., Coker, C. A statistical characterization of local mid-latitude total electron content. J. Geophys. Res., 98, 15.717-15.727, 1993.

Gao, Y., Heroux, P., Kouba, J. Estimation of GPS receiver and satellite L1/L2 signal delay biases using Data from CACS. Proceedings of KIS-94, Banff, Canada, August 30 – September 2, 1994.

Gao, Y., Liu, Z. Z. Precise ionosphere modeling using regional GPS Network data, J. of GPS., 1, 18-24, 2002.

Garriot, O. K., Little, C. G. The use of Geostationary Satellites for the study of Ionospheric Electron Content and Radio-Wave Propagation. J. Geophys. Res., 65, pp. 2025, 1960.

Garriot, O. K., Smith, F. L., Yuen, P. C. Observations of ionospheric electron content using a geostationary satellite. Plan. Space Sci., 13, pp. 829, 1965.

Hobiger, T. Kashima Space Research Center, National Institute of Information and Communications Technology, Kashima, Japan, Private Communication, 2007.

Hobiger, T., Kondo, T., Schuh, H. Very long baseline interferometry as a tool to probe the ionosphere. Radio Sci., 41, RS1006, doi:10.1029/2005RS003297, 2006.

Hobiger, T., Schuh, H. How VLBI contributes to ionospheric research. in International Service for Geodesy and Astrometry 2004 General Meeting Proceedings, edited by N. R. Vanderberg and K. D. Baver, NASA Conf. Publ. CP-2004-212255, 437-441, 2004.

Hoffmann-Wellenhof, B., Lichtenegger, H., Collins, J. GPS Theory and Practice. 3rd rev. ed., Springler-Verlag Wien, Vienna, Austria, 1994.

Hovestadt, D. et al. CELIAS-Charge, Element, and Isotope Analysis System for SOHO. Sol. Phys. 162, 441-481,1995.

Huang, X., Reinisch, B. W., Song, P., Green, J. L., Gallagner, D. L., Developing empirical density model of the plasmasphere. Adv. Space Res., 33, 829-832, 2003.

Hunsucker, R. D. Radio Techniques for probing the ionosphere. Springer-Verslag, New-York, 1991.

Immel, T. J., Mende, S. B., Frey, H. U., Ostgaard, N., Gladstone, G. R. Effect of the 14 July 2000 solar flare on Earth's FUV emissions. J. Geophys. Res., 108, 1155, doi:10.1029/2001JA009060, 2003.

Jakowski, N. TEC monitoring by Using Satellite Positioning Systems. in: Kohl, H., Rüster, R., Schlegel, K. (Eds.), Modern Ionospheric Science. Max-Planck-Intitut für Aeronomie, pp.371-390, 1996.

Jakowski, N., Heise, S., Wehrenpfenning, S., Schlüter, S. TEC Monitoring by GPS – A possible contribution to space weather monitoring. Phys. Chem. Earth (C), 26, 609-613, 2001.

Jakowski, N., Heise, S., Wehrenpfenning, S., Schlüter, S., Reimer, R. GPS/GLONASS-based TEC measurements as a contributor for space weather forecast. J. Atmos. and Sol. Terr. Phys., 64, 729-735, 2002.

Jakowski, N., Jungstand, A., Schlegel, K., Kohl, H., Rinnert, K. The ionospheric response to perturbation electric fields during the onset phase of geomagnetic storms. Canadian Journal of Physics, 70(7), 575-581, 1992.

Jakowski, N., Paasch, E. Report on the observations of the total electron content of the ionosphere in Neustrelitz/GDR from 1976 to 1980. Ann. Geophys., 2, 501-504, 1984.

Jakowski, N., Schlüter, S., Sardón, E. Total electron content of the ionosphere during the geomagnetic storm on 10 January 1997. J. Atmos. Sol. Terr. Phys., 61, 299-307, 1999.

Jee, G., Schunk, R. W., Scherliess, L., Comparison of IRI-2001 with TOPEX TEC measurements, J. Atmos. Sol. Terr. Phys., 67, 365-380, 2005.

Jones, A. R. Space Science Center, University of South California, Los Angeles, Private communication, 2005.

Judge, D. L. First solar EUV irradiance obtained from SOHO by CELIAS/SEM. Sol. Phys., 177, 261, 1998.

Judge, D. L., McMullin, D. R., Gangopadhyay, P., Ogawa, H. S., Ipavich, F. M., Galvin, A. B., Möbuis, E., Bochsler, P., Wurz, P., Hilchenbach, M., Grünwaldt, H., Hovestadt, D., Klecker, B., Gliem, F. Space weather observations using SOHO CELIAS complement of instruments. J. Geophys. Res., 106, 29963-29968, 2001.

Judge, D. L., Ogawa, H. S., McMullin, D. R., et al. The SOHO CELIAS/SEM EUV database from SC23 minimum to the present. Adv. Space Res. 29, 1063-1968, 2002.

Junkins, J. L., Miller, G. W., Jancaitis, J. R. A weighting function approach modelling of irregular surfaces. J. Geophys. Res.,78, 1794-1803, 1973.

Kaplan, E. D. Understanding GPS principles and applications. Artech House, Boston, 1996.

Klobuchar, J. A. Ionospheric time-delay algorithm for single frequency users. IEEE transactions on Aerospace and Electronic Systems, 23, 325-331, 1987.

Klobuchar, J. A. Ionospheric effects on GPS. GPS World, 2, 48-51, 1991.

Komjathy, A. Global Ionospheric Total Electron Content Mapping Using the Global Positioning System. Dept. of Geodesy and Geomatics Engineering, Technical Report No. 188), PhD. Dissertation, University of New Brunswick, 1997.

Komjathy, A., Langley, R. B. An assessment of predicted and measured ionospheric total electron content using a regional GPS Network. The proceedings of the National Technical Meeting of the Institute of Navigation., pp. 615-624, 1996.

Komjathy, A., Langley, R. B., Bilitza, D. Ingesting GPS-derived TEC data into International Reference Ionosphere for single frequency radar altimeter ionospheric delay corrections. Adv. Space Res., 22, 793-801, 1998.

Kondo, T. Application of VLBI data to measurements of ionospheric total electron content, J. Comm. Res. Lab., 38, 613-622, 1991.

Langley, R. B., The GPS observables. GPS world, 4, 52-59, 1993.

Langley, R. B. Propagation of GPS signals. In GPS for Geodesy. International School, Delft, The Netherland, 26 March – 1 April, 1995, Springer verlag, New York, 1996.

Lanyi, G., Roth, T. A comparison of mapped and measured total ionospheric electron content using global positioning system and beacon satellite observations. Radio Sci., 23(4), 483-492, 1988.

Liu, J. Y., Lin, C. H., Chen, Y. I., Lin, Y. C., Fang, T.W., Chen, C. H., Chen, C. Y., Hwang, J. J., Solar flare signatures of the ionospheric GPS total electron content, J. Geophys. Res., 111, A05308, doi:10.1029/2005JA011306, 2006.

Liu, H., Lurh, H., Watanbe, S., Kohner, W., Manoj, C. Contrasting behavior of the thermosphere and ionosphere in response to 28 October 2003 solar flare. J. Geophys. Res., 112, A07305, doi:10.1023/2007JA012313, 2007.

Lui, Z. Z., Gao, Y. Ionospheric tomography using GPS measurements. Proceedings of KIS-2001, Banff, Alberta, Canada, June 5-8, 2001.

Lunt, N., Kersely, L., Bishop, G. J., Manzella, A. J. The contribution of the protonsphere to GPS total electron content: Experimental measurements. Radio Sci., 34, 1273-1280, 1999.

Mannucci, A. J., Tsurutani, B. T., Iijima, B. A., Komjathy, A., Saito, A., Gronzalez, W. D., Guarneiri, F. L., Kozyra, J. U., Skoug, R. Dayside global ionospheric response to the major interplanetary events of October 29-30 “Halloween Storms”. Geophys. Res. Lett., 32, L12S02, doi:10.1029/2004GL021467, 2005.

Mannucci, A. J., Wilson, B. D., Edwards, C. D. A new method for monitoring the Earth's ionospheric total electron content using the GPS global network. Proceedings of the ION GPS-93, 6th International Technical Meeting of the Satellite division of the Institute of Navigation, Salt lake, Utah, USA, VII, pp. 1323-1332, 1993.

Mannucci, A. J., Wilson, B., Yuan, D. An improved ionospheric correction method for wide-area augmentation systems. Proceedings of ION GPS-95, the 8th International Technical Meeting of the satellite Division of Institute of Navigation, Palm Springs, CA, 12-15 September, The Inst. Nav., Alexandria, VA, 1199-1208, 1995.

Mannucci, A. J., Wilson, B. D., Yuan, D. N., Ho, C. M., Lindqwister, U. J., Runge, T. F. A global mapping Technique for GPS-derived ionospheric total electron content measurements, Radio Sci., 33, 565-582, 1998.

McKinnell, L. A. A neural network based ionospheric model for the bottomside electron density profile over Grahamstown, Ph.D. Thesis, Rhodes University, South Africa, pp. 1-155, 2002.
McKinnell, L. A., Opperman, B., Cilliers, P. J. GPS TEC and Ionosonde TEC over Grahamstown, South Africa: First Comparisons. Adv. Space Res., 39, 816-820, 2007.

McKinnell, L. A., Poole, A. V. W. The development of a neural network based short-term foF2 forecast program. Phys. Chem. Earth, 24, 287-290, 2000.

McKinnell, L. A., Poole, A. V. W. Neural Network-based ionospheric modelling over the South African region, S. Afr. J. Sci., 100, 519-523, 2004.

McNamara, L. F. The ionosphere Communications, Surveillance, and Direction Finding. Krieger Publishing Company, Malabar, FL., 1991.

McNamara, L. F. Radio amateur guide to the ionosphere. Krieger publishing Company, Malabar, FL, 1994.

Meggs, R. W., Mitchell, C. N. A study into the errors in vertical total electron content mapping using GPS data. Radio Sci., 41, RS1008, doi:10.1029/2005RS003308, 2006.

Meggs, R. W., Mitchel, C. N., Spencer, S. J. A comparison of techniques for mapping total electron content over Europe using GPS signal. Radio Sci., 39, RS1S10, doi:10.1079/2002RS002846, 2004.
Mendillo, M. Storms in the ionosphere: Patterns and processes for total electron content, Rev. Geophys., 44, RG4001, doi:10.1029/2005RG000193, 2006.

Miro, G., Jakowski, N., de la Morena, B. A., Equivalent slab thickness of the ionosphere in the middle latitude based on TEC/foF2 obserfations over EL Arenosillo. Proc. 3rd COST251 Workshop, (Eds. R. Hanbaba and B. A. dela Morena), September, 1998, 87-92, 1999.

Mitchell, C. N., Kersley, L., Heaton, J. A. T., Pryse, S. E. Determination of the vertical electron-density profile in ionospheric tomography: experimental results. Annales Geophys., 15, 747-752, 1997.

Mitra, A. P. Ionospheric effects of Solar flares. Springer, New York, pp 294, 1974.

Moeketsi, D. M. Modelling of Galactic and Jovian electrons in the heliosphere. MSc Thesis, Northwest University, Potchefstroom Campus, South Africa, pp.1-121, 2004.

Moeketsi, D. M., Combrinck, W. L., McKinnell, L. A., Combrink, A. Z. A. Comparison of ionospheric Total Electron Content derived from collocated GNSS receivers over HartRAO during Solar X-flares. S. Afr. J. Geol., 110(2-3), 219-224, 2007 (a).

Moeketsi, D. M., Combrinck, W. L., McKinnell, L. A., Fedrizzi, M. Mapping GPS-derived ionospheric Total Electron Content over Southern Africa during different epochs of Solar Cycle 23. Adv. Space Res. 39, 821-829, 2007 (b).

Ngcobo, S., Moeketsi, D. M., Combrink, A. Z. A., W. L. Combrinck. Ionospheric total electron content observed using the southern African GPS networks. S. Afr. J. Sci., 101, 537-539, 2005.

Opperman, B. D. L., Cilliers, P. J., McKinnell, L. A., Haggard, R. Development of a regional GPS-based model for South Africa. Adv. Space Res., 39, 808-815, 2007.

Otto, A. The Magnetosphere. Lect. Notes., Springer Verlag, Berlin, Heidenberg, (Edited by K. Scherer, H. Fichtner, B. Heber, U. Mall: Space Weather, The Physics behind the slogan), 656, 133-192, 2005.

Oyeyemi, E. O. A global ionospheric F2 region peak electron density model using neural networks and extended geophysically relevant inputs. PhD thesis, Rhodes University, South Africa, pp. 1-183, 2005.

Oyeyemi, E. O., McKinnell, L. A., Poole, A. W. V. Neural network-based prediction techniques for global modeling of M(3000) F2 ionospheric parameter. Adv. Space Res., 39, 643-650, 2007.

Oyeyemi, E., Poole, A. W. V. On the development of a global foF2 empirical model using neural networks. Adv. Space Res., 34, 1966-1972, 2004.

Parker, E. N. Cosmic ray modulation by the solar wind. Phys. Rev., 110, 1445, 1958.

Parker, E. N. Interplanetary dynamical processes, Interscience, New York, 1963.

Prölss, G. W. On explaining the local time variation of ionospheric storm effects. Ann. Geophys., 11, 1-9, 1993.

Poole, A. W. V., McKinnell, L. A. On the predictability of foF2 using neural networks. Radio Sci. 35, 225-234, 2000.

Ratcliffe, J. A. Magneto-ionic theory and its application to the ionosphere. Cambridge University Press, Cambridge, 1959.

Raymund, T. D. Comparison of several ionospheric tomography algorithms, Ann. Geophys., 13, 1254-1262, 1995.

Raymund, T. D., Austen, J. R., Franke, S. J., Liu, C. H., Klobuchar, J. A., Stalker, J. Application of computerized tomography to the investigation of Ionosphere Structure. Radio. Sci., 25, 771-789, 1990.

Raymund, T. D., Bresler, Y., Anderson, D. N., Daniell, R. E. Model-assisted ionospheric tomography: new algorithm. Radio Sci., 1493-1512, 1994.

Reinisch, B. W. New techniques in ground-based ionospheric sounding and studies, Radio Sci., 21, 331-336, 1986.

Reinisch, B. W. Modern Ionosondes. in: Kohl, H., Rüster, R., Schlegel, K. (Eds.), Modern Ionospheric Science. Max-Planck-Intitut für Aeronomie, pp.440-458, 1996.

Reinisch, B. W., Huang, X. Deducing topside profiles and total electron content from bottomside Ionogram. Adv. Space Res., 27, 23-30, 2001.

Ros, E., Marcaide, J. M., Guirando, J. C., Sardon, E., Shapiro, I. I. A GPS-based method to model the plasma effects in VLBI observations. Astron. Astrophys. 356, 357-362, 2000.

Schaer, S. Mapping and predicting the Earth's ionosphere using the global positioning system. Ph.D. Dissertation, University of Bern, Bern, Switzerland, 1999.

Sekido, M., Kondo, T., Kawai, E. Evaluation of GPS-based ionospheric TEC map by comparing with VLBI data. Radio Sci., 38, 1069, doi:10.1029/2000RS002620, 2003.

Shetti, D. J. Studies of the dynamics of the upper atmosphere at low latitudes (0 to 30°N Latitude) by airglow technique. PhD Thesis, Shivaji University, Kolhapur, India, pp. 1-162, 2006.

Smith, E. J., Marsden, R. G. Ulysses observations at solar maximum: Introduction. Geophys. Res. Lett., 30, 8027, doi:10.1029/2003GL018223, 2003.

Skone, S., Yousuf, R., Perfomance of satellite-based navigation for marine users during ionospheric disturbances, Space Weather, 5, s01006, doi:1029/2006SW000246, 2007.

Skoug, R. M., Gosling, J. T., Steinberg, J. T., McComas, D. J., Smith, C. W., Ness, N. F., Hu, Q., Burlaga, L. F. Extremely high speed solar wind: 29-30 October 2003. J. Geophys. Res., 109, A09102, doi:10.1029/2004JA010494, 2004.

Stewart, P. J. The reduction of differential ionospheric delay for GPS carrier phase ambiguity resolution, M.Sc.E thesis, Department of Geodesy and Geomatics Engineering, Technical Reports No. 185, University of New Brunswick, Fredericton, New Brunswick, Canada, pp. 104, 1997.

Stubbe, P. The ionosphere as a Plasma Laboratory. in: Kohl, H., Rüster, R., Schlegel, K. (Eds.), Modern Ionospheric Science. Max-Planck-Intitut für Aeronomie, pp.274-321, 1996.

Sugira, M. Hourly values of equatorial DST for IGY. pp.945-948, in annals of the international geophysical year. 35, Pergamon press, Oxford, 1964.

Tascione, T. F. Introduction to Space Enviroment. Orbit Book Company, Malibar, Florida, 1988.

Thome, G. D., Wagner, L. S. Electron density enhancements in the E and F regions of the ionosphere during solar flares. J. Geophys Res., 76, 6883, 1971.

Titheridge, J. E. The electron content of the southern mid-latitude ionosphere: 1965-1971, J. Atmos. Terr. Phys., 35, pp. 981, 1973.

Tsurutani, B. T., Gonzalez, W. D. The interplanetary causes of magnetic storms: A review, in Magnetic storms, Geophys. Monogr. Ser., 98, edited by Tsurutani et al., pp. 77-89, AGU, Washington, D. C., 1997.

Tsurutani, B. T., Judge, D. L., Guarnieri, F. L., Gangopadhyay, P., Jones, A. R., Nuttal., Zambon, G. A., Didkovsky, L., Mannucci, A. J., Iijima, B., Meier, R. R., Immel, T. J., Woods, T. N., Prasad, S., Floyd, L., Huba, J., Solomon, S. C., Straus, P., Viereck, R. The October 28, 2003 extreme EUV solar flare and resultant extreme ionospheric effects: Comparison to other Hallowen events and the Bastille Day event. Geophys. Res. Lett., 32, L003S09, doi:1029/2004GL021475, 2005.

Tsurutani, B T., Mannucci, A., Iijima, B., Abdu, M. L., Sobral, J. H. A., Gonzalez, W., Guarnieri, F., Tsuda, T., Saito, A, Yumoto, K., Fejer, B., Fuller-Rowell, T. J., Kozyra, J., Foster, J. C., Coster,

A., Vasyliunas, V. M. Global dayside ionospheric upliftment and enhancement associated with interplanetary electric fields. J. Geophys. Res., 109, A08302, doi:10.1029/2003JA010342, 2004.

van der Wal, A. D. Evaluation of Strategies for Estimating residual neutral atmosphere propagation delay in high precision global positioning system data analysis. M.Sc.E. Thesis, Department of Geodesy and Geomatics Engineering Technical Report No. 177, University of New Brunswick, Frederiction. N.B., Canada, 1995.

Walker, J. K. Spherical cap harmonic modeling of high latitude magnetic activity and equivalent sources with sparse observations. J. Atmos. Terr. Phys., 51, 67-80, 1989.

Warnant, R., Pottiaux, E. The increase of the ionospheric activity as measured by GPS. Earth and Planet. Space. 52, 1055-1060, 2000.

Warnninger, L. Effects of the equatorial ionosphere on GPS. GPS world, 4, 48-53, 1993.

Webb, P. A., Essex, E. A. Modelling the Plasmasphere. IPS Radio and Space Serv., Sydney, Austria, 2002.

Williscroft, L. A., Poole, A. W. V. Neural Networks, foF2, sunspot number and magnetic activity. Geophys. Res. Lett., 23, 3659-3662, 1996.

Zhang, M. L., Radicella, S. M., Shi, J, K., Wang, X., Wu, S. Z. Comparison among IRI, GPS-IGS and ionogram-derived total electron contents. Adv. Space Res., 37, 972-977, 2006.

Zhang, D. H., Xiao, Z. Study of ionospheric response to the 4B flare on 28 October 2003 using International GPS Service network data. J. Geophys. Res., 110, A03307, doi:10.1029/2004JA010738, 2005.